SECTION B

RESULTS AND DISCUSSION

CHAPTER 4

Microscopic, Spectroscopic, Electrochemical and Electrocatalytic Properties of Nanostructured Iron(II) and Cobalt(II) Phthalocyanine*

* The following publications resulted from part of the research work presented in this chapter and they are not referenced further in this thesis:

1. S.A. Mamuru, K.I. Ozoemena, *Materials Chemistry and Physics*, **114** (2009), 113-119
2. S.A. Mamuru, K.I. Ozoemena, *Electroanalysis*, **22** (2010), 985-994

4.1 Microscopic and Spectroscopic Characterisation

Following the synthesis of the nanostructured iron(II) and cobalt(II) phthalocyanine complexes from their bulk counterpart, their surface morphologies were examined to obtain microscopic and spectroscopic information. Atomic force microscopy, scanning electron microscopy and energy dispersive x-ray spectroscopy were employed for this investigation.

4.1.1. *Comparative SEM, AFM and EDX*

Scanning electron microscope (SEM) images of the MPc and nanoMPc as depicted in Scheme 3.1 clearly confirm the successful nanostructuring of the bulk (crystallite form) MPc molecules to their amorphous nanoparticles protected by surfactant layer (CTAB particles). The main principle of the synthesis as depicted in Scheme 3.1 is simply the breaking of the intramolecular forces of the MPc and protecting the species in CTAB environments. As observed in the SEM images, these nanoparticles form aggregates which is an indication of the existence of an attractive interaction among nanoparticles. The preservation of their individuality suggests the existence of a stabilisation mechanism resulting from the surfactant layer adsorbed at the nanoparticle surface.[1] Figure 4.1 shows AFM images of the bulk FePc and nanoFePc, it closely resembles that of the SEM.

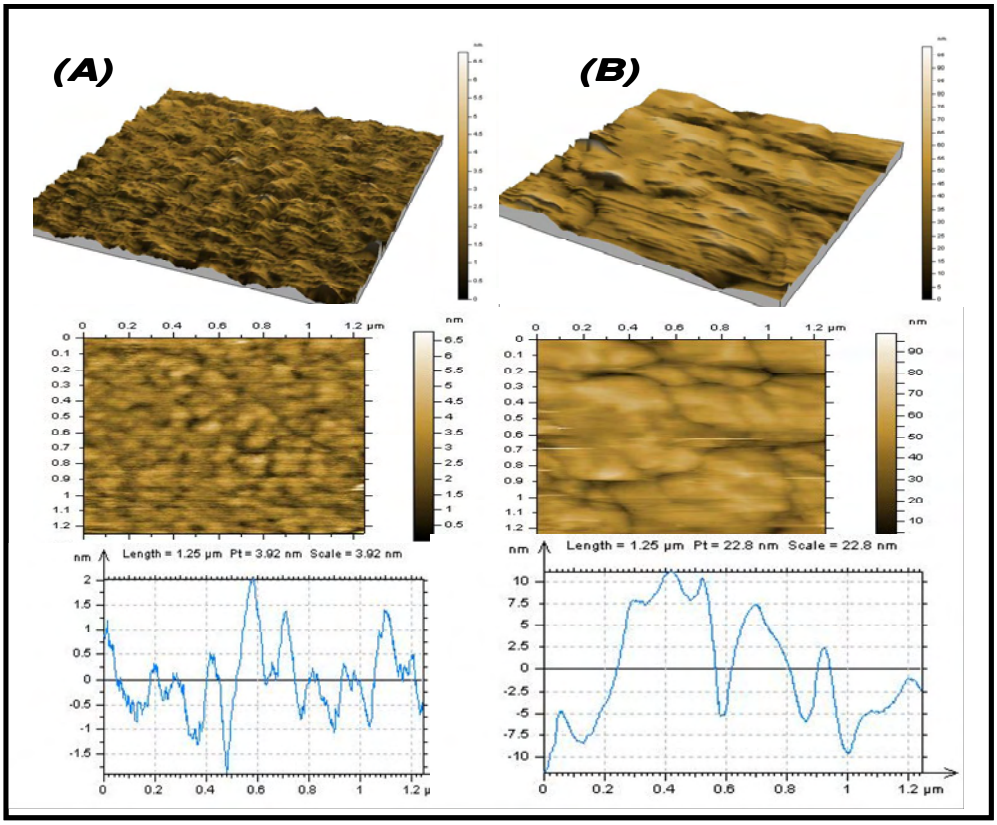

Figure 4.1: *AFM images of bulk FePc (A) and nanostructured FePc (B)*

The energy dispersive x-ray (EDX) profile (Figure. 4.2) clearly shows the analytical details of the elemental composition of the bulk FePc, nanostructured FePc and surfactant (CTAB).The FePc (A) was dominated by carbon and iron. With CTAB (B), carbon and bromine were observed only. Similarly, as expected, with the nanoFePc (C), the presence of these two species (FePc and CTAB) was clearly evident. The sulphur peak at 2.4 *e*V could have arisen from the sulphuric acid solution used in the synthesis. Similar profiles were observed for the cobalt (II) phthalocyanine.

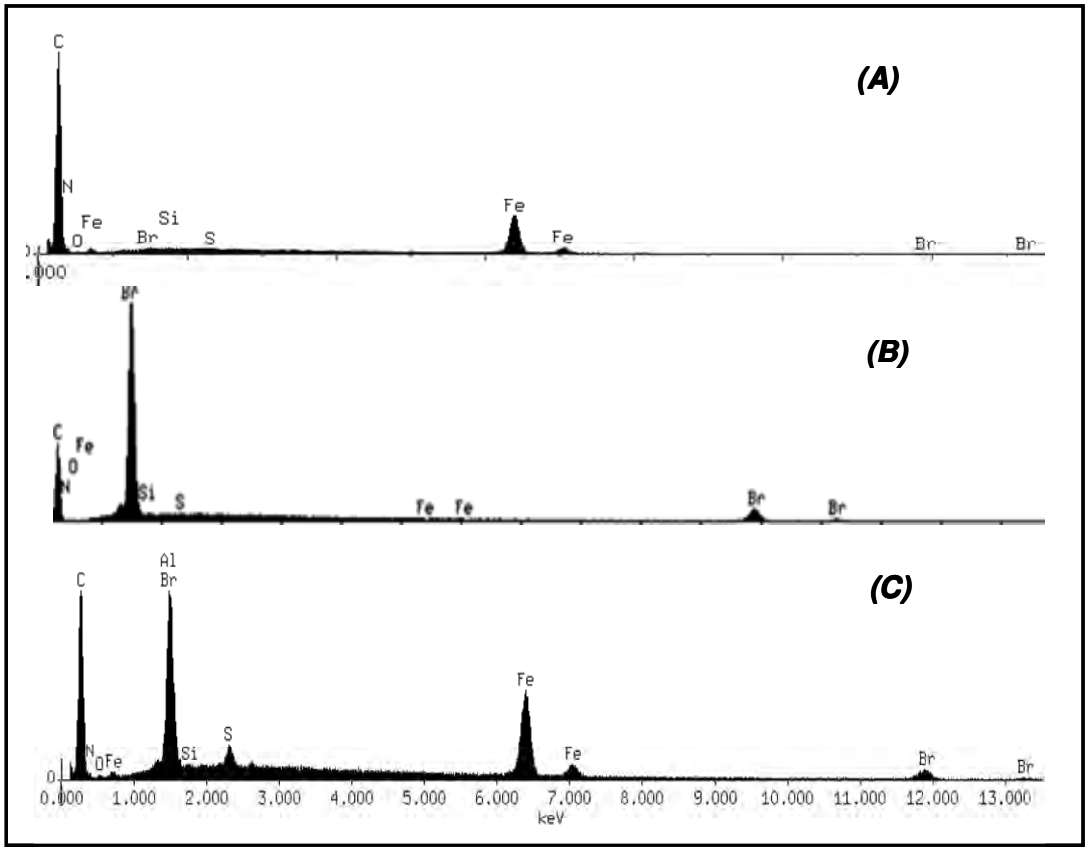

***Figure 4.2:** EDX profile of bulk FePc (A), CTAB (B) and nanoFePc (C)*

4.2 Electrochemical Characterisation

4.2.1. *Electron transfer behaviour: cyclic voltammetry*

Figure 4.3 compares typical cyclic voltammetric evolutions of the bare EPPGE, EPPGE-FePc, EPPGE-nanoFePc,EPPGE-MWCNT, EPPGE-MWCNT-FePc and EPPGE-MWCNT-nanoFePc and the corresponding CoPc derivatives recorded in 0.1 M $[Fe(CN_6)]^{3-}/[Fe(CN_6)]^{4-}$ solution containing 1.0 M KCl. It should be noted that $[Fe(CN)_6]^{3-}/[Fe(CN)_6]^{4-}$ is an important redox probe known to exhibit 1-electron reversible process. The choice of this redox probe in this work is to answer the question as to what extent can the modifying species permit the electron transfer of the $[Fe(CN)_6]^{3-}/[Fe(CN)_6]^{4-}$ species to the underlying EPPG electrode. In Figure 4.3 (a) the bare EPPGE gave similar voltammogram as those of the EPPGE-FePc and EPPGE-nanoFePc. This cyclic voltammetric result has certain implications. First, the result is in excellent agreement with the reports of Griveau *et al*[2] and Ozoemena and Nyokong.[3] These workers[2,3] had examined the cyclic voltammetric responses of $[Fe(CN)_6]^{3-}/[Fe(CN)_6]^{4-}$ at both bare and MPc-modified electrodes and found that they produced similar voltammetric shapes with no detectable change in the redox potential and with nearly equal peak current intensities. However, there was a huge current difference between the MWCNT-based electrodes and the other electrodes. A similar trend was observed with the EPPGE-CoPc derivatives and the EPPGE-MWCNT-CoPc derivatives. Analysis of the

potential peak-to-peak separation (ΔE_p) of the electrodes are essentially similar (approximately 100 mV), suggesting that no meaningful electron transfer kinetics could be obtained using the ΔE_p values.

4.2.2. *Diffusion Domain Approximation Theory*

The type of diffusion process that could be occurring at these electrodes was interrogated by using the "diffusion domain approximation" theory developed by Davies and Compton for the voltammetric responses at spatially heterogeneous electrodes/partially blocked electrodes,[4,5,6] which can also be applied to a 3-dimensional electrochemically heterogeneous electrode, for example, EPPGE modified with gold and anthraquinone.[4] More information on this theory can be found in the cited references. As shown in Figure 4.3, and according to the theory, radial diffusion plays the dominant role where there is near complete electrolysis of the redox probe to the surface of the electrodes in the bare EPPGE and the EPPGE-MPc electrodes. The questions that then arise should include: (a) what is the origin of the large current response observed at the EPPGE-MWCNT, a negatively-charged surface, that should have been lower considering that a repulsive interactions should have existed between this electrode and the negatively-charged redox probe, ($[Fe(CN)_6]^{3-}$/ $[Fe(CN)_6]^{4-}$)?; (b) why is the current response at the EPPGE-MWCNT-

nanoFePc (a positively-charged surface) the same as that of the EPPGE-MWCNT?, and (c) why is the current response at the EPPGE-MWCNT-nanoFePc larger than that observed at the EPPGE-MWCNT-FePc?

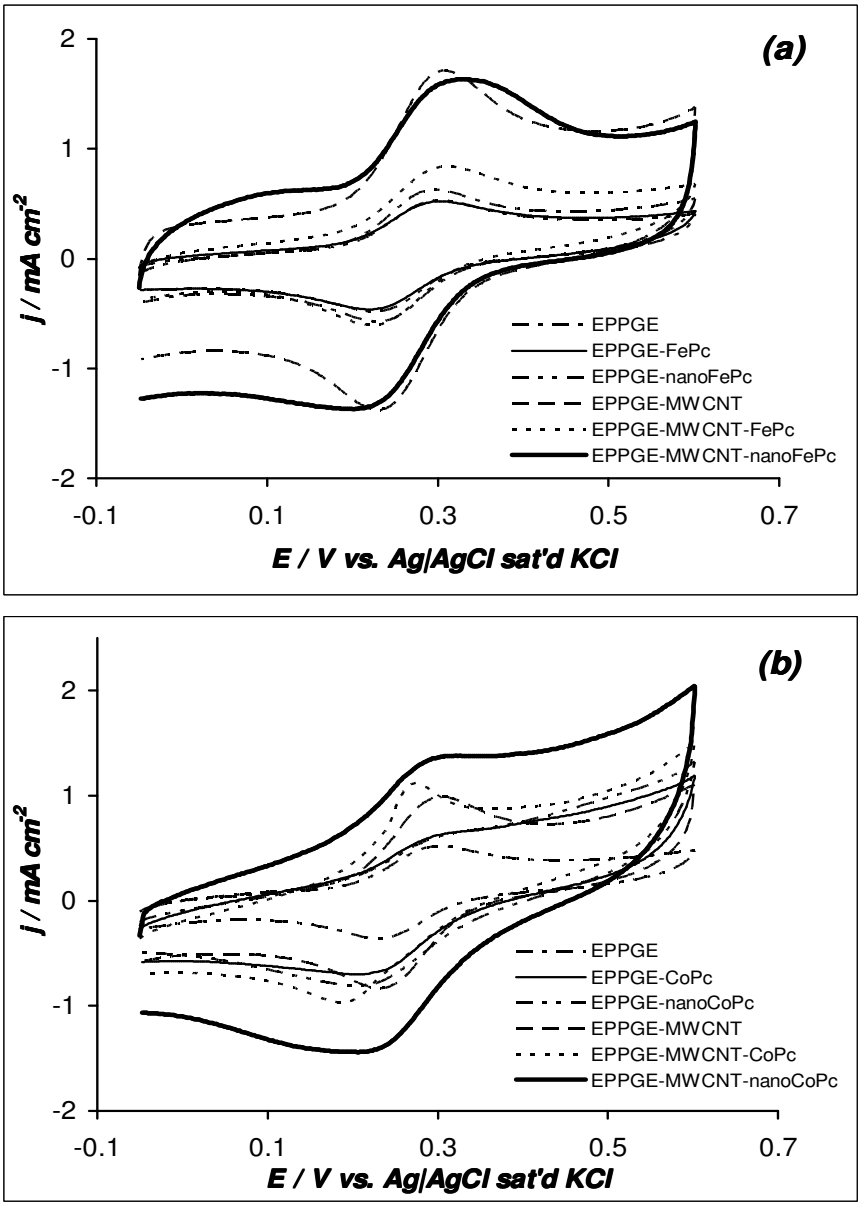

Figure 4.3: *Comparative cyclic voltammograms of the electrodes in 1.0 M KCl containing 0.1 M $[Fe(CN)_6]^{3-}/[Fe(CN)_6]^{4-}$ solution (a) FePc derivatives (b) CoPc derivatives*

The answers to these questions may be found in the work of Compton and co-workers,[7] where the authors cautioned on the interpretation of the current response at CNT-based electrodes where the electrode surface is not truly planar. According to them, such large current response could arise from (i) electrocatalysis, (ii) a change in diffusion regime (i.e., semi-infinite linear diffusion and / or thin layer diffusion processes, the latter process arising from the oxidation of electroactive species/electrolytes trapped in pockets in between the nanotubes), or (iii) a combination of (i) and (ii). Thus, it may suffice to say that in this case, this may be due to the redox processes of the ferrocyanide/ferricyanide species that were trapped within the porous layers of the high surface area MWCNTs or MWCNT-nanoFePc. The slightly lower capacitive current (in the region between +0.1 and -0.1 V) at the MWCNT-nanoFePc compared to the MWCNT alone may be attributed to the enhanced Faradaic response induced by the electrostatic attraction between the nanoFePc and the redox probe.

According to Davies and Compton, the diffusion layer thickness, δ, which helps in categorizing the type of diffusion occurring at the electrodes, can be obtained from the modified Einstein equation for the root mean square displacement of diffusing particles,[4,5,6] equation (4.1):

$$\delta = \sqrt{2D\frac{\Delta E}{v}} \qquad (4.1)$$

where *D* is diffusion coefficient of aqueous ferrocyanide ($6.3x10^{-6}$ cm^2 s^{-1})[6], Δ*E* is the potential "width" of the voltammogram (i.e., the distance between the onset potential to where the peak potential or limiting current is attained)[6] and υ is the scan rate (0.05 V s^{-1} in the case of Figure 4.3 (a)). Using ΔE of 0.197 V (for the EPPGE, EPPGE-FePc and EPPGE-nanoFePc), 0.186 V for the EPPGE-MWCNT-FePc, 0.176 V for the EPPGE-MWCNT and 0.170 V for the EPPGE-MWCNT-nanoFePc for the EPPGE-MWCNT-FePc, 0.135 V for EPPGE-CoPc and EPPGE-nanoCoPc, 0.129 V for EPPGE-MWCNT-CoPc and 0.148 V for the EPPGE-MWCNT-nanoCoPc, an approximate value of 51 μm was estimated as the diffusional distance for the FePc derivatives while 59 μm was obtained for the CoPc derivatives. These values correspond to the type 3 behaviour of the voltammetric responses at spatially heterogeneous electrodes,[5] and is associated with an overlap of adjacent diffusion layers resulting from the small size of the inert part of the electrode.

4.2.3. *Electron transport behaviour: Impedimetric characterization*

Since the potential peak-to-peak separation (ΔE_p) of the electrodes are essentially similar (approximately 100 mV), suggesting that no meaningful electron transfer kinetics could be obtained using

the ΔE_p values. This prompted the exploration of the electrochemical impedance spectroscopy route to follow the heterogeneous electron transfer kinetics at these electrodes. EIS is a complementary technique to CV; while the latter represents only part of an electrochemical system, the results of the EIS measurements give fuller description of the electrochemical system,[8] providing vital information about processes occurring at the electrode/electrolyte interface. Figures 4.4 (a) and 4.5 (a) shows examples of the Nyquist plots obtained for the electrodes in the $[Fe(CN)_6]^{3-}/[Fe(CN)_6]^{4-}$ solution. As seen in Figure 4.4 (a) and 4.5 (a) (data summarized in Table 4.1), the impedance spectra of the electrodes were satisfactorily fitted (especially in terms of the low fitting errors and the pseudo-chi square ($\leq 10^{-4}$) from the Kramers-Kronig tests) with the proposed modified Randles equivalent electrical circuits (Fig. 4.4 (d)). The bare EPPGE, EPPGE-FePc and EPPGE-nanoFePc were fitted with circuit (i) while the EPPGE-MWCNT, EPPGE-MWCNT-FePc and EPPGE-MWCNT-nanoFePc were fitted with circuit (ii). In Figure 4.5, the impedance spectra were fitted with the equivalent electrical circuit as proposed in Figure 4.5 (d). The EPPGE-CoPc was fitted with circuit (i), while EPPGE-nanoCoPc, EPPGE-MWCNT-CoPc and EPPGE-MWCNT-nanoCoPc were fitted with circuit (ii). The fitting parameters involve the electrolyte resistance (R_s), electron-transfer resistance (R_{ct}), constant phase element (CPE), double layer capacitance (C_{dl}) and Warburg-type impedance (Z_w) which is

associated with the diffusion of the ions of the redox probe. The apparent electron-transfer rate constant (k_{app}) values of the electrodes were obtained from the equation (4.2):[9]

$$k_{app} = \frac{RT}{n^2 F^2 A R_{ct} c} \qquad (4.2)$$

where n is the number of electron transferred, A is the area of the electrode, c is the concentration of the $[Fe(CN)_6]^{3-}$ (in mol cm^{-3}, the concentration of $[Fe(CN)_6]^{3-}$ and $[Fe(CN)_6]^{4-}$ are equal), R is the ideal gas constant, T is the absolute temperature (K) and F is the Faraday constant. The calculated values are shown in Table 4.1. The k_{app} values decrease as: EPPGE-MWCNT-nanoFePc > EPPGE-MWCNT-FePc > EPPGE-nanoFePc > EPPGE-FePc, for the FePc derivatives while for the CoPc derivatives is as: EPPGE-MWCNT-nanoCoPc > EPPGE-MWCNT-CoPc > EPPGE-nanoCoPc > EPPGE-CoPc indicating that electron transfer processes between the redox probe and the underlying EPPGE surface is much easier at the EPPGE-MWCNT-nanoMPc compared to the other electrodes.

The impedance of the CPE (Z_{CPE}) is defined as equation (2.26):

$$Z_{CPE} = \left[Q(j\omega)^n\right]^{-1} \qquad (2.26)$$

where Q is the frequency-independent constant related to the interface, $j = \sqrt{-1}$, ω is the radial frequency, the exponent n arises from the slope of log Z vs. log f (and has values $-1 \leq n \leq 1$). If n=0, the CPE behaves as a pure resistor; n=1, CPE behaves as a pure capacitor, n=

-1 CPE behaves as an inductor; while n=0.5 corresponds to Warburg impedance (Z_w) which is associated with the domain of mass transport control arising from the diffusion of ions. In short, CPE arises from several factors such as (i) the nature of the electrode (e.g., roughness and polycrystallinity), (ii) distribution of the relaxation times due to heterogeneities existing at the electrode/electrolyte interface, (iii) porosity and (iv) dynamic disorder associated with diffusion. In the circuits, notice that the Warburg in the ideal Randles circuit has been replaced by the CPE_2, which simply describes the porous nature of the concerned electrodes. From the Bode plots (Figs. 4b and 4c), the slopes of the log Z vs. log f plot at the mid frequency region are less than the ideal -1.0 for pure capacitive behaviour, which is indicative of pseudocapacitive behaviour. It is worthy to mention here that all attempt to replace the C_{dl} in circuit (i) with a CPE (which is a more practical situation) led to huge fitting errors. This should not be interpreted to signify that the C_{dl} is a pure double layer capacitance. According to Orazem and Tribollet,[10] frequency dispersion leading to CPE behaviour takes place through the distribution of time constants along either the area of the electrode surface (involving a 2-dimensional aspect of the electrode, which mimics an ideal RC behaviour) or along the axis normal to the electrode surface (involving a 3-dimensional surface). Thus, suffice to say here that the observed impedimetric behaviour of the modified electrodes is CPE. The data

from the Bode plots (i.e., -phase angle vs. log f) further confirms the absence of ideal capacitive behaviour as the observed phase angles are less than the 90° expected of an ideal capacitive behaviour.

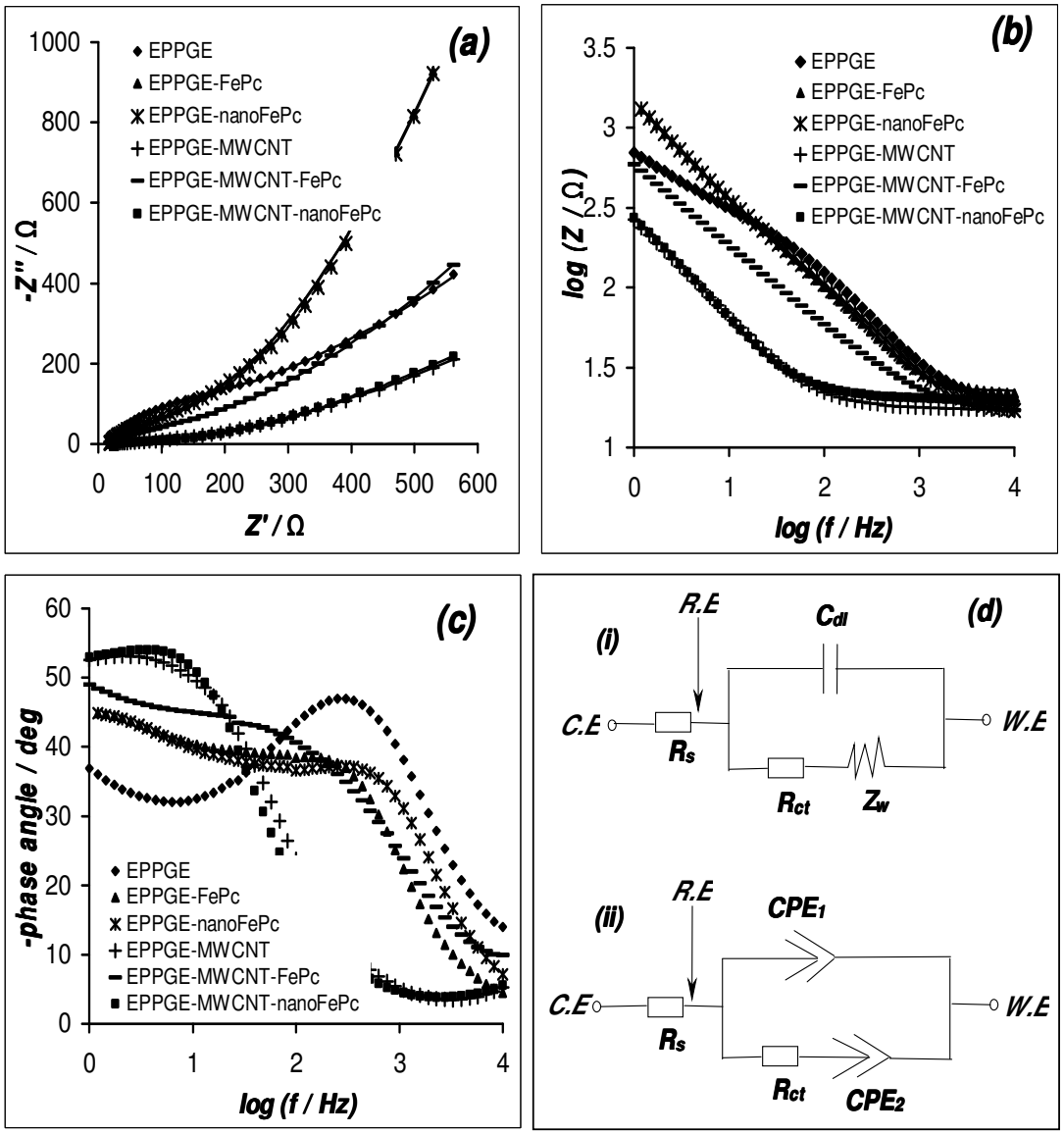

Figure 4.4: *Comparative (FePc derivatives) Nyquist plots (a) and Bode plots (b) and (c) obtained for the various electrodes studied in 1.0 M KCl containing 0.1 M* $[Fe(CN)_6]^{3-}/[Fe(CN)_6]^{4-}$*, equivalent electrical circuit diagrams (d)*

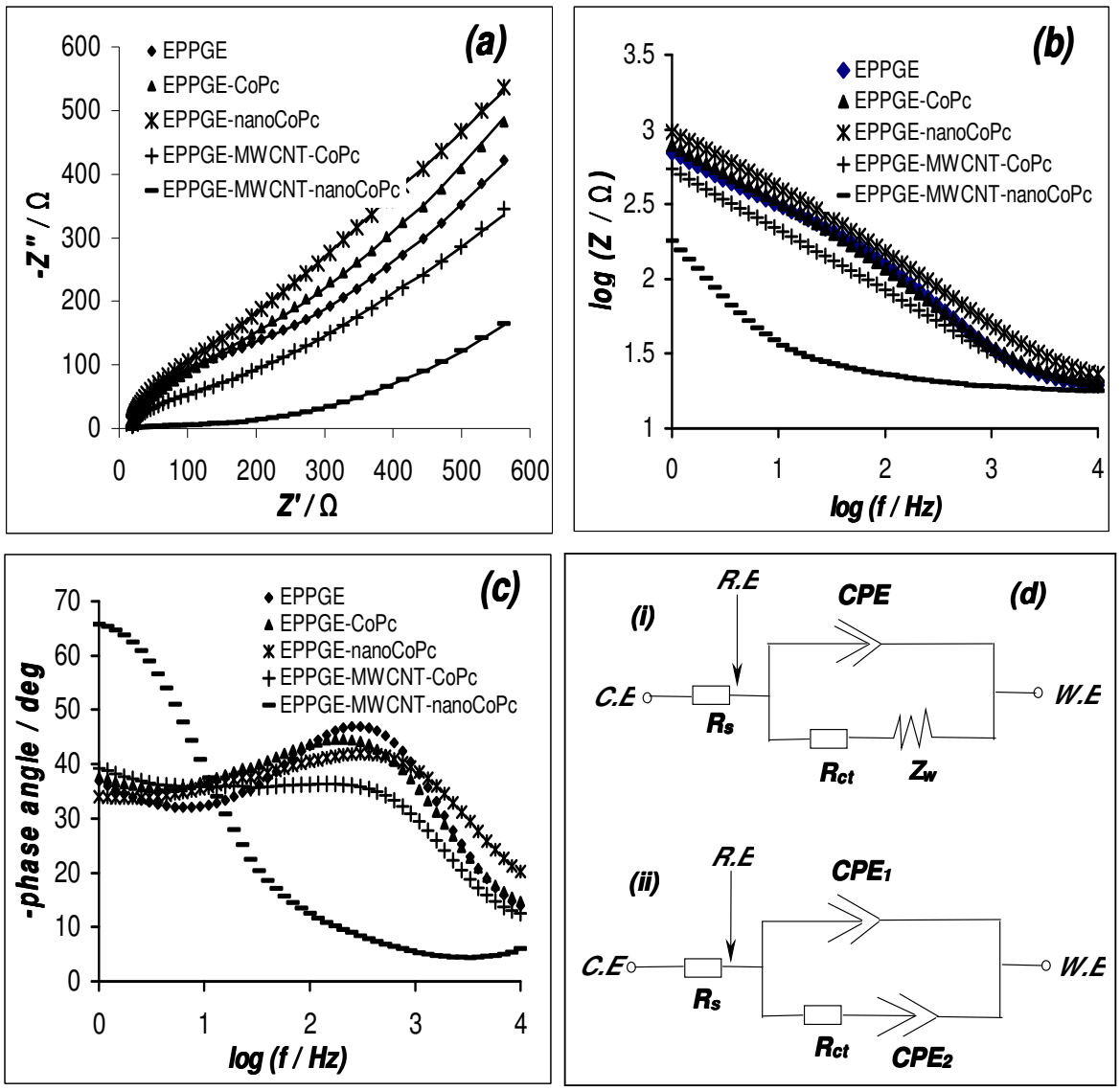

Figure 4.5: *Comparative(CoPc derivatives) Nyquist plots (a) and Bode plots (b) and (c) obtained for the various electrodes studied in 1 M KCl containing 0.1 M $[Fe(CN)_6]^{3-}/[Fe(CN)_6]^{4-}$, equivalent electrical circuit diagrams (d)*

***Table 4.1:** Impedance parameters obtained for the various electrodes studied in 0.1 M $[Fe(CN)_6]^{3-/4-}$ 1.0 M KCl solution*

EPPGE Modifier	R_s /Ω	R_{ct} /Ω	CPE_1/μF	n_1	CPE_2 /μF	n_2	C_{dl} /μF	$10^6 Z_w$	$10^2 k_{app}$/cms^{-1}
FePc	22.7±0.2	30.9±2.0	-	-	-	-	20.7±0.7	966±9	12.0±0.8
NanoFePc	17.6±0.3	29.4±1.5	-	-	-	-	12.8±0.4	971±10	13.0±0.7
CoPc	17.3±0.2	324±9.7	78.8±3.0	0.71	-	-	-	551±6	1.2±0.1
nanoCoPc	17.2±0.2	169±31	55.7±6.3	0.71	523±4.9	0.36	-	-	2.2±0.4
MWCNT	16.5±0.5	4.5±0.4	1290±77	0.51	304±11	0.85	-	-	84.1± 6.5
MWCNT-FePc	16.4±0.4	15.01±0.8	565±16	0.60	205±3	0.93	-	-	25.3± 1.3
MWCNT-nanoFePc	15.3±0.5	6.8±0.4	1106±19	0.44	299±9	0.90	-	-	55.6± 3.3
MWCNT-CoPc	17.6±0.2	105±13	95.2±12.1	0.71	797±17	0.45	-	-	3.6±0.5
MWCNT-nanoCoPc	17.5±0.2	12.5±1.7	819±147	0.70	544±4	0.92	-	-	30.3±3.8

4.3 Electrocatalytic Properties

4.3.1. *Electrocatalytic reduction of oxygen*

Transition metal macrocyclic complexes can catalyze the oxygen reduction reaction through a 2-electron or 4-electron transfer pathway to produce either H_2O_2 or H_2O. They can sometimes catalyze ORR through a mixed pathway of 2- and 4- electron transfer reduction and in rare cases, can also catalyze a 1-electron oxygen reduction, producing superoxide. Hence, comparative studies for oxygen reduction reaction were performed in 0.1 M NaOH solution with a view to establishing the catalytic efficiency of the different electrodes and determine their catalytic pathway. As shown in Figure 4.6(a), the catalytic efficiency of EPPGE-MWCNT-nanoFePc towards oxygen reduction was better (in terms of onset potential, -5 mV, and catalytic current response of approximately -1.7 mA cm^{-2}) compared to other electrodes that were observed at negative onset potentials (between -20 and -50 mV) and lower current densities (between -0.6 and -1.05 mA cm^{-2}).

In Figure 4.6(b), the EPPGE-MWCNT-nanoCoPc and EPPGE-MWCNT-CoPc showed better electrocatalytic activity towards ORR (with onset potential at approximately -60 mV and current densities of -2.26 and -1.51 mA cm^{-2} respectively) compared to the other electrodes with onset potential at approximately -100 mV and current density of 0.60 mA cm^{-2}. Two peaks were observed at -200 mV and -600 mV for the

CoPc derivatives (Fig. 4.6(b)), which is attributed to the two 2-electron reduction of oxygen to peroxide and then to water at high potential. Moreover, mononuclear Co-N_4 complexes are known to favour the 2-electron transfer pathway to peroxide,[11] at the standard electrode potential of -264 mV (Ag|AgCl saturated KCl) in alkaline medium.[12]

At the EPPGE-MWCNT-nanoFePc electrode, three peaks were observed at approximately -100, -200 and -500 mV. The origin of these peaks was explored by performing further cyclic voltammetric experiments using the EPPGE-MWCNT and EPPGE-MWCNT-nanoFePc electrodes in 0.1 M NaOH solution saturated with pure nitrogen (Figure. 4.7). Three peaks can be observed in EPPGE-MWCNT-nanoFePc (Fig. 4.7(b)); peaks I and II can be attributed to Fe^{2+}/Fe^{3+} and Fe^{2+}/Fe^{1+} redox couples, respectively,[13] while peak III can be attributed to the surface bound carboxylic or quinone-type group on the MWCNT. This explanation is in agreement with the report by Zagal and co-workers[13] who observed that compounds with M^{2+}/M^{3+} redox couples close to the onset of oxygen reduction promote the 4-electron reduction of oxygen at that potential region. As a consequence, the observed peak at -100 mV might be due to the direct reduction of oxygen to water. X-ray absorption spectroscopy was used by Yang *et al*.[14] to identify the ferrous ion coordinated with 4 nitrogen atoms as the electrocatalytic active sites for oxygen reduction in an aligned carbon nanotubes with built in Fe-N_4 molecule. The existence of carboxylic acid and quinone-

type groups on functionalized carbon nanotubes has also been claimed to most likely determine their electrocatalytic properties,[14,15,16] hence the role played by various surface bound quinones in the electrocatalysis of oxygen reduction has been well established.[16,17]

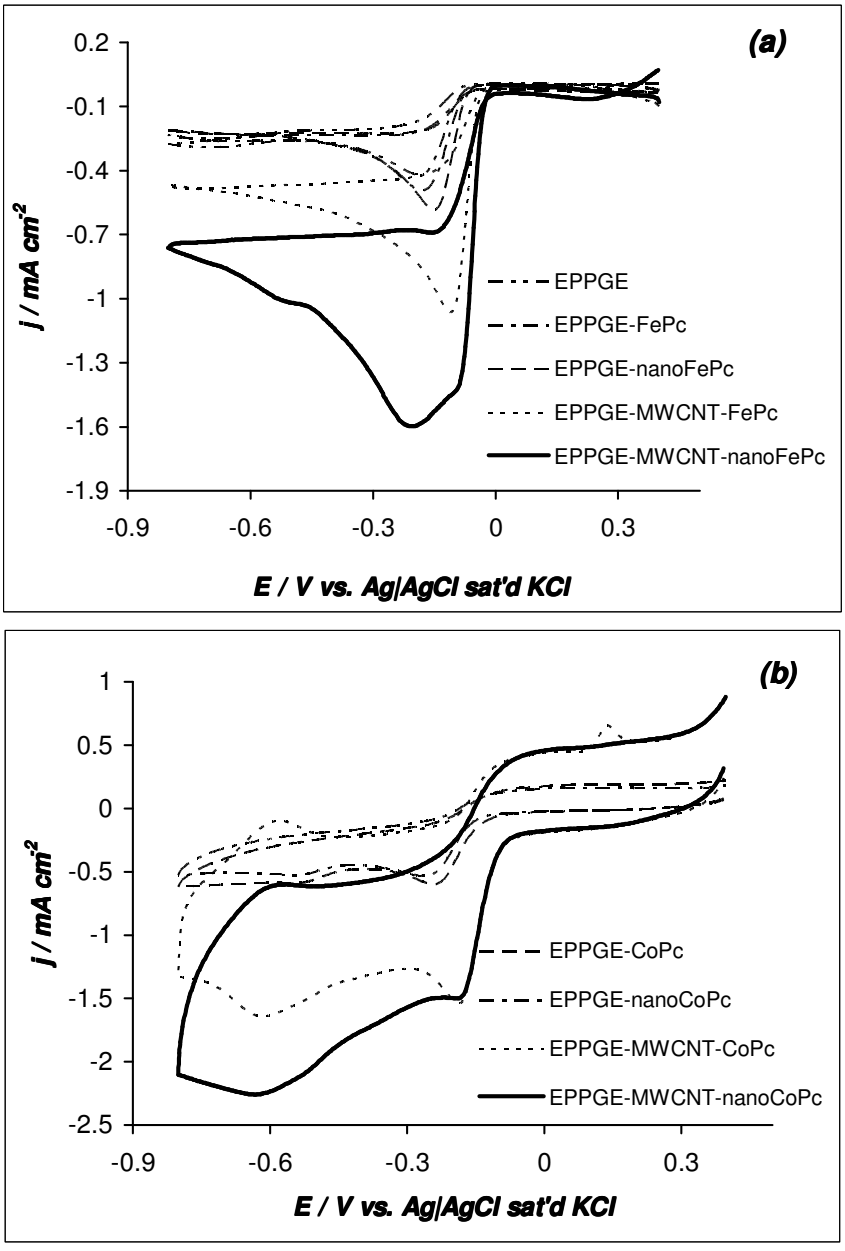

Figure 4.6: *Comparative cyclic voltammograms of the various electrodes in oxygen saturated 0.1 M NaOH solution. FePc derivatives (a), CoPc derivatives (b)*

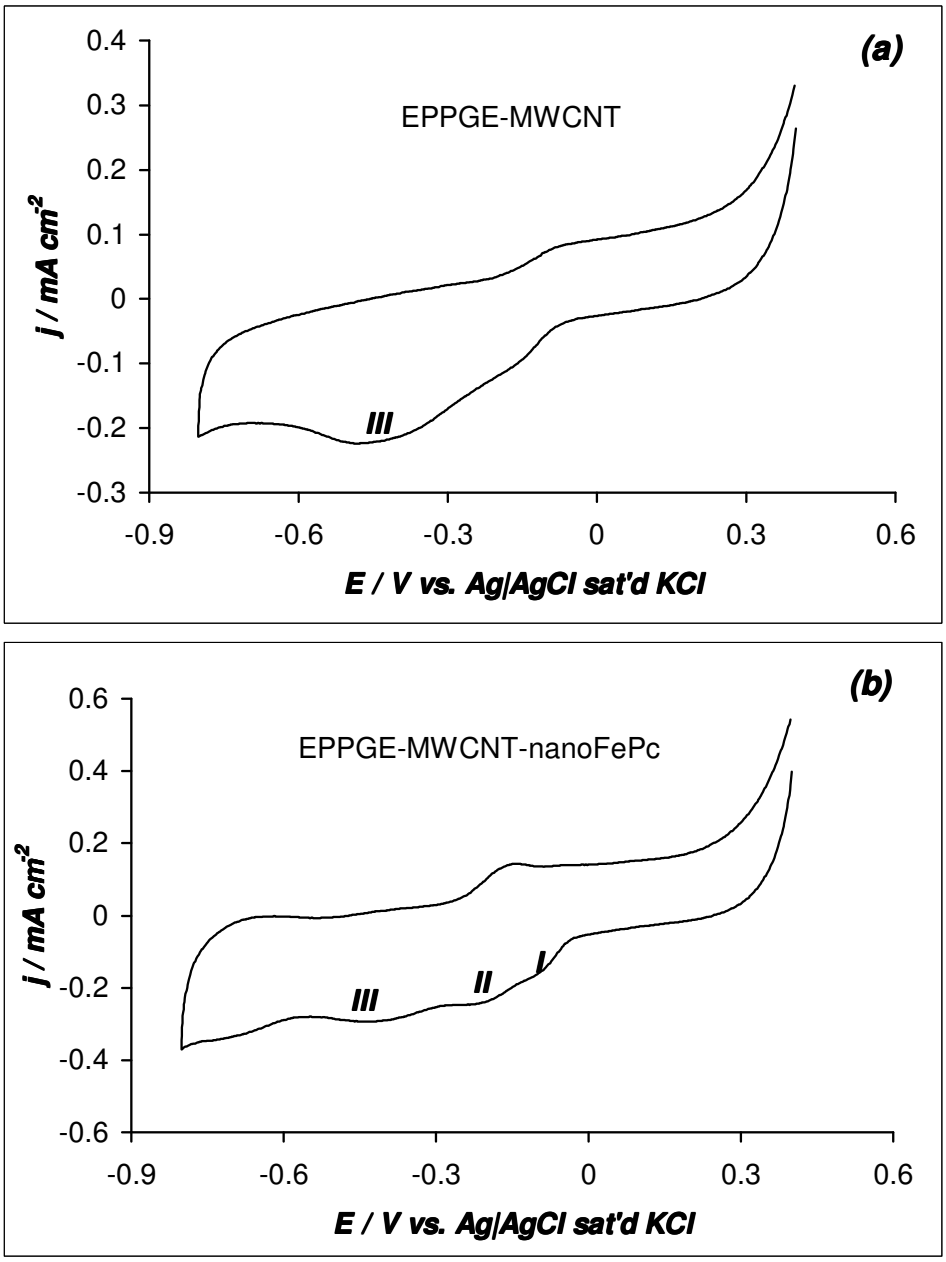

Figure 4.7: *Comparative cyclic voltammograms of the different electrodes in nitrogen saturated 0.1 M NaOH (a) EPPGE-MWCNT, (b) EPPGE-MWCNT-nanoFePc. Scan rate: 25 mV* s^{-1}

It is known that these electrodes catalyze the 2-electron reduction of oxygen to peroxide in alkaline solution at more negative potential.[18,19] Therefore, the observed peak at -500 mV might be due

to the 2-electron reduction of oxygen to peroxide and subsequent reduction of the peroxide to water by the quinone group. The enhanced catalytic activity of the MWCNT-nanoFePc nanocomposite may be due to the large surface area of these two electrocatalytic π-electron species which provides more active sites for the adsorption of molecular oxygen. Given the high activity of the EPPGE-MWCNT-nanoFePc, all subsequent studies were performed with the electrode.

Given that multiple peaks were observed for the reduction of oxygen at EPPGE-MWCNT-nanoFePc, further analysis was carried out to establish the peak that is responsible for the 4–electron reduction of oxygen.

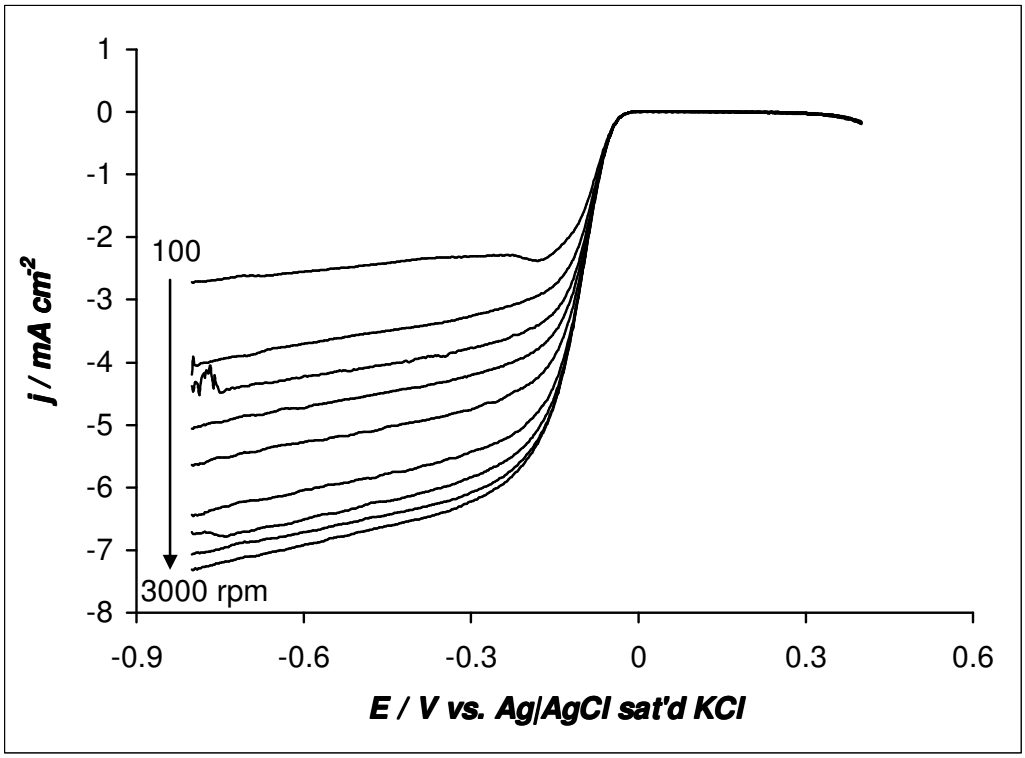

Figure 4.8: *RDE polarization curves of EPPGE-MWCNT-nanoFePc in oxygen saturated 0.1 M NaOH solution*

Figure 4.8 presents the results of the rotating disk electrode (RDE) measurement in oxygen saturated 0.1 M NaOH. It can be seen that the limiting current densities increases with increasing rotation. If we assume an electrode of first order in reactant and negligible contribution from the film diffusion resistance to the measured current density, the voltammetric response of a porous RDE is described by the Koutecky–Levich (K–L) equation (equation 2.12) used to determine the number of electrons (n) involved in the reaction:[20]

$$\frac{1}{j} = \frac{1}{j_{Lev}} + \frac{1}{j_{kin}} \tag{2.12}$$

$$j_{kin} = nFkc_O\Gamma \tag{2.13}$$

$$j_{Lev} = 0.21nFD^{2/3}\gamma^{-1/6}c_{O_2}\omega^{1/2} \tag{2.14}$$

where j_{kin} and j_{Lev} are the kinetic and diffusion limited current densities respectively, F is Faraday constant (96485 C mol^{-1}), D is the diffusion coefficient of oxygen ($1.51x10^{-5}$ cm^2 s^{-1}),[20] c_{O_2} is the concentration of the dissolved oxygen in the electrolyte solution ($0.25x10^{-6}$ mol cm^{-3}),[21] γ is the kinematic viscosity of the electrolyte solution (0.01 cm^2 s^{-1}),[20] ω is the rotation rate in rpm, (0.21 is used when ω is expressed in rpm), *k* is the kinetic rate constant for the catalyzed oxygen reduction reaction and Γ is the surface concentration of the adsorbed species (~ 1.8×10^{-8} mol cm^{-2}).

Figure 4.9(a) shows the K–L plots obtained from the RDE data, it can be seen that the K–L lines are approximately linear; indicating that the

reaction order with respect to O_2 was unity for the electrode. The number of electrons transferred was estimated as 4.0, indicating that oxygen was reduced to water at approximately -100 mV as observed in Fig. 4.6(a).

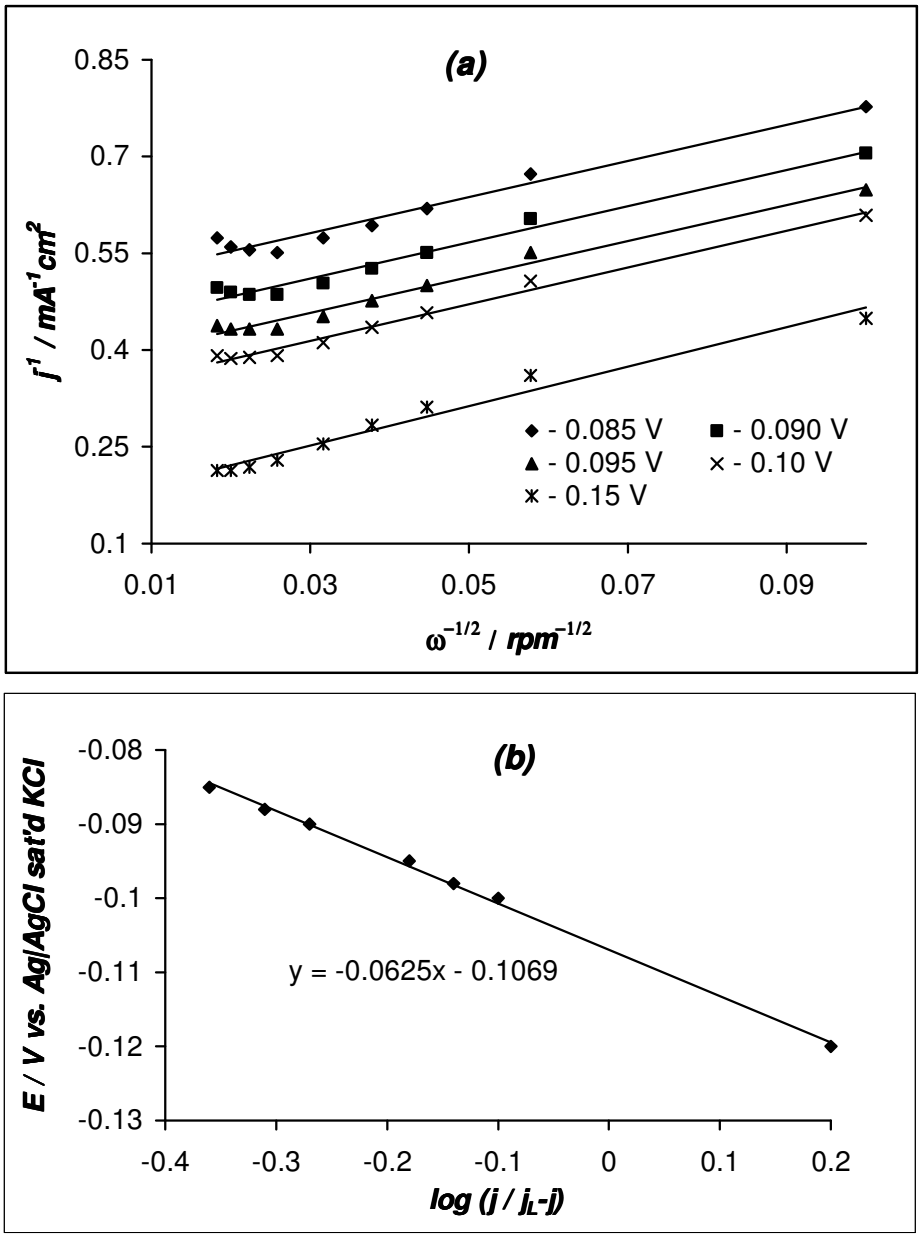

Figure 4.9: *Koutecky-Levich plot (a) and Tafel plot (b) of EPPGE-MWCNT-nanoFePc generated from Figure 4.8*

This is not completely surprising considering that FePc based electrodes are well known to reduce oxygen to water. The kinetic rate constant (k) was estimated from the intercept of the K–L plot as 2.2 x 10^8 M^{-1} s^{-1}, a value in the same range as reported by other workers for ORR.[22,23] On correction of the polarization curve for diffusion effects for first order reaction, one obtains the Tafel equation as equation (4.3):[24]

$$E = E_{eq} - b \log j_k \tag{4.3}$$

$$j_K = \left(\frac{j}{j_L - j} \right) \tag{4.4}$$

where E is the applied potential, E_{eq} is the equilibrium potential, αn is the kinetic parameter for the electrode process, j is the disk current density, j_L is the diffusion limiting current density, b is the Tafel slope described as in equation (4.5):

$$b = \frac{2.3RT}{\alpha nF} \tag{4.5}$$

where the symbols represent their usual meaning. The Tafel slope was from the plot of E vs. log (j/j_L-j), Fig. 4.9(b), with j and j_L obtained directly from Figure 4.8. Tafel slope was estimated as -63 mV dec^{-1}, resulting to αn=0.94. Assuming a transfer coefficient (α) of 0.5, the number of electron (n) involved in the rate-determining step would be 2. Although Beck[25] proposed a 2-electron process as the rate determining step in acidic medium, rate determining step involving a 2-electron process is not usually favoured.[20,26] Indeed, several workers have observed FePc complexes to give small Tafel slopes at

low potentials and also promote the 4-electron reduction of oxygen at that potential.[13,26,27] For example, Zagal *et al*.[27] observed a Tafel slope of -60 $mVdec^{-1}$ for oxygen reduction reaction using water-soluble iron(II) phthalocyanine-based electrode and proposed a single-electron rate determining step. The small Tafel slope was associated to such factors as redox potentials and pKa's of the phthalocyanine catalyst as well as the pH of the electrolytes.[27] In this case, it seems reasonable therefore to assume a single-electron rate determining step process, suggesting that α value is 0.94. The α value gives an indication on the conductivity of the electrode; for the most conductive electrodes, α = 0.5, the least conductive ones give α = 0.25, while α > 0.5 is an indication of enhanced electrocatalytic process.[28] Also, from several literature,[29-33] it may be speculated here that the global oxygen reduction reaction leading to water may be due to combined processes involving MWCNTs and nanoFePc; reaction involving nanoFePc leading to direct four-electron pathway[26] and the other due to the quinone (Q) group on the surface of the MWCNTs involving a two-electron pathway.[33] The combined high surface area of the MWCNT-nanoFePc nanocomposites is expected to encourage the adsorption of the oxygen molecule on the surface of the nanocomposites.

4.3.2. *Electrocatalytic oxidation of thiocyanate*

Figure 4.10 shows the comparative CV of the FePc derivative (a) and the CoPc derivative electrodes (b), in 1mM SCN^- solution contained in phosphate buffer (pH 5). In both figures the MWCNT-nanoMPc electrodes gave the highest peak current densities, this is mostly likely due to the large surface area provided by the MWCNT and the nanostructured MPc species. The onset potential for the oxidation of thiocyanate is ~ 50 mV less positive at the EPPGE-MWCNT-nanoFePc compared to the EPPGE-MWCNT-nanoCoPc, with a peak current density of 3.62 mA cm^{-2}. This means that the electrocatalytic activity of EPPGE-MWCNT-nanoFePc towards thiocyanate oxidation is better than at EPPGE-MWCNT-nanoCoPc. Surface immobilized FePc complexes are known to sometimes show better catalysis compared to their surface immobilized CoPc counterparts.[34]

The effect of varying the scan rate on the response of EPPGE-MWCNT-nanoFePc and EPPGE-MWCNT-nanoCoPc in the thiocyanate solution was also interrogated (Figure 4.11(a) and (b)). Scan rates studies where only possible at scan rate range between 10–150 mV s^{-1}. This suggests that the SCN^- is prone to adsorption on the EPPGE-MWCNT-nanoMPc electrodes. All plots of the peak current density against the square root of scan rate shows linearity (Figure 4.11 (c) and (d)), indicating diffusion-controlled electrode reactions.

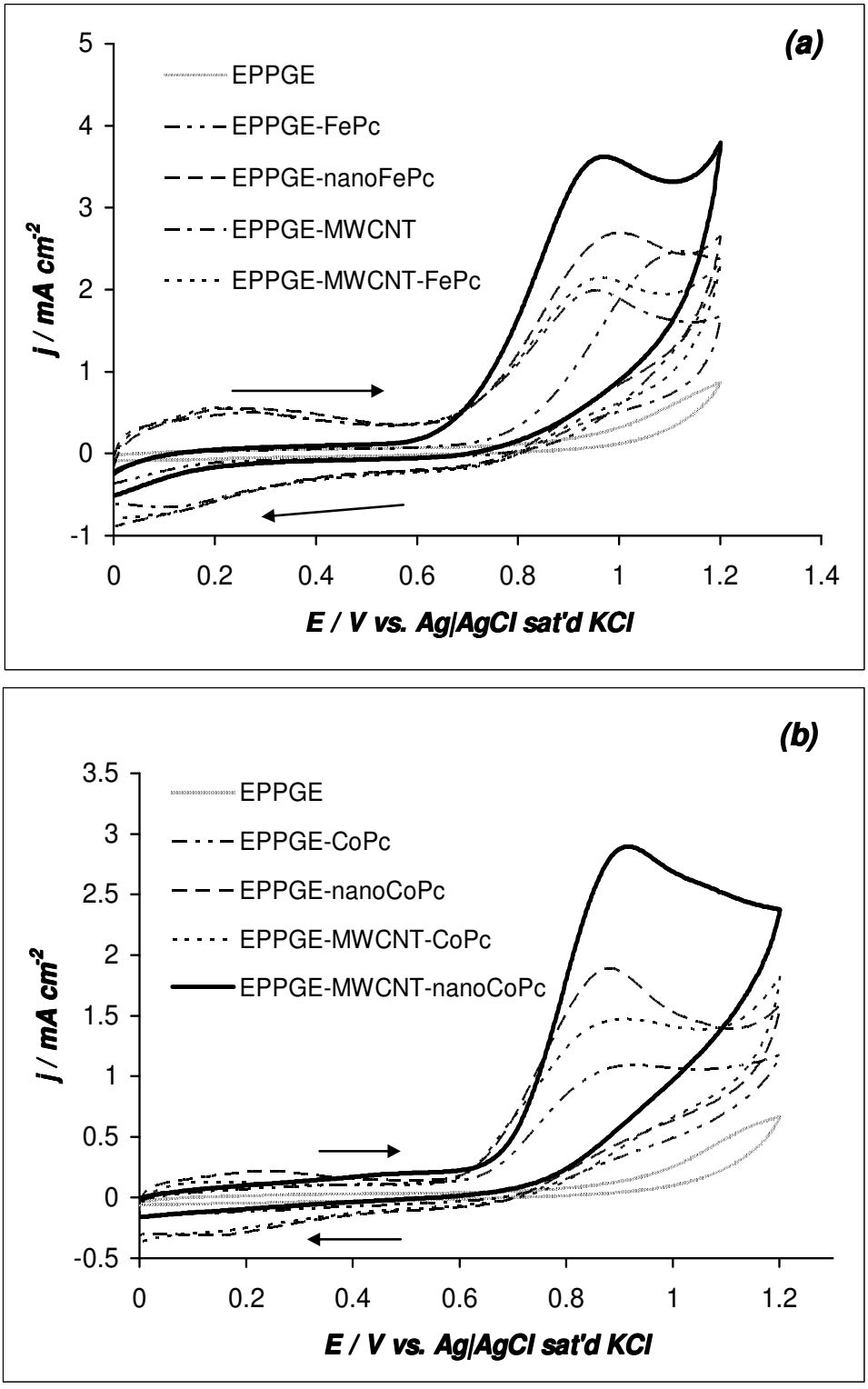

***Figure 4.10:** Comparative cyclic voltammograms of the various electrodes in 1 mM SCN^- solution contained in phosphate buffer (pH 5). FePc derivatives (a), CoPc derivatives (b)*

The current density function ($j_p/v^{1/2}$) decreased with the scan rate for both electrodes (exemplified in Figure 4.12 (a) and (b)) confirming that the electrocatalytic processes observed here are coupled with chemical reaction, EC_{cat} mechanisms.[35]

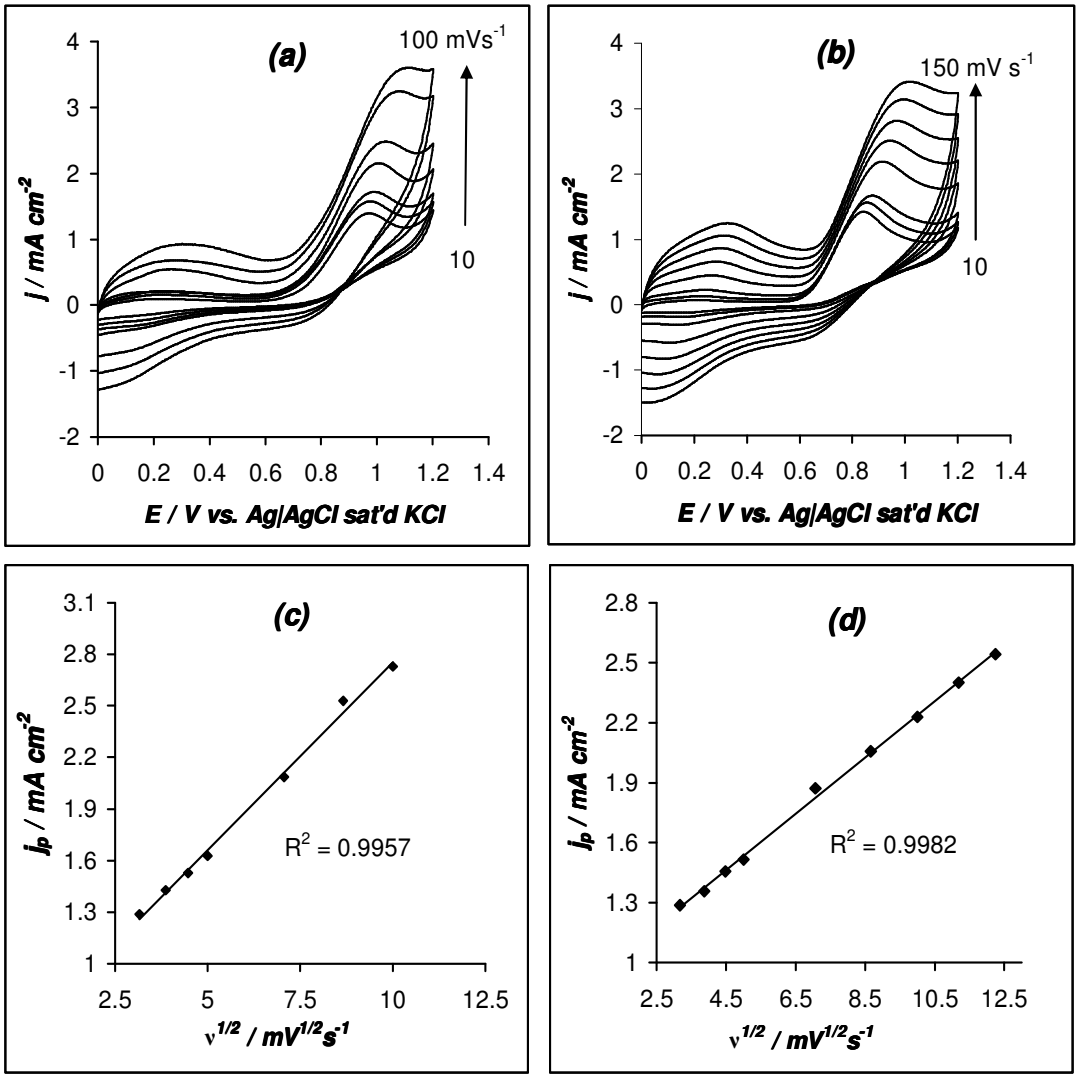

***Figure 4.11:** Cyclic voltammetric evolutions at different scan rates of (a) EPPGE-MWCNT-nanoFePc and (b) of EPPGE-MWCNT-nanoCoPc in 1.0 mM of thiocyanate (pH 5). Plots of peak current density vs. square root of scan rate (c) EPPGE-MWCNT-nanoFePc and (d) of EPPGE-MWCNT-nanoCoPc*

For irreversible reactions where diffusion and charge-transfer control the rate of reaction, the peak potentials should vary with the scan rates according to:

$$E_p = E^o - b'\left[0.78 + \ln\left(\frac{D^{1/2}}{k^o}\right) + \ln(b')^{1/2}\right] - \frac{2.303RT}{2\alpha nF}\log\nu \qquad (2.9)$$

where $k°$ is the standard heterogeneous rate constant at the standard potential ($E°$), and b' is as in equation (4.5). equation (2.9) can be simplified as:

$$E_p = \frac{b}{2}\log\nu + \text{constant} \qquad (4.6)$$

where b = Tafel slope = 2.303b' and all symbols retain their usual meanings. On the basis of the $\delta E_p/\delta\log\nu$ slopes of the plots of E_p vs. log ν, (Figure 4.12 (c) and (d)), the Tafel slopes were obtained as -163 and -181 mV dec^{-1} at EPPGE-MWCNT-nanoFePc and EPPGE-MWCNT-nanoCoPc, respectively in the analyte solution. This result indicates the involvement of a 1-electron transfer electrode process in the rate-determining step (i.e., assuming electron transfer coefficient of α= 0.50). The high Tafel slopes is associated with adsorption since it is known that Tafel slope greater than the 120 mV dec^{-1} value expected for a 1- electron process is indicative of adsorption of the analytes onto the electrodes.[36,37]

The following mechanism for the electrocatalytic reactions for the thiocyanate ion is proposed:

$$\text{nano}M^{2+}\text{Pc} \rightarrow \text{nano}M^{3+}\text{Pc} + e^- \qquad (4.7)$$

$$nanoM^{2+}Pc + SCN^{-} \rightarrow [SCN\text{-}nanoM^{3+}Pc]^{-} \quad (4.8)$$

$$[SCN\text{-}nanoM^{3+}Pc]^{-} \rightarrow [SCN\text{-}nanoM^{3+}Pc] + e^{-} \quad \text{rate determining step} \quad (4.9)$$

$$[SCN\text{-}nanoM^{3+}Pc] \rightarrow nanoM^{2+}Pc + {}^{\cdot}SCN \quad (4.10)$$

$${}^{\cdot}SCN + {}^{\cdot}SCN \rightarrow (SCN)_2 \quad \text{fast} \quad (4.11)$$

$$(SCN)_2 + H_2O \rightarrow \text{reaction products} \quad (4.12)$$

(Where M is Fe or Co)

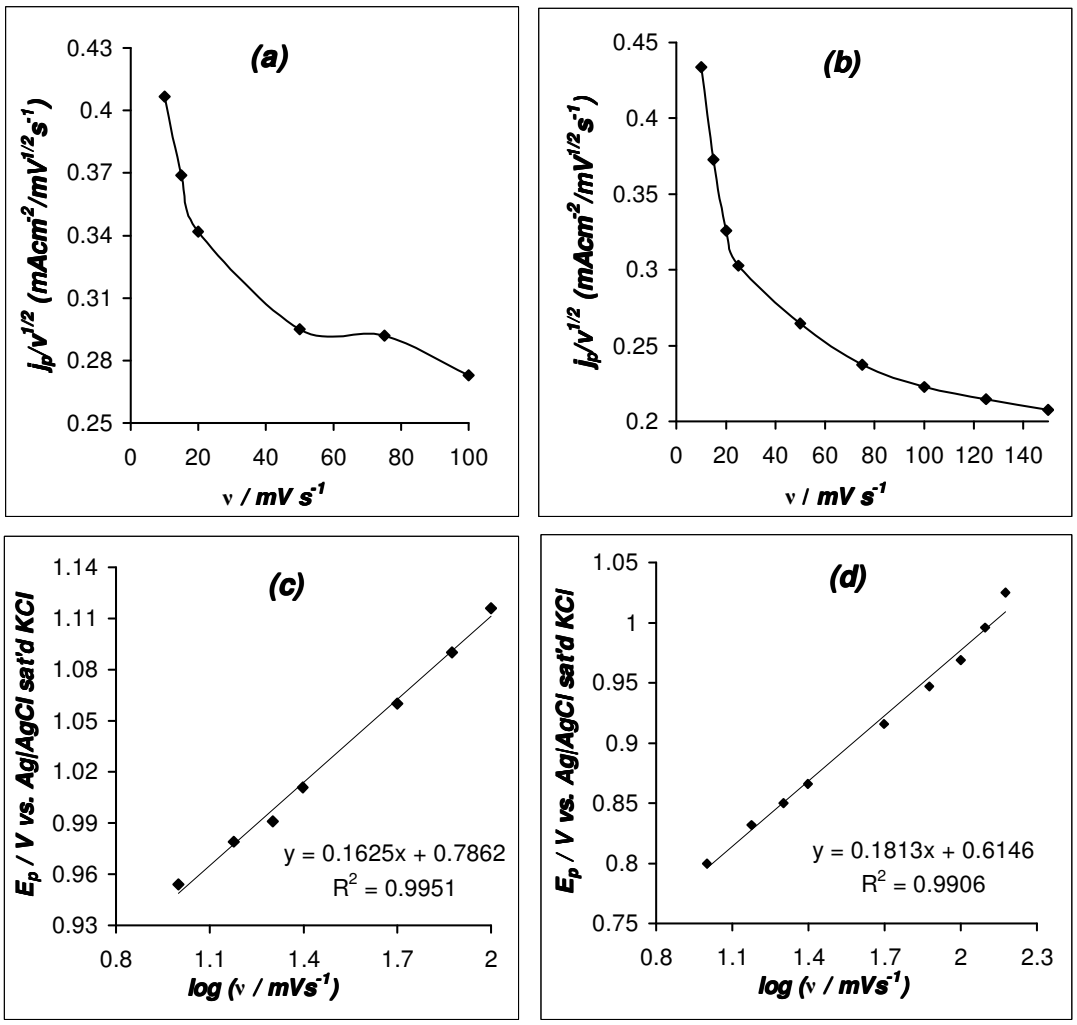

***Figure 4.12:** Current function plots: (a) EPPGE-MWCNT-nanoFePc, (b) EPPGE-MWCNT-nanoCoPc and Tafel plots: (c) EPPGE-MWCNT-nanoFePc, (d) EPPGE-MWCNT-nanoCoPc*

It is also well established that iron porphyrins and phthalocyanine-catalysed reactions of SCN^- occur by initial binding of the SCN^- to the Fe^{3+}.[38,39,40] Also, FePc complex is a natural mimic of the Horseradish peroxidase (HRP), and HRP-catalysed oxidation of SCN^- occurs via the formation of the thiocyanate radical as an intermediate product, which readily dimerises to form the unstable thiocyanogen $(SCN)_2$. The $(SCN)_2$ is unstable in aqueous solution and readily hydrolyses to form some stable intermediate products.

As shown in Figure 4.13, well resolved single-step chronoamperometric evolutions were obtained at the EPPGE-MWCNT-nanoFePc (a) and EPPGE-MWCNT-nanoCoPc (b) electrodes in the absence and presence of consecutive addition of 40 µM thiocyanate in phosphate buffer solution (pH 5). The numbers 1 to 8 in Figure 4.13, correspond to 0.0, 40.0, 80.0, 120, 160, 200, 240, and 280 µM, respectively. It shows that at the conditions employed for this work, the SCN^- was irreversible. Inset Figure.4.13 (a) and (b) depicts linearity between j_p vs. $[SCN^-]$. Also, a linear relationship was obtained when log j_p vs. log $[SCN^-]$ was plotted for both electrodes with slope values approximately 0.7143 and 0.6157, respectively which is close to unity, suggesting that one SCN^- species interacts with one molecule of the nanoMPc species. From the slope and the relative standard deviation of the intercept obtained from a plot of j_p vs. $[SCN^-]$, the limit of detection (LoD) were estimated as 26.34 and 21.37 µM for the

EPPGE-MWCNT-nanoFePc and EPPGE-MWCNT-nanoCoPc electrodes, respectively. $LoD = \frac{3.3s}{m}$, where s is the relative standard deviation of the intercept and m the slope.[41]

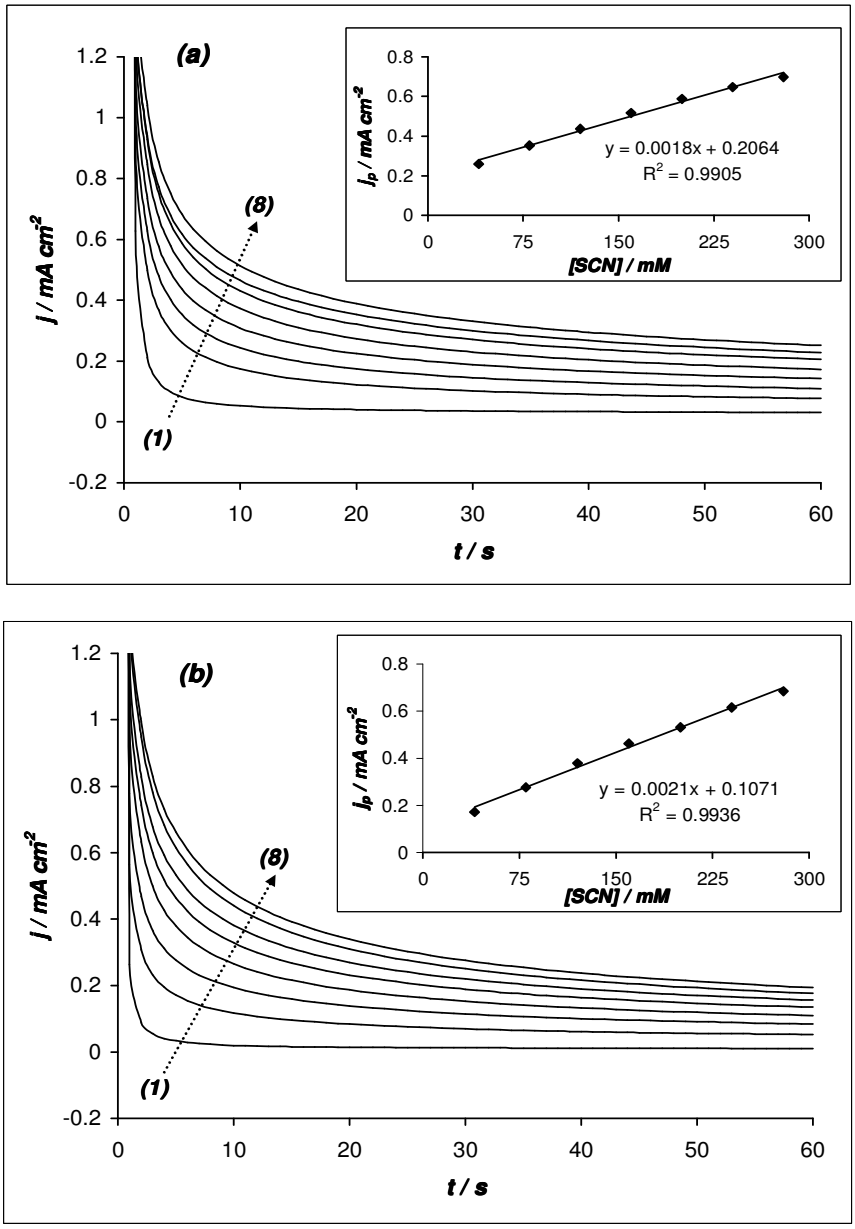

***Figure 4.13:** Chronoamperometric evolutions obtained at the EPPGE-MWCNT-nanoFePc (a) and EPPGE-MWCNT-nanoCoPc (b) electrodes in the absence and presence of consecutive addition of 40 µM thiocyanate in phosphate buffer solution (pH 5). Insets, plot of peak current density vs. concentration of thiocyanate*

4.3.3. *Electrocatalytic oxidation of nitrite*

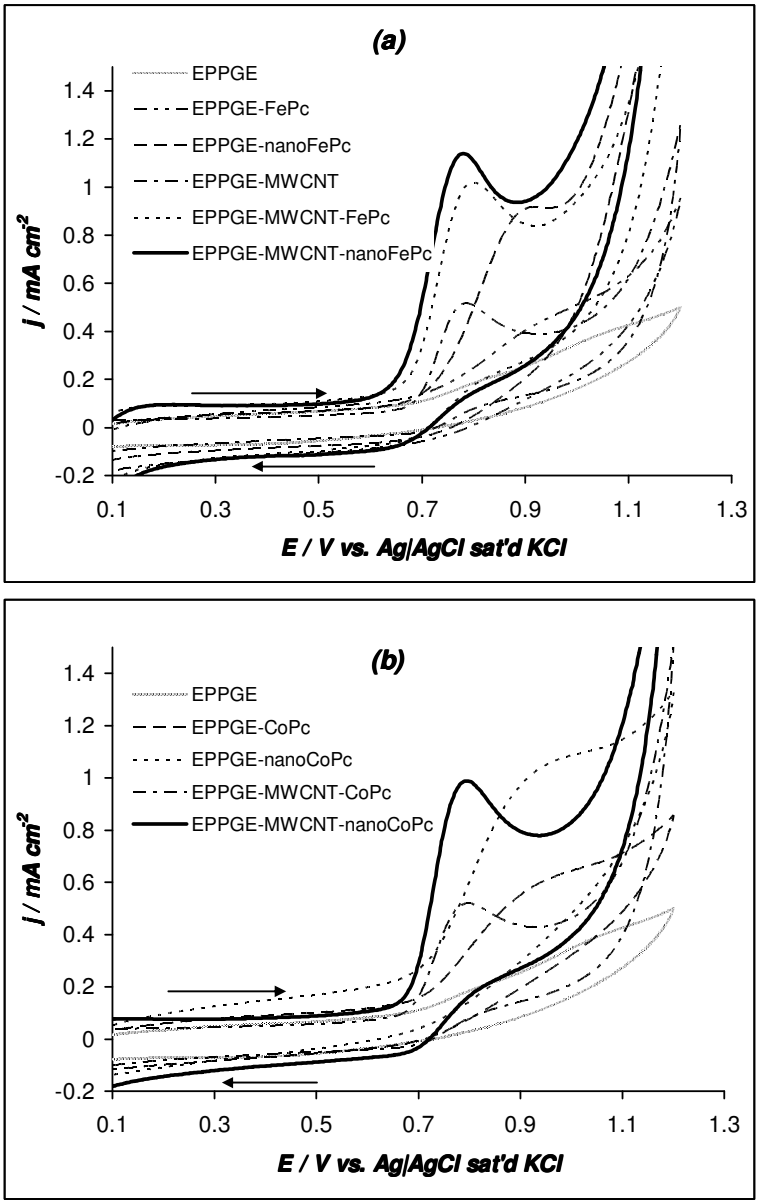

Figure 4.14: *Comparative cyclic voltammograms of the various electrodes in 1mM nitrite solution contained in phosphate buffer (pH 7.4). FePc derivatives (a), CoPc derivatives (b)*

Figure 4.14 shows the cyclic voltammograms of 1mM nitrite in phosphate buffer (pH 7.4) at (a) the FePc derivative and (b) the CoPc

derivative electrodes. As observed in the figures, the EPPGE-MWCNT-nanoMPc electrodes showed better catalytic activity towards nitrite oxidation with peak potential at approximately 0.80 V compared to the other electrodes (peak potentials between 0.83 – 0.97 V) and at increased current densities, (~ 1 mA cm^{-2}).

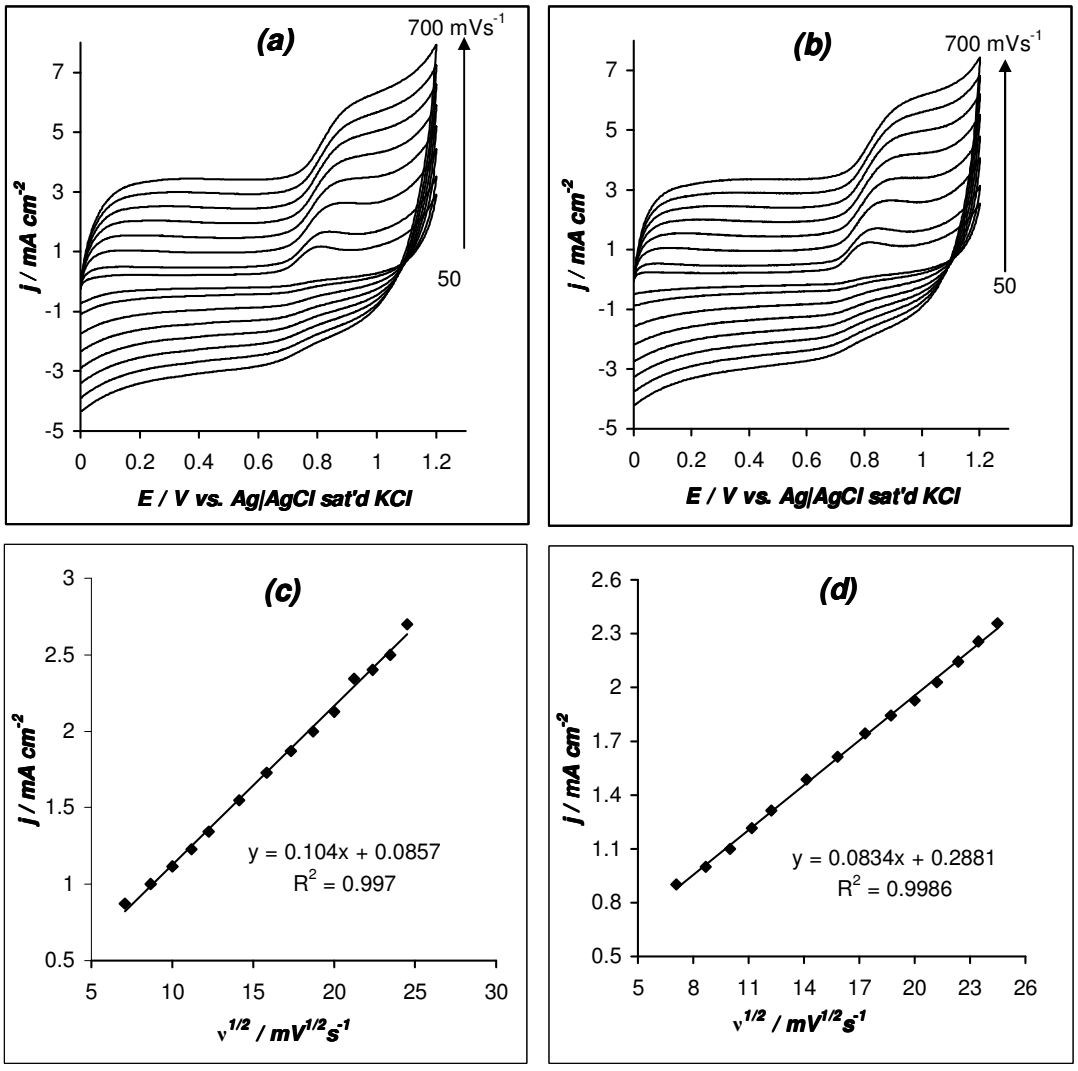

Figure 4.15: *Cyclic voltammetric evolutions at different scan rates of (a) EPPGE-MWCNT-nanoFePc and (b) of EPPGE-MWCNT-nanoCoPc in 1.0 mM of nitrite (pH 7.4). Plots of peak current density vs. square root of scan rate (c) EPPGE-MWCNT-nanoFePc and (d) of EPPGE-MWCNT-nanoCoPc*

Figure 4.15 (a) and (b) shows the effect of varying the scan rate on the response of EPPGE-MWCNT-nanoFePc and EPPGE-MWCNT-nanoCoPc in the nitrite solution. Analysis of the scan rate reveals that the electrocatalytic oxidation of nitrite is a diffusion-controlled process judging from the linearity observed when the peak current density (j_p) was plotted against the square root of scan rate (Figure 4.15 (c) and(d)

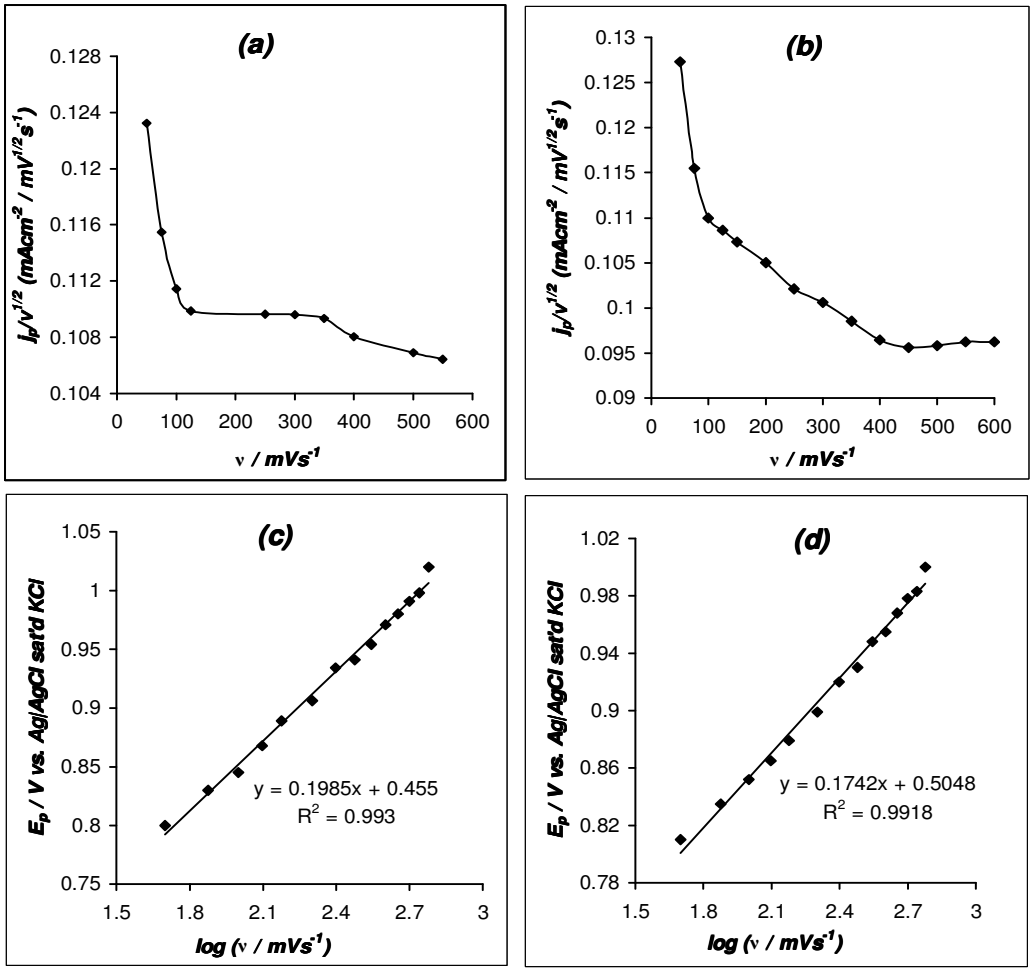

Figure 4.16: *Current function plot (a) EPPGE-MWCNT-nanoFePc, (b) EPPGE-MWCNT-nanoCoPc and Tafel plot (c) EPPGE-MWCNT-nanoFePc, (d) EPPGE-MWCNT-nanoCoPc*

The electrocatalytic oxidation of nitrite by the EPPGE-MWCNT-nanoMPc electrodes was further confirm as a catalytic process judging from the shape of the plot of current density function against scan rate which is typical of a catalytic process [42] (Figure 4.16 (a) and (b)). Catalysis of nitrite oxidation by the electrodes, shows that the peak potentials shifted with the log of scan rate (Figure 4.16 (c) and (d)), this indicates that the electrocatalytic oxidation of nitrite is irreversible.[43] From the plot of E_p vs. log of scan rate, and governed by equation (4.6), Tafel slope values corresponding to 199 and 174 mV dec^{-1} were obtained for EPPGE-MWCNT-nanoFePc and EPPGE-MWCNT-nanoCoPc, respectively.

It is known that nitrite ion form axial ligation with central transition metal of the MPc,[44,44] it can be speculated here that the same mechanism as observed by others occurs in this case, thus the following mechanism:

$$\text{nanoM}^{2+}\text{Pc} + NO_2^- \rightarrow (NO_2^-)\text{nanoM}^{2+}\text{Pc} \quad (4.13)$$

$$(NO_2^-)\text{nanoM}^{2+}\text{Pc} \rightarrow (NO_2^-)\text{nanoM}^{3+}\text{Pc} + e^- \quad \text{rate determining step} \quad (4.14)$$

$$(NO_2^-)\text{nanoM}^{3+}\text{Pc} \rightarrow \text{nanoM}^{2+}\text{Pc} + NO_2 \quad (4.15)$$

$$NO_2 + H_2O \rightarrow NO_2^- + NO_3^- + 2H^+ \quad \text{fast} \quad (4.16)$$

(Where M is Fe or Co)

Chronoamperometric experiments, polarized at 0.80 V was carried out on the two electrodes. Figure 4.17 (a) and (b) shows the chronoamperometric evolutions of the two electrodes after successive additions of 40 μM nitrite solution in phosphate buffer (pH 7.4).

The numbers (1) to (8) corresponds to 0.0, 40.0, 80.0, 120, 160, 200, 240 and 280 μM respectively. Inset Figure.4.16 (a) and (b) depicts linearity between j_p vs. [NO_2]. From the slope and the relative standard deviation of the intercept obtained from a plot of j_p vs. [SCN^-], the limit of detection (LoD) were estimated as 21.89 and 23.08 μM for the EPPGE-MWCNT-nanoFePc and EPPGE-MWCNT-nanoCoPc electrodes, respectively.

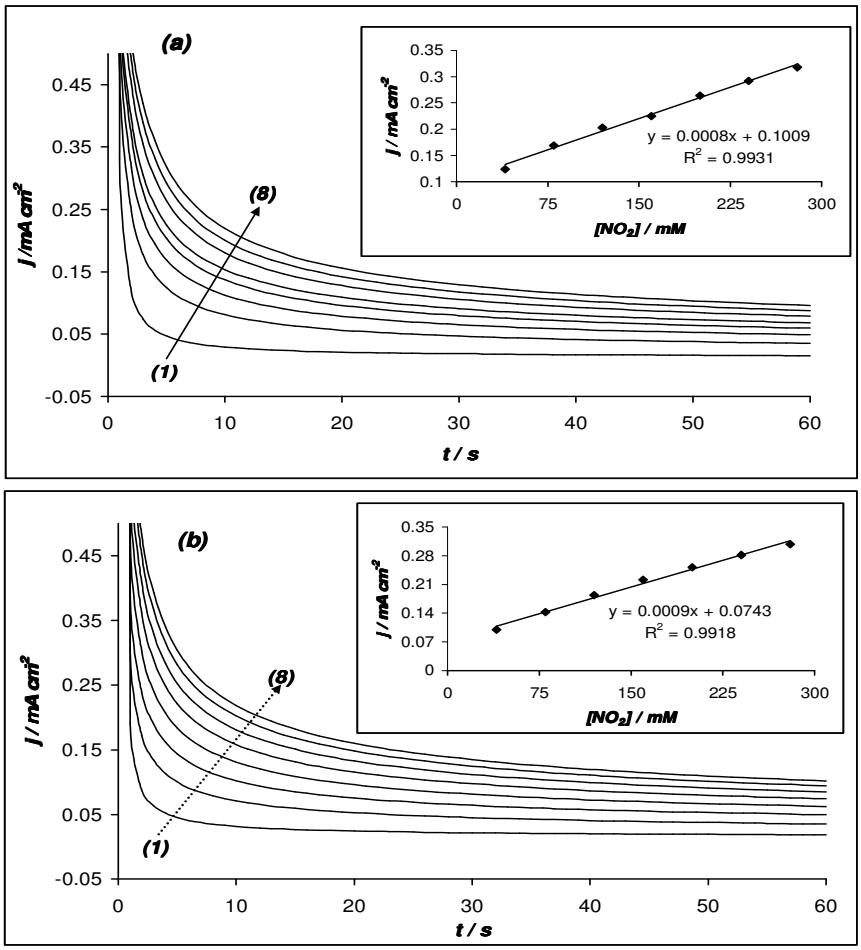

***Figure 4.17:** Chronoamperometric evolutions obtained at the EPPGE-MWCNT-nanoFePc (a) and EPPGE-MWCNT-nanoCoPc (b) electrodes in the absence and presence of consecutive addition of 40 μM nitrite in phosphate buffer solution (pH 7.4).Insets, plot of peak current density vs. concentration of nitrite*

References

1. V. Arcoleo, V.T. Liveri, *Chem.Phys.Lett*. **258** (1996) 223
2. S. Griveau, J. Pavez, J.H. Zagal, F. Bedioui, *J. Electroanal. Chem*. **497** (2001) 75
3. K.I. Ozoemena, T. Nyokong, *Electrochim. Acta* **42** (2002) 4035
4. T.J. Davies, R.G. Compton, *J. Electroanal. Chem*. **585** (2005) 63
5. T.J. Davies, C.E. Banks, R.G. Compton, *J. Solid State Electrochem.* **9** (2005) 797
6. R.G. Compton, C.E. Banks, *Understanding Voltammetry*, World Scientific Publishing Company, London, 2007
7. I. Streeter, G.G. Wildgoose, L. Shao, R.G. Compton, Sens. Actuators B **133** (2008), 462
8. B-Y. Chang, S-Y. Hong, J-S. Yoo, S-M. Park, *J. Phys. Chem*. *B* **110** (2006) 19385
9. E. Sabatani, I. Rubinstein, *J. Phys. Chem*. **91** (1987),6663
10. M. E. Orazem, B. Tribollet, *Electrochemical Impedance Spectroscopy*, Wiley, Hoboken, NJ 2008
11. J. Zagal, P. Bindra, E. Yeager, *J. Electrochem. Soc.* **127** (1980),1506
12. E. Yeager, *J. Mol. Catal*., **38** (1986) 5
13. J. Zagal, M. Paez, A. A. Tanaka, J. R. dos Santos Jr, C. A. Linkous, *J. Electroanal. Chem.* **339** (1992) 13

14. J. Yang, D-J. Liu, N. N. Kariuki, L. X. Chen, *Chem. Commun*. (2008), 329
15. P. J. Britto, K. S. V. Santhanam, *Adv. Mater.* **11** (1999), 154
16. C. E. Banks, T. J. Davies, G. G. Wildgoose, R. G. Compton, *Chem. Commun*. (2005), 829
17. K. Tammeveski, K. Kontturi, R. J. Nichols, R. J. Potter, D. J. Schiffrin, *J. Electroanal. Chem*. **515** (2001), 101
18. G. Jurmann, K. Tammeveski, *J. Electroanal. Chem.* **597** (2006), 119
19. A. Sarapuu, K. Vaik, D. J. Schiffrin, K. Tammeveski, *J. Electroanal. Chem*. **541** (2003), 23
20. A. J. Bard, L. R. Faulkner, *Electrochemical Methods: Fundamentals and Applications* 2nd ed., Wiley, Hoboken, NJ 2001.
21. D. H. Evans, J. J. Lingane, *J. Electroanal. Chem*. **6** (1963), 283
22. R. Baker, D. P. Wilkinson, J. Zhang, *Electrochim. Acta* **53** (2008), 6906
23. N. Kobayashi, Y. Nishiyama, *J. Phys. Chem*. **89** (1985), 1167
24. I. Koç, M. Camur, M. Bulut, A. R. Özkaya, *Catal. Lett.* **131** (2009), 370
25. F. Beck, *J. Appl. Electrochem*. **7** (1977), 241
26. A. J. Appleby, J. Electroanal. Chem. **357** (1993), 117

27. J. Zagal, P. Bindra, E. Yeager, *J. Electrochem. Soc*. **127** (1980), 1506
28. J. N. Soderberg, A. C. Co, A. H. C. Sirk, V. I. Birss, *J. Phys*. *Chem. B* **110** (2006), 10401
29. C. Ercolani, M. Gardini, F. Monacelli, G. Pennesi, G. Rossi, *Inorg. Chem*. **22** (1983), 2584
30. R. Holtze, *Electrochim. Acta* **33** (1988), 1619
31. F. Monacelli, C. Ercolani, *Inorg. Acta* **346** (2003), 95
32. S. Baranton, C. Coutanceau, E. Garnier, J.-M. Leger, *J. Electroanal. Chem*. **590** (2006), 100
33. I. Kruusenberg, N. Alexeyeva, K. Tammeveski, *Carbon* **47** (2009), 651
34. K.I. Ozoemena, T. Nyokong*, Electrochemical sensors based on phthalocyanines and related complexes:* Encyclopeadia of sensors, (C.A Grimes, E.C Dickey and M.V Pishko Eds) Vol. 3 American Scientific Publishers (2006) 157-199
35. P.M.S. Monk, *Fundamentals of Electroanalytical Chemistry*, Wiley, New York, 2002
36. J-M. Zen; A. Senthil Kumar; M-R. Chang, *Electrochim. Acta* **45** (2000) 1691
37. M.E.G. Lyons, C.A. Fitzgerald, M.R. Smyth, *Analyst* **119** (1994) 855

38. K.I. Ozoemena, T. Nyokong, *J. Electroanal. Chem*. **579** (2005) 283
39. D. Nkosi, K.I. Ozoemena, *J. Electroanal. Chem*. **621** (2008) 304
40. D. Gao, J-Z. Li, R-Q. Yu, *Anal. Chem*. **66** (1994) 2245
41. G. D. Christian, *Analytical Chemistry*, 6th ed. John Wiley and Sons, New York, 2004, p.113
42. C.A. Caro, F. Bedioui, J.H. Zagal, *Electrochim. Acta* **47** (2002) 489
43. T. Malinsky, Z. Taha, *Nature* **358** (1992) 676
44. B. Agboola, T. Nyokong, *Anal. Chim. Acta* **587** (2007) 116
45. F. Matemadombo, T. Nyokong, *Electrochim. Acta* **52** (2007) 6856

CHAPTER 5

Microscopic, Spectroscopic, Electrochemical and Electrocatalytic Properties of Iron(II) and Cobalt(II) Octabutylsulphonylphthalocyanine*

* The following publications resulted from part of the research work presented in this chapter and they are not referenced further in this thesis:

3 K.I. Ozoemena, S.A. Mamuru, T. Fukuda, N. Kobayashi, T. Nyokong, *Electrochemistry Communication*, **11** (2009) 1221-1225

4 S.A. Mamuru, K.I. Ozoemena, T. Fukuda, N. Kobayashi, T. Nyokong, *Electrochimica Acta*, **55** (2010) 6367-6375

5.1 Microscopic and Spectroscopic Characterisation

Following the synthesis of the iron(II) and cobalt(II) octabutylsulphonylphthalocyanine, their surface morphologies were examined to obtain microscopic and spectroscopic information. Scanning electron microscopy and UV-visible spectroscopy were employed for this investigation.

5.1.1. *SEM characterisation*

Fig. 5.1 shows typical comparative SEM images of the MOBSPc (a), MWCNT (b) and MWCNT/MOBSPc (c), showing porous morphology. The images are perhaps not surprising as MWCNT-based electrodes are known to exhibit porous morphology.[1] Also; the drop-cast method used in the fabrication of the electrode mostly gives layers of modifiers rather than just a layer or mono-layer.

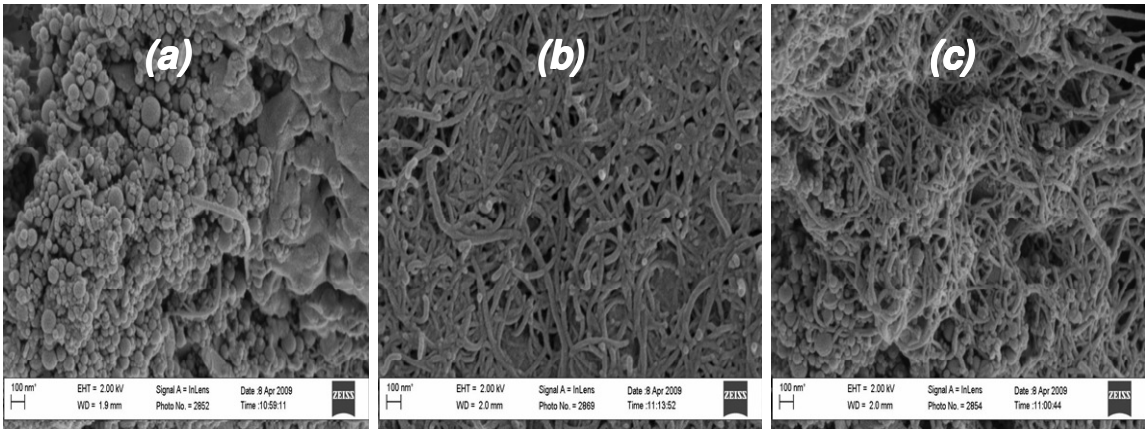

Figure 5.1: *SEM images of MOBSPc (a), MWCNT (b) and MWCNT/MOBSPc*

5.1.2. *Characterization using UV-visible Spectrophotometer*

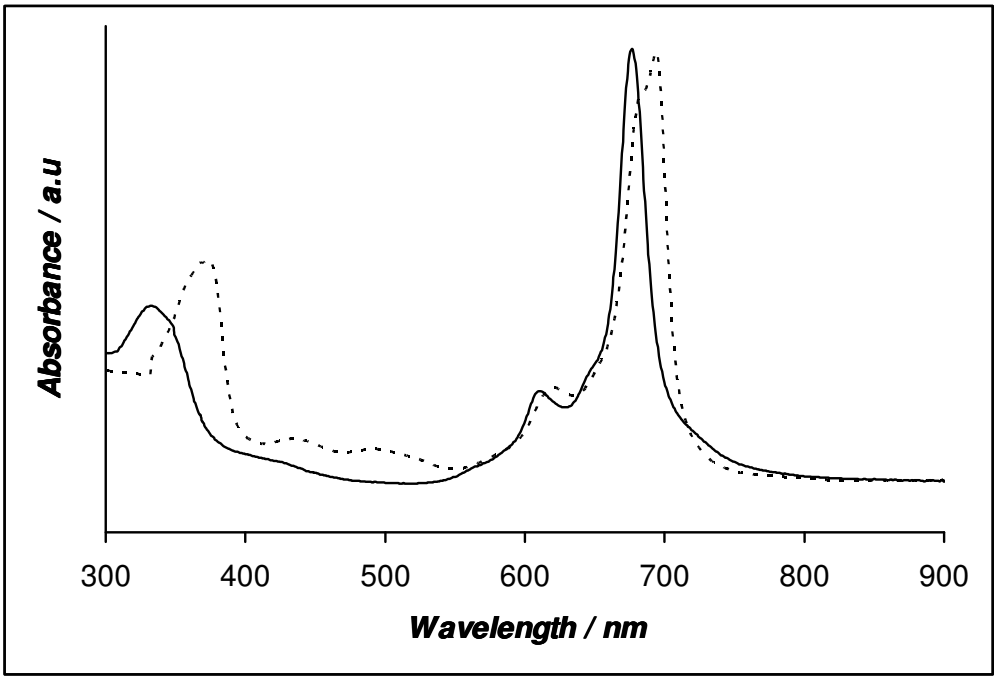

Figure 5.2: *UV-visible spectrum of CoOBSPc (bold lines) and FeOBSPc (dashed lines) in chloroform.*

Figure 5.2 shows the comparative UV – visible spectrum for CoOBSPc and FeOBSPc in chloroform. The observed spectra exhibited the characteristic Q – band typical for monomeric species of metallophthalocyanine complexes. The CoOBSPc complex shows two absorption bands at 343 nm (B – band) and 678 nm (Q – band), while for FeOBSPc, the B – band and the Q – band appears at 360 nm and 696 nm respectively. The two weak bands at 435 nm and 495 nm observed for the FeOBSPc complex is typical of a low-spin six-coordinate $Fe^{II}Pc$ species and is usually associated with Fe^{II} – to - ligand transfer transition.[2] Hence its presence is a good indication that

the central metal ion remain in the +2 oxidation state. Both B and Q bands of the FeOBSPc complex slightly shifted to longer wavelength when compared to the CoOBSPc complex, such a shift is an indication that the energy gap between the highest occupied molecular orbital (HOMO) and the lowest unoccupied molecular orbital (LUMO) of the FeOBSPc are narrower than those of CoOBSPc complex.[3]

5.2 Electrochemical Characterisation

5.2.1. *Solution Electrochemistry*

Figure 5.3 (a) and (b) shows typical cyclic voltammograms and inset, corresponding square wave voltammograms obtained in DMF containing about 1 mM of FeOBSPc and CoOBSPc in 0.1 M TBAP (second scans). All the redox processes were diffusion-controlled as the plots of j_p vs. $\nu^{1/2}$ (not shown) were linear. The values of the redox potentials are summarized in Table 5.1. From Table 5.1, we can conclude the following. First, the first reduction and oxidation processes of the FeOBSPc and CoOBSPc complexes are attributed to the metal centers (M^{3+}/M^{2+}), in comparison with literature.[4] The other reduction processes of the MOBSPc complexes are ascribed to the Pc rings; Peak III' seen at the FeOBSPc species is ascribed to the electrolyte as it was unstable, disappeared at high scan rates or during repetitive scans.

Table 5.1*: Redox potentials of compounds recorded in DMF containing 0.1 M TBAP.*

Compound	**Potential, $E_{1/2}$ (V vs. Ag/AgCl wire)**				
	V	**IV**	**III**	**I**	**II**
FeOBSPc	-1.62	-1.16	-0.67	0.76	1.48
CoOBSPc	-1.61	-1.06	-0.58	0.32	1.63

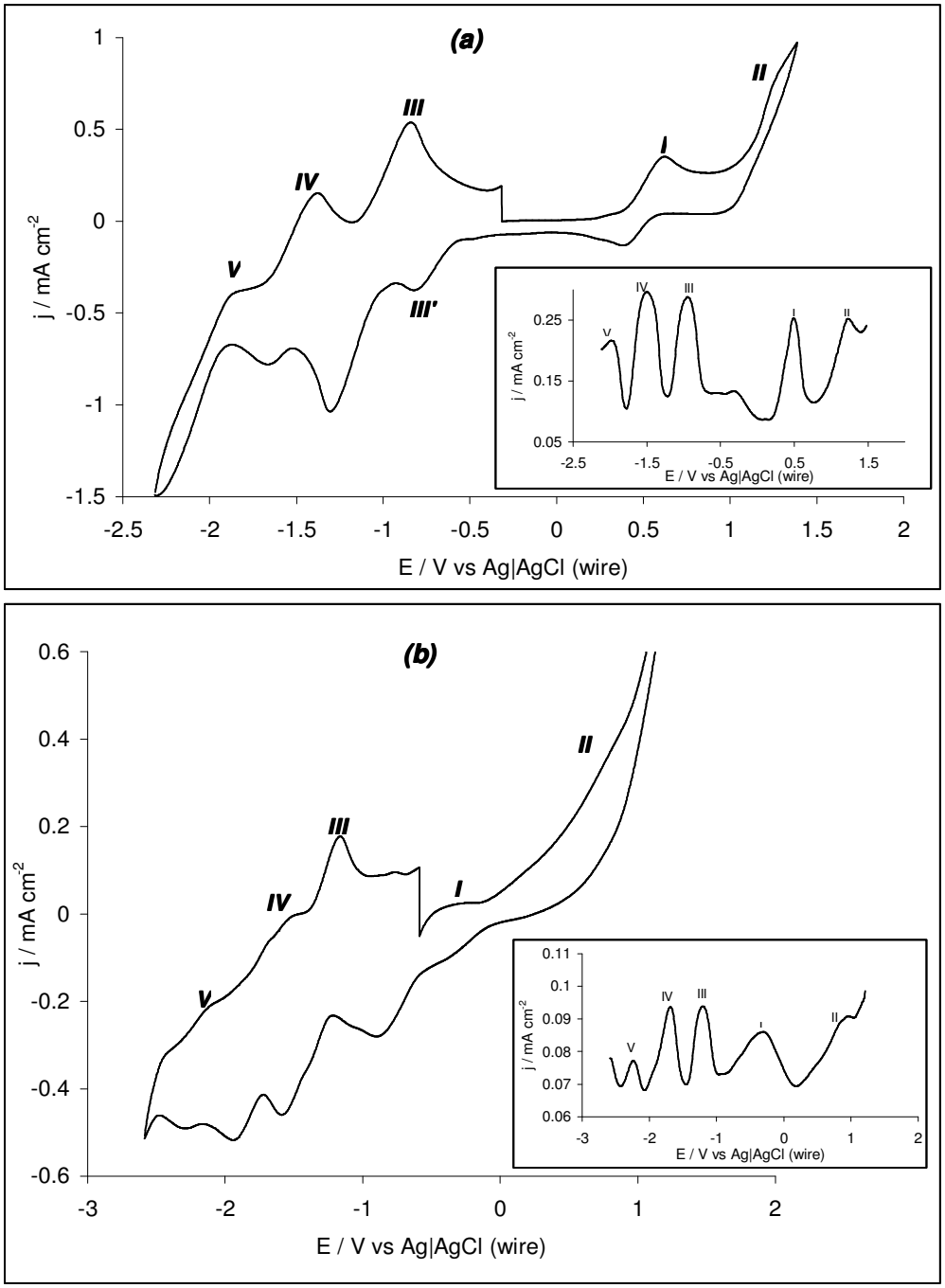

Figure 5.3: *Typical cyclic voltammograms and inset square wave voltammograms for FeOBSPc (a) and CoOBSPc (b) recorded in DMF containing 0.1 M TBAP.*

5.2.2. *Electron transfer behaviour: cyclic voltammetry*

Figure 5.4 presents the comparative cyclic voltammograms of the various electrodes studied in a 1.0 M KCl solution containing 0.1 M $[Fe(CN)_6]^{3-}/[Fe(CN)_6]^{4-}$. This experiment is to explore the extent to which the modifying species permit the electron transfer of the $[Fe(CN)_6]^{3-}/[Fe(CN)_6]^{4-}$ to and from the underlying EPPG electrode. Analysis of the potential peak-to-peak separation (ΔE_p) of the various electrodes gave the following values: EPPGE–CoOBSPc (122mV) > EPPGE–FeOBSPc (95mV) > EPPGE–MWCNT–CoOBSPc (92mV) > bare EPPGE(83mV)>EPPGE–MWCNT≈EPPGE–MWCNT–FeOBSPc (56mV).This result shows that EPPGE–MWCNT–FeOBSPc gave the fastest electron transfer, while the EPPGE–CoOBSPc was the worst. In general, the result indicates that the MPc complexes gave the best electron transport in the presence of MWCNTs rather than when alone, suggesting that MWCNT platform acts as efficient electron-conducting nanowires.

Next, the diffusion domain approximation theory as discussed in Chapter 4 was used to interrogate the type of diffusion process that could be occurring at these electrodes. It can be seen in Figure 5.4 that the voltammetric responses by the EPPGE–FeOBSPc and EPPGE–CoOBSPc electrodes are about half the current of the bare EPPGE electrode, suggesting that these electrodes behave as single macro-

blocks where "linear" diffusion plays the active role without any significant depletion in the concentration of the redox couple hence a reduced current response. The increased current response observed for the MWCNT-based electrodes is as discussed in 4.2.1.1.

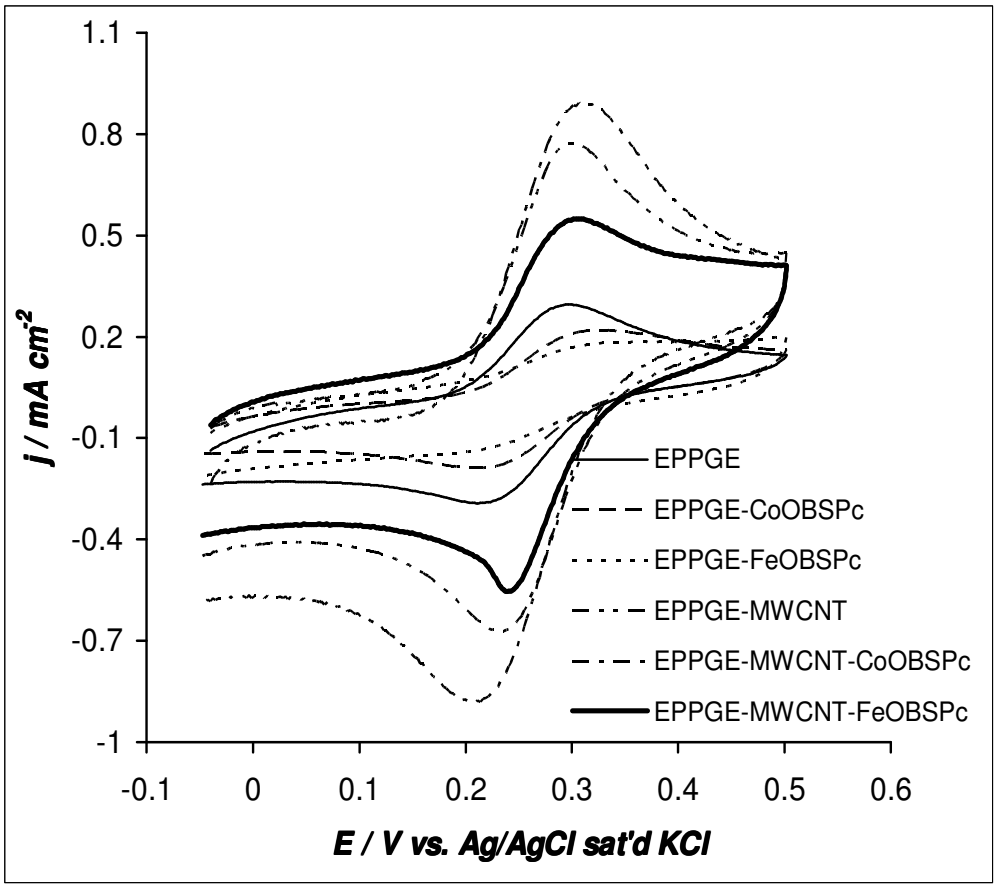

Figure 5.4: *Comparative cyclic voltammograms of the various electrodes in 0.1 M* $[Fe(CN)_6]^{3-}/[Fe(CN)_6]^{4-}$ *in 1.0 M KCl solution.*

The type of diffusion occurring at the electrodes was categorized using the modified Einstein equation for the root mean square displacement of diffusing particles (equation 4.1) From the estimated ΔE values of the electrodes, ~0.15 V for the EPPGE and EPPGE–

MWCNT–FeOBSPc, ~0.17 V for the EPPGE–FeOBSPc and EPPGE–MWCNT–CoOBSPc, and ~0.19 V for the EPPGE–CoOBSPc, an approximate value of 63.5 μm was estimated as the diffusional distance, which corresponds to the type 3 behaviour of the voltammetric responses at spatially heterogeneous electrodes. This type of voltammetric behaviour is associated with an overlap of adjacent diffusion layers resulting from the small size of the inert part of the electrode.

5.2.3. *Electron transfer behaviour: impedimetric characterisation*

Figure 5.5(a) presents the Nyquist plots for the various electrodes studied in 1.0 M KCl solution containing 0.1M $[Fe(CN)_6]^{3-}/[Fe(CN)_6]^{4-}$. The impedance spectra of the electrodes were satisfactorily fitted with the proposed modified Randles equivalent electrical circuits (Figure 5.5(d)). The bare EPPGE and EPPGE–CoOBSPc electrodes were fitted with circuit (i), while EPPGE–FeOBSPc and the MWCNT- based electrodes were fitted with circuit (ii).The fitting parameters involve the electrolyte resistance (R_s), electron transfer resistance (R_{ct}), constant phase element (CPE), double layer capacitance (C_{dl}) and Warburg-type impedance (Z_w) which is associated with the diffusion of the ions of the redox probe. The apparent heterogeneous electron transfer rate constant (k_{app}) values of the electrodes were obtained using equation.

(4.2) The calculated values are shown in Table 5.2, wherein the k_{app} values decreased as: EPPGE–MWCNT (782×10^{-3} cms^{-1}) > EPPGE–MWCNT–FeOBSPc (372×10^{-3} cms^{-1}) > EPPGE–MWCNT–CoOBSPc (215×10^{-3} cms^{-1}) > EPPGE–FeOBSPc (93×10^{-3} cms^{-1}) > EPPGE (6.1×10^{-3} cms^{-1}) > EPPGE–CoOBSPc (0.2×10^{-3} cms^{-1}), indicating that electron transfer processes between the redox probe and the underlying EPPGE surface are much easier at the EPPGE–MWCNT modified electrodes compared to the other electrodes. This result closely agrees with the ΔE_p trend from the CV data. The impedance of the CPE (Z_{CPE}) is defined as in (equation (2.26)). From the Bode plots (Figure 5.5(b) and (c)), the slopes of the log Z vs. log f plot at the mid frequency region are less than the ideal −1.0 for pure capacitive behaviour, which is indicative of pseudocapacitive behaviour. In circuit Figure 5.5(d) (ii), notice that the Warburg impedance in the ideal Randles circuit has been replaced by the C_{dl}, which simply describes the porous nature of the concerned electrodes. All attempt to replace the C_{dl} in circuit (ii) with a CPE (which is a more practical situation) led to huge fitting errors. This should not be interpreted to signify that the C_{dl} is a pure double layer capacitance. According to Orazem and Tribollet,[5] frequency dispersion leading to CPE behaviour takes place through the distribution of time constants along either the area of the electrode surface (involving a 2-dimensional aspect of the electrode, which mimics an ideal RC behaviour) or along the axis normal to the

electrode surface (involving a 3-dimensional surface). Thus, one may conclude here that the observed impedimetric behaviour of the modified electrodes is CPE. The data from the Bode plots (i.e.,–phase angle vs. log f) further confirms the absence of ideal capacitive behaviour as the observed phase angles are less than the 90° expected of an ideal capacitive behaviour.

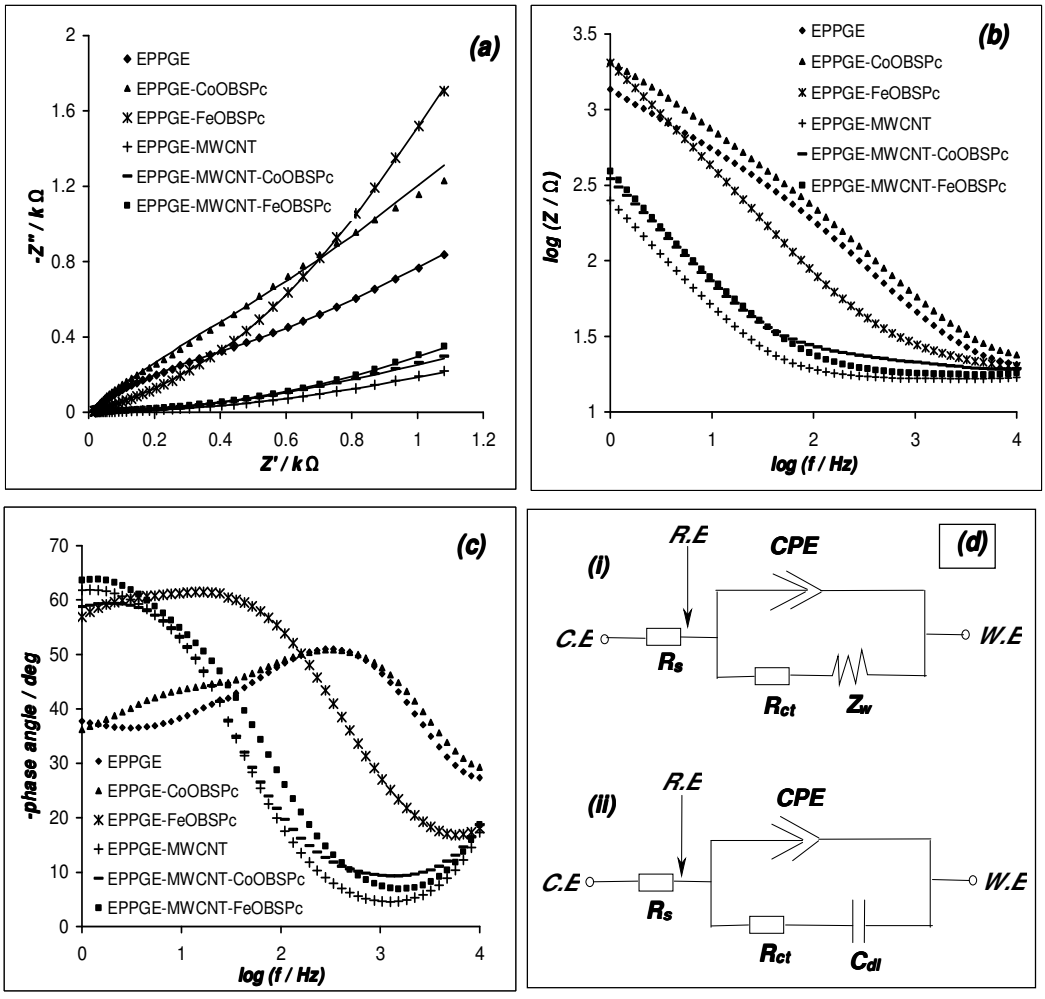

Figure 5.5: *(a) Comparative Nyquist and (b), (c) Bode plots of the various electrodes in 0.1 M $[Fe(CN)_6]^{3-}$/$[Fe(CN)_6]^{4-}$ 1.0 M KCl solution. Proposed equivalent electrical circuits (d)*

Table 5.2: *Impedance parameters and ΔE_p values obtained for the various electrodes studied in 0.1 M $[Fe(CN)_6]^{3-}$ /$[Fe(CN)_6]^{4-}$ in 1 M KCl solution*

EPPGE modifier	**Electrochemical impedance spectroscopic parameters**						
	R_s / Ω	R_{ct} / kΩ	CPE / µF	n	C_{dl} /µF	$10^3 k_{app}$ /cm s^{-1}	ΔE_p / mV
EPPGE*	13.8±0.35	0.627±0.004	51.9±3.22	0.70±0.08	-	6.1±0.4	83
CoOBSPc*	13.6±0.53	1.438±0.015	62.3±4.05	0.70±0.08	-	~ 0.2	122
FeOBSPc	14.8±0.41	0.040±0.003	143.9±2.73	0.60±0.07	652±51.51	93.2±7.8	95
MWCNT-CoOBSPc	14.9±0.89	0.018±0.001	875±50.75	0.50±0.03	137±10.14	214.7±16.5	92
MWCNT-FeOBSPc	16.2±0.49	0.010±0.003	697.4±35.57	0.70±0.03	54±1.73	371.7±14.6	56
MWCNT	14.7±0.49	0.005±0.002	1066± (6.1)	0.60±0.04	177±24.25	782.3±23.3	56

*Z_w of EPPGE and CoOBSPc is (319±0.008) x 10^{-6} Ω and (186±0.009) x 10^{-6} Ω, respectively.

5.3 Electrocatalytic Properties

5.3.1. *Electrocatalytic reduction of oxygen*

Figure 5.6 shows the comparative CV of the various electrodes studied in oxygen saturated 0.1M NaOH solution. The EPPGE–MWCNT–FeOBSPc electrode showed the best response in terms of current density, peak potential and less onset potential compared to other electrodes. The current density is about three times higher with a peak potential at ~−0.18 V and an onset potential of ~0.0 V compared to the EPPGE–MWCNT–CoOBSPc electrode with an onset potential of ~−0.15 V. Expectedly, both EPPGE–MWCNT and EPPGE–MWCNT–CoOBSPc electrodes showed two peaks at ~−0.2 and −0.5 V, which maybe attributed to the two-step 2-electron reduction of oxygen. This result agrees with literature as it is well known that while the FePc catalysts follow the direct 4-electron pathway,[6,7] CNT-based electrodes[8,9] and CoPc-based electrodes[10] catalyze the ORR via the 2-electron reduction of oxygen to hydrogen peroxide and then the hydrogen peroxide to water in alkaline medium at more negative potentials. The enhanced ORR activity of the EPPGE–MWCNT–FeOBSPc might be due to the structural properties of the carbon nanotube; comprising multiple cylindrical shell of graphite sheets of nanometer diameters, channels in the tubular structure, and the topological defects on the tube surface,

all make the carbon nanotubes provide enough effective reaction sites to increase electron exchange rate and at less negative potentials.[9]

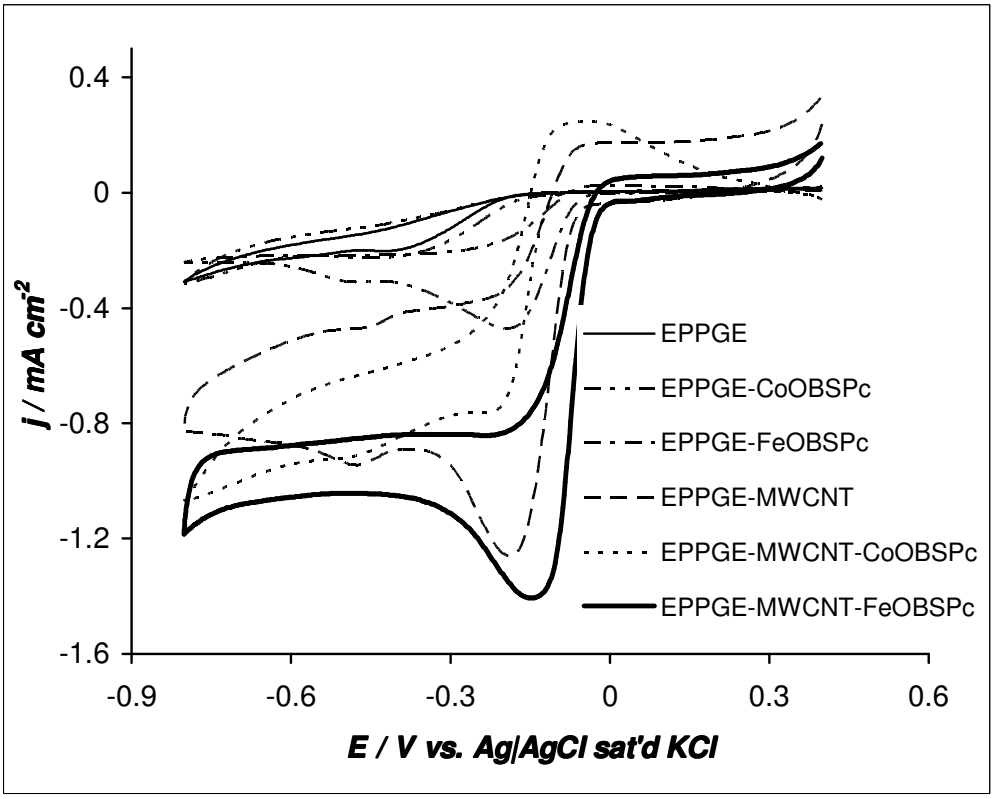

Figure 5.6: *Comparative cyclic voltammograms of the electrodes in 0.1 M NaOH saturated with oxygen. Scan rate: 10 mV* s^{-1}

The central Fe of the FePc complexes undergo axial co-ordination with O-donor and N-donor molecules, faster and more stable, than their CoPc counterparts,[11-14] which further explains the higher ORR activity of the FeOBSPc than the CoOBSPc. Indeed, it is exciting to observe here that the onset potential of the oxygen reduction at the EPPGE–MWCNT–FeOBSPc electrode (0.0 V vs. Ag|AgCl) is much better than that recently reported by Gong *et al*.[15] (approximately −0.2 V vs.

Ag|AgCl) for a commercial platinum catalyst supported on carbon, but comparable to the recent work (−0.08 V vs. Ag|AgCl) by Chen and Chen[16] for gold nanoclusters supported on glassy carbon. Because of its best performance, the EPPGE–MWCNT–FeOBSPc electrode was used for subsequent studies.

5.3.1.1. *Effect of scan rates*

Cyclic voltammetry was employed to investigate the effect of varying scan rate on the response of the EPPGE–MWCNT–FeOBSPc electrode in the reduction of molecular oxygen in 0.1M NaOH solution saturated with pure oxygen. Figure 5.7(a) presents the CV evolutions of the EPPGE–MWCNT–FeOBSPc electrode at different scan rates (25–500 mVs^{-1}). Inset of Figure 5.7(a) describes the linear relationship between the reduction peak current (I_p) and the square root of scan rate ($\nu^{1/2}$), implying that the process is diffusion controlled.

As an irreversible process, it can be observed that the peak potential (E_p) shifts to more negative values with increasing scan rate (ν). This process is governed by equation (4.6):[17,18]

$$E_p = \frac{b}{2}\log \nu + \text{constant} \qquad (4.6)$$

$$b = \frac{2.3RT}{\alpha nF} \qquad (4.5)$$

where R is the ideal gas constant, T the absolute temperature, F the Faraday constant, α the charge transfer coefficient and n is the number of electrons involved in the rate-determining step. The plot of peak potential (E_p) against logarithm of scan rate (log ν), Figure 5.7(b), gave a straight line with a Tafel slope of approximately 124 mV dec^{-1}, with an α value of 0.48.The Tafel slope is close to the theoretical 118 mV dec^{-1} for a 1-electron process involved in the rate-determining step

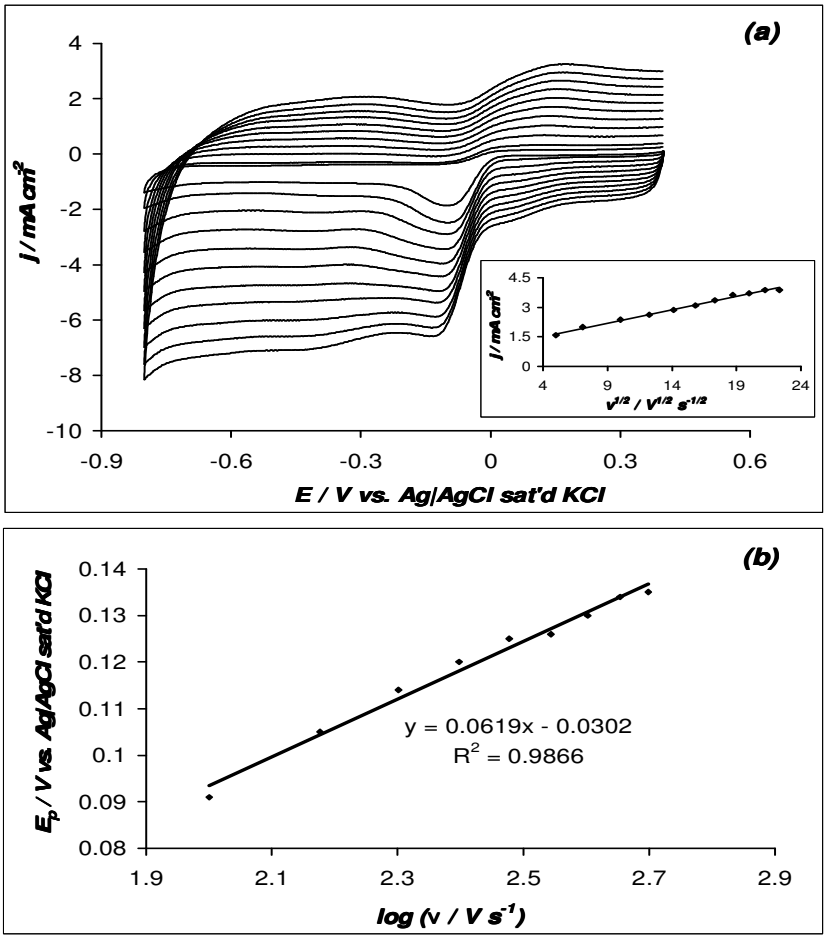

Figure 5.7: *(a) Cyclic voltammetric evolutions of the EPPGE-MWCNT-FeOBSPc electrode at varying scan rates. Inset shows linear relationship between the reduction peak current (I_p) and square root of scan rate ($\nu^{1/2}$). (b) Plot of peak potential (E_p) against the logarithm of scan rate (log ν).*

5.3.1.2. *Chronocoulometric studies*

Figure 5.8 presents the chronocoulometric evolutions of the EPPGE–MWCNT–FeOBSPc electrode in oxygen saturated and nitrogen saturated 0.1M NaOH solution. The charge on the oxygen-saturated electrode is about 3 folds more than the nitrogen-saturated electrode, this is indicative of the electro-active nature of the electrode towards the reduction of oxygen. After subtraction of the background charge, a plot of charge (Q) against square root of time ($t^{1/2}$) was generated from the plot in Figure 5.8(a) for the oxygen-saturated electrode. The plot in Figure 5.8(b) reveals a linear relationship (R^2 = 0.9995), characteristic of diffusion-controlled electrode process. According to Cottrell equation,[18] the number of electrons (n) involved in the reduction of oxygen can be estimated from the slope of the plot of Q vs. $t^{1/2}$ using equation (5.1):[18]

$$Q = \frac{2nFAcD^{1/2}t^{1/2}}{\pi^{1/2}} \qquad (5.1)$$

where F is Faraday constant, A is the electroactive area of the EPPGE–MWCNT–FeOBSPc (~0.1cm^2), c is the concentration of oxygen in oxygen saturated 0.1 M NaOH (0.25×10^{-6} mol cm^{-3}), D is the diffusion coefficient of oxygen in an aqueous solution (1.51×10^{-5} cm^2 s^{-1})[19] and slope = 30 μCs$^{-1/2}$. The number of electrons involved in the reduction of oxygen was estimated to be ≈4.

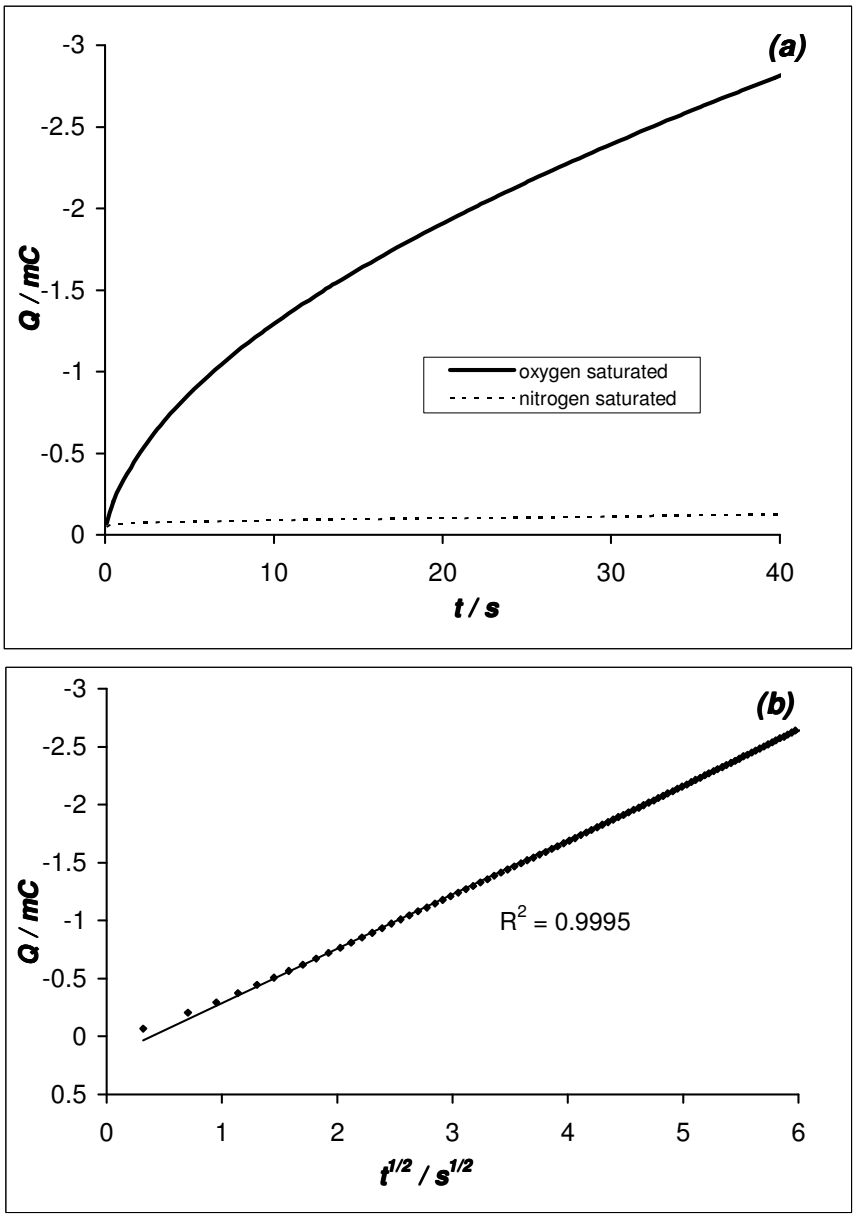

Figure 5.8: (a) Chronocoulometry curves of EPPGE-MWCNT-FeOBSPc in 0.1 M NaOH saturated with oxygen (bold line) and saturated with nitrogen (dashed line). (b) Plot of charge (Q) against square root of time ($t^{1/2}$).

5.3.1.3. *Hydrodynamic voltammetry investigation*

Hydrodynamic voltammetry was used to carry out further study on the electro-reduction of molecular oxygen on the EPPGE–MWCNT–FeOBSPc

electrode by scanning linearly from 0.4 to −0.8V in oxygen saturated 0.1 M NaOH electrolyte solution (Figure 5.9(a)). The result presented in Figure 5.9(a) clearly shows that as the rotation rate increases there is an enhancement of the limiting current. Figure 5.9(b) presents the Koutecky–Levich plot for the electro-catalytic reduction of molecular oxygen on EPPGE–MWCNT–FeOBSPc electrode in oxygen saturated 0.1 M NaOH generated from Figure 5.9(a), and govern by the Koutecky–Levich equation (2.12). The linearity observed when the inverse of the current density was plotted against the inverse square root of rotation rate implies that the electrode process is diffusion controlled and the reaction is first order. Furthermore, the slope and intercept from the straight line, respectively correspond to j_{Lev} (equation (2.14)) and j_{kin} (equation (2.13)). The number of electrons (n) transferred per oxygen molecule was calculated from equation (2.14) and estimated to be ~4 at −0.15 V. This potential is close to the peak potential observed for EPPGE–MWCNT–FeOBSPc electrode in Figure 5.6. Also, this result supports our finding using chronocoulometry. The dashed lines in Figure 5.9(b) are theoretical lines calculated using equation(2.14) for n = 4 and n = 2.The figure reveals that oxygen reduction at EPPGE–MWCNT–FeOBSPc electrode follows the 4-electron transfer Levich plot, suggesting that oxygen reduction at EPPGE–MWCNT–FeOBSPc electrode proceeds via a single 4-electron transfer.

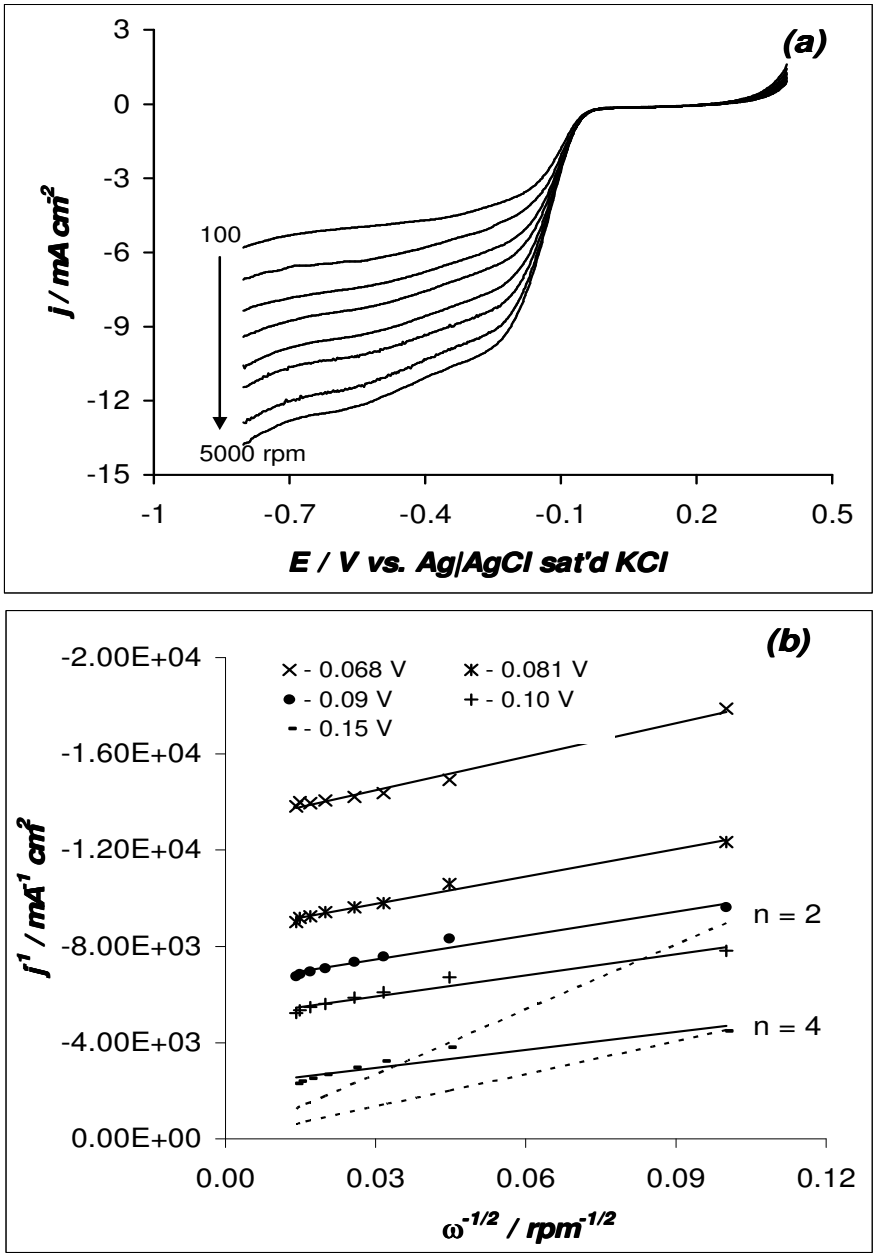

Figure 5.9: *(a) RDE voltammetry for oxygen reduction on an EPPGE-MWCNT- FeOBSPc electrode in oxygen saturated 0.1 M NaOH. Scan rate: 10 mV s^{-1}. (b) Koutecky-Levich plots for oxygen reduction on EPPGE-MWCNT-FeOBSPc electrode in oxygen saturated 0.1 M NaOH solution.*

5.3.2. *Electrocatalytic oxidation of thiocyanate*

Figure 5.10 presents the comparative cyclic voltammograms of the electrodes studied in 1mM thiocyanate solution (phosphate buffer pH 5). As seen, the EPPGE-MOBSPc electrodes shows no catalytic response towards thiocyanate oxidation, this is probably due to the strong electron-withdrawing effect of the substituents attached to the ring of the phthalocyanine which makes oxidation difficult. However, the EPPGE-MWCNT gave the best catalytic response towards thiocyanate oxidation with oxidation peak at approximately 0.80 V. The catalytic activity of MWCNT has been reported,[20] and was attributed to the edge-plane- like sites nanotube ends where there is a possibility of the presence of oxygenated groups, as in this case, the purification of the MWCNT introduces some oxygenated groups. In comparison, the EPPGE-MWCNT-CoOBSPc and EPPGE-MWCNT-FeOBSPc exhibited irreversible oxidation peaks at approximately 0.90 and 1.0 V respectively, suggesting that the introduction of the MOBSPc shifted the potential to more positive potential hence the slow electron transfer at these electrodes.

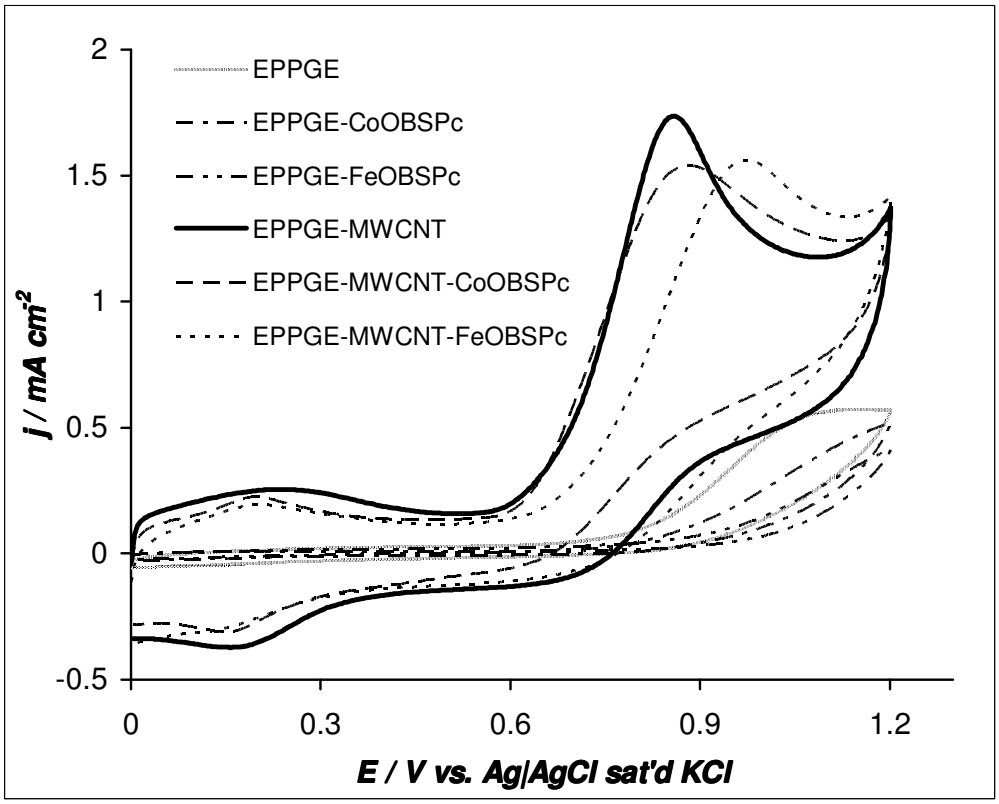

Figure 5.10: *Comparative cyclic voltammograms of the various electrodes in 1mM thiocyanate solution contained in phosphate buffer (pH 5).*

5.3.3. Electrocatalytic oxidation of nitrite

Figure 5.11 presents the comparative CV of the various electrodes studied in 1mM nitrite solution (phosphate buffer pH 7.4). As seen, a similar trend as observed for thiocyanate oxidation was noticed. Considering that the aim of the of the study is to establish the electrocatalytic activity of the MOBSPc complexes, no further analysis

was carried on these electrodes because of their poor performance or the MWCNT electrode.

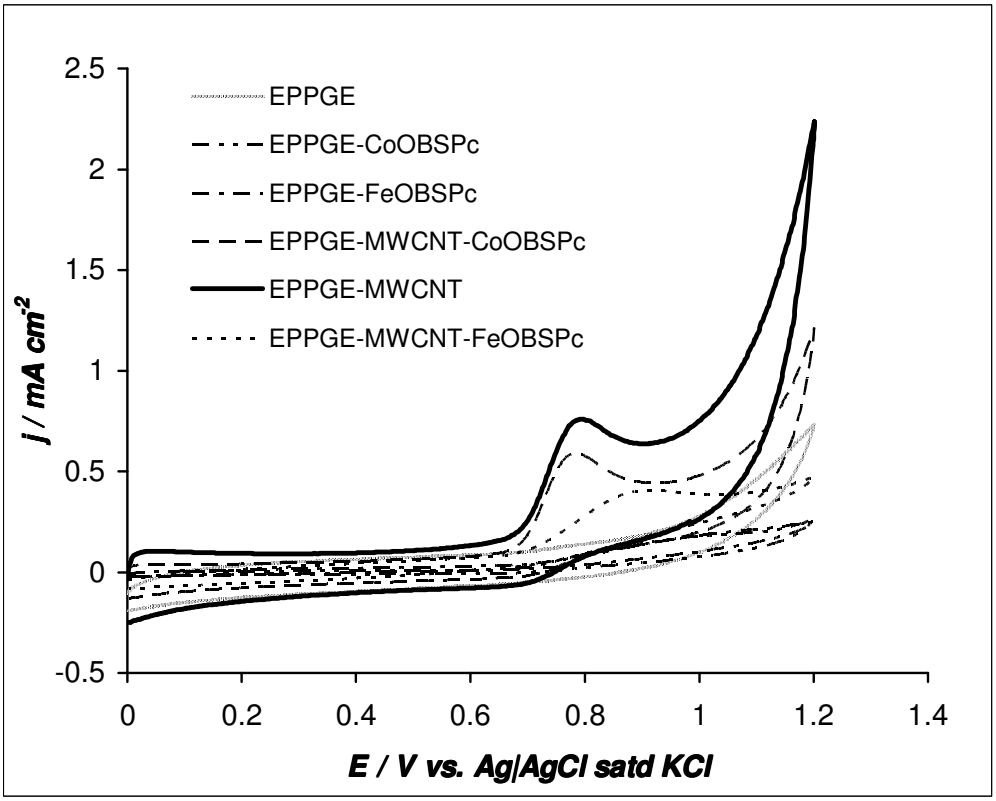

Figure 5.11: *Comparative cyclic voltammograms of the various electrodes in 1mM nitrite solution contained in phosphate buffer (pH 7.4).*

References

1. I. Streeter, G.G. Wildgoose, L. Shao, R.G. Compton, *Sens. Actuators* B **133** (2008) 462
2. K.I. Ozoemena, T. Nyokong, *Dalton Trans* (2002), 1806
3. M.J. Stillman, T. Nyokong, *Phthalocyanines: Properties and Applications*, eds. C.C. Lenznoff, A.B.P. Lever, VCH, New York, 1989, vol. 1
4. A.B.P. Lever, E.R. Milaeva, G. Spieer, *Phthalocyanines: Properties and Applications*, vol. 3, VCH Publishers, 1993, Chapter 1
5. M. E. Orazem, B. Tribollet, Electrochemical Impedance Spectroscopy, John Wiley & Sons Inc, Hoboken, NJ, 2008
6. N. Kobayashi, P. Janda, A.B.P. Lever, *Inorg. Chem.* **31** (1992) 5172
7. G. Wang, N. Ramesh, A. Hsu, D. Chu, R. Chen, *Mol. Simul.* **34** (2008) 1051
8. A. Sarapuu, K. Vaik, D.J. Schriffin, K. Tammeveski, *J. Electroanal. Chem.* **541** (2003) 23
9. F. Wang, S. Hu, *J. Electroanal. Chem.* **589** (2005) 68
10. J. Zagal, M. Paez, A.A. Tanaka, J.R. dos Santos Jr., C.A. Linkous, *J. Electroanal. Chem.* **339** (1992) 13
11. S. Griveau, J. Pavez, J.H. Zagal, F. Bedoui, *J. Electroanal. Chem*. **497** (2001) 75

12. M.P. Siswana, K.I. Ozoemena, T. Nyokong, *Electrochim. Acta* **52** (2006) 114
13. M. Siswana, K.I. Ozoemena, T. Nyokong, *Talanta* **69** (2006) 1136
14. K.I. Ozoemena, T. Nyokong, P. Westbrooke, *Electroanalysis* **15** (2003) 1762
15. K.P. Gong, F. Du, Z.H. Xia, M. Durstock, L.M. Dai, *Science* **323** (2009) 760
16. W. Chen, S. Chen, *Angew. Chem. Int. Ed*. **48** (2009) 4386
17. J.A. Harrison, Z.A. Khan, *J. Electroanal. Chem.* **28** (1970) 131
18. A.J. Bard, L.R. Faulkner, *Electrochemical Methods: Fundamentals and Applications*, 2nd ed., John Wiley & Sons, Hoboken, NJ, 2001.
19. D.H. Evans, J.J. Lingane, *J. Electroanal. Chem*. **6** (1963) 283
20. C.E. Banks, T.J. Davies, G.G. Wildgoose, R.G. Compton, *Chem. Commun.* (2005) 829

CHAPTER 6

Microscopic, Spectroscopic, Electrochemical and Electrocatalytic Properties of Iron(II) tetrakis(diaquaplatinum)octa-carboxy phthalocyanine*

* The following publications resulted from part of the research work presented in this chapter and they are not referenced further in this thesis:

5 S. A. Mamuru, K. I. Ozoemena, T. Fukuda, N. Kobayashi, *Journal of Materials Chemistry*, **20** (2010) 10705.

6 S. A. Mamuru, K. I. Ozoemena, *Electrochemistry Communication*, **12** (2010) 1539.

6.1. Microscopic and Spectroscopic Characterisation

Microscopic and spectroscopic information of iron(II) tetrakis (diaquaplatinum)octa-carboxyphthalocyanine, were obtained with transmission electron microscope, scanning electron microscope, UV-visible spectrophotometer, mass spectrophotometer, X-ray diffraction spectrophotometer, and elemental analyser.

6.1.1. *UV-visible characterisation*

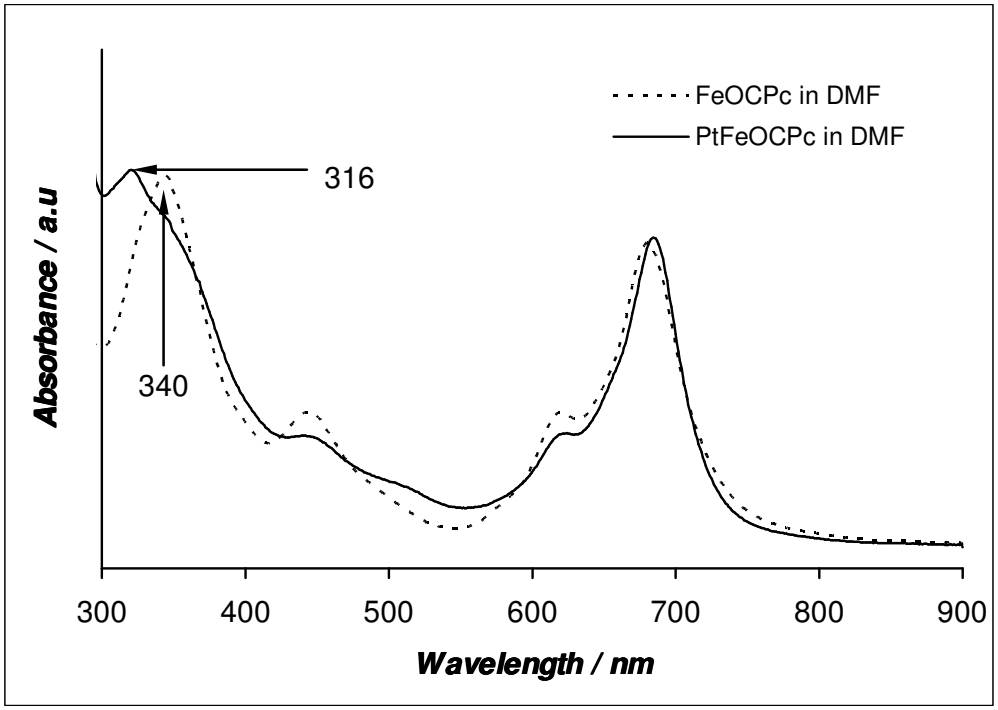

Figure 6.1: *Comparative UV-visible spectrum of FeOCPc and PtFeOCPc in DMF*

Figure 6.1 shows the comparative UV-visible spectrum of FeOCPc and PtFeOCPc in DMF. The Q-bands of the two complexes occur almost at the same wavelength (685 nm), with a slight shift to the red region

(~ 2 nm) by the PtFeOCPc complex. Second, there is a notable change in the spectral pattern of the B-band region (316 – 340 nm range); such change is characteristic of the introduction of the Pt at the periphery of the phthalocyanine ring and can conveniently serve for monitoring the formation of PtFeOCPc complex.[1] Third, notice the peak at ~ 450 nm, which is characteristic of the metal-to-ligand charge transfer band of iron-containing phthalocyanine complexes.

6.1.2. *Elemental analysis and mass spectroscopy characterisation*

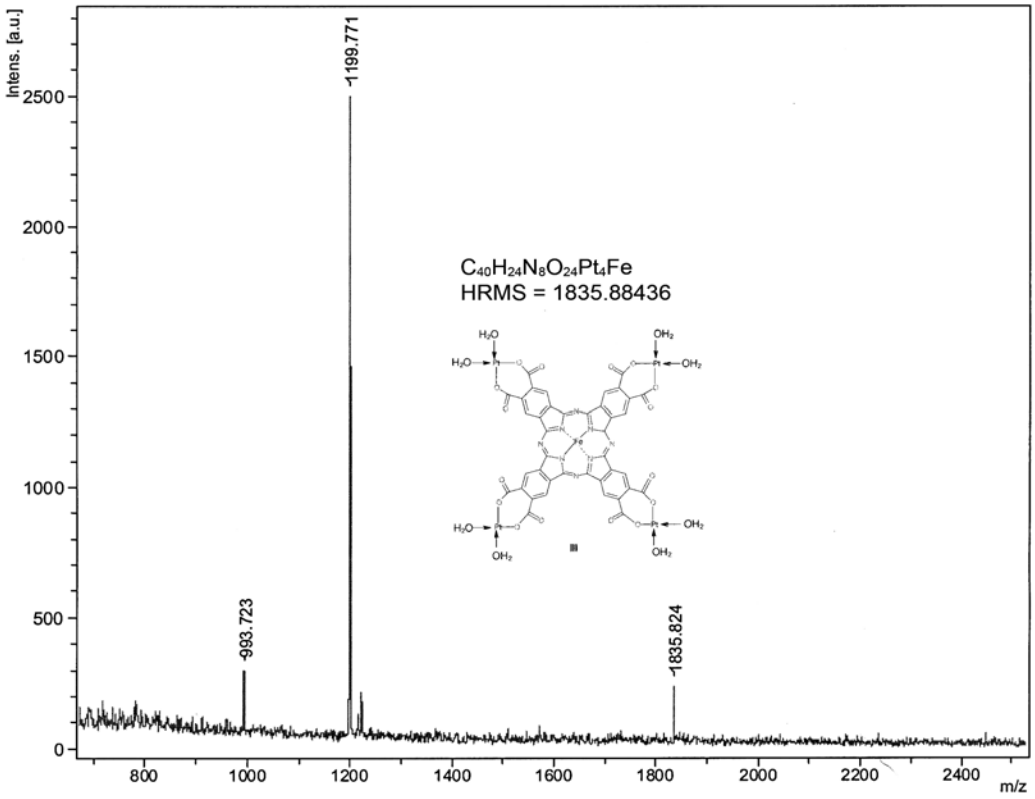

Figure 6.2: *High resolution mass spectra of iron(II) tetrakis (diaquaplatinum)octa-carboxyphthalocyanine ($C_{40}H_{24}N_8FeO_{24}Pt_4$)*

Elemental analysis data (CHN) of the two FePc complexes closely agree with the expected values (as presented in section 3.2.3). The PtFeOCPc was further analysed with mass spectroscopy (Figure 6.2). The peak at m/z 1199.771 is attributed to the $C_{36}H_{18}N_8O_{12}Pt_2Fe$ molecular ion, while that at m/z 993.732 may be related to the $C_{37}H_{10}N_8O_{11}PtFe$ fragment.

6.1.3. *XRD and EDX Characterisation*

Figure 6.3(a) presents the x-ray diffraction pattern of FeOCPc and PtFeOCPc. The PtFeOCPc compound exhibited diffraction peaks different from its precursor, FeOCPc, confirming the presence of Pt particles.[2,3] The broad diffraction peak observed at 2θ of 31° is due to C (003) which we associate with the phthalocyanine. This peak is more pronounced at the FeOCPc compound than its PtFeOCPc counterpart. The FeOCPc is amorphous, in agreement with reported results where MPcs were found to be amorphous.[4]

Figure 6.3(b) presents the EDX profile of PtFeOCPc; elemental analysis gave the expected atomic ratio of 1:4 (Fe:Pt).

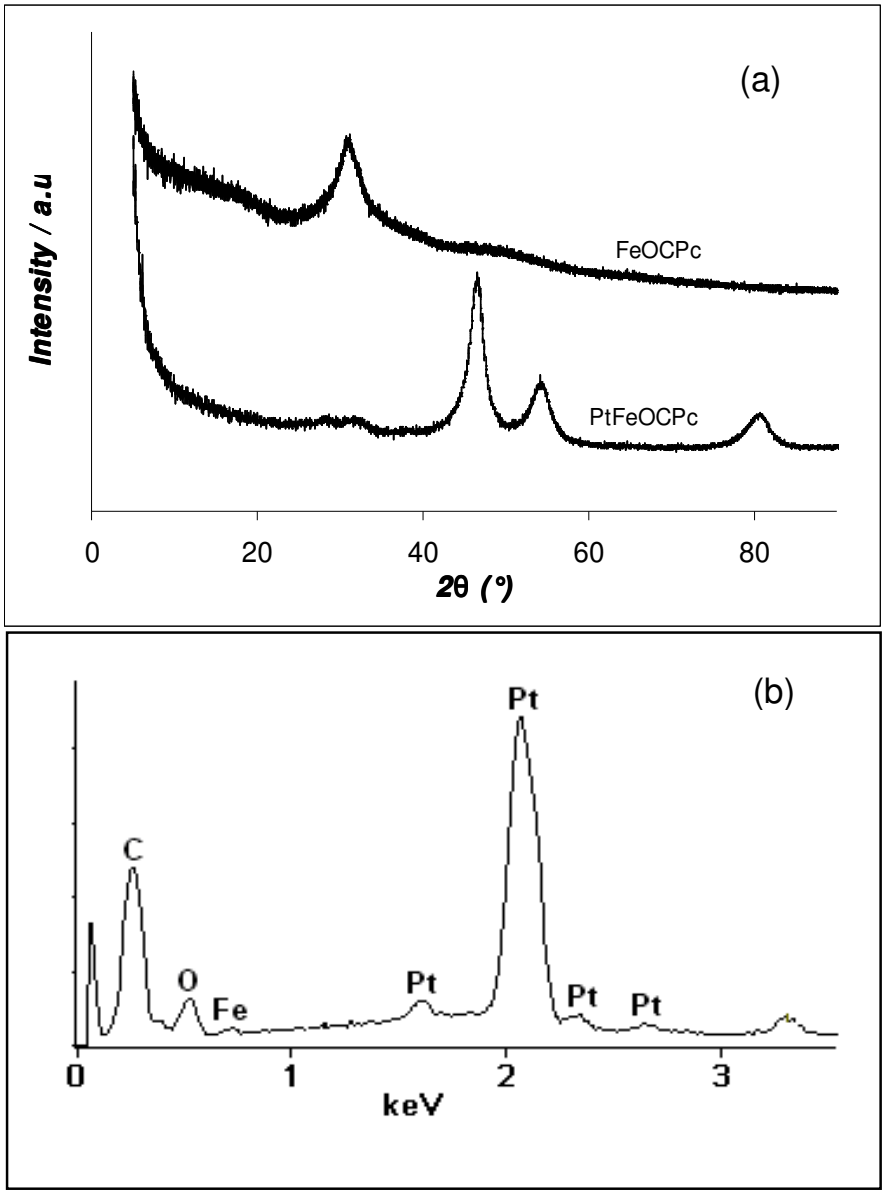

Figure 6.3: *Comparative XRD pattern of FeOCPc and PtFeOCPc (a), EDX spectra of PtFeOCPc (b)*

6.1.4. *Comparative SEM and TEM characterisation*

Figure 6.4 (a) and (b) presents the SEM images of MWCNT and MWCNT/PtFeOCPc respectively. The image shows the porosity in the structure of the complex. Figure 6.4 (c) and (d) shows the crystallinity and attachment of the PtFeOCPc to the MWCNTs. In (d) the

entrapment of the PtFeOCPc onto the cylindrical or the nanofibril structures of the MWCNTs might have been enhanced by some electrostatic interactions between the negatively-charged MWCNTs and the positively-charged platinum particles attached to the metallophthalocyanine, the platinum particle can be seen aligned along the MWCNT surface they form clusters and this favours high degree of dispersion and large surface area which increases electrocatalysis.[5]

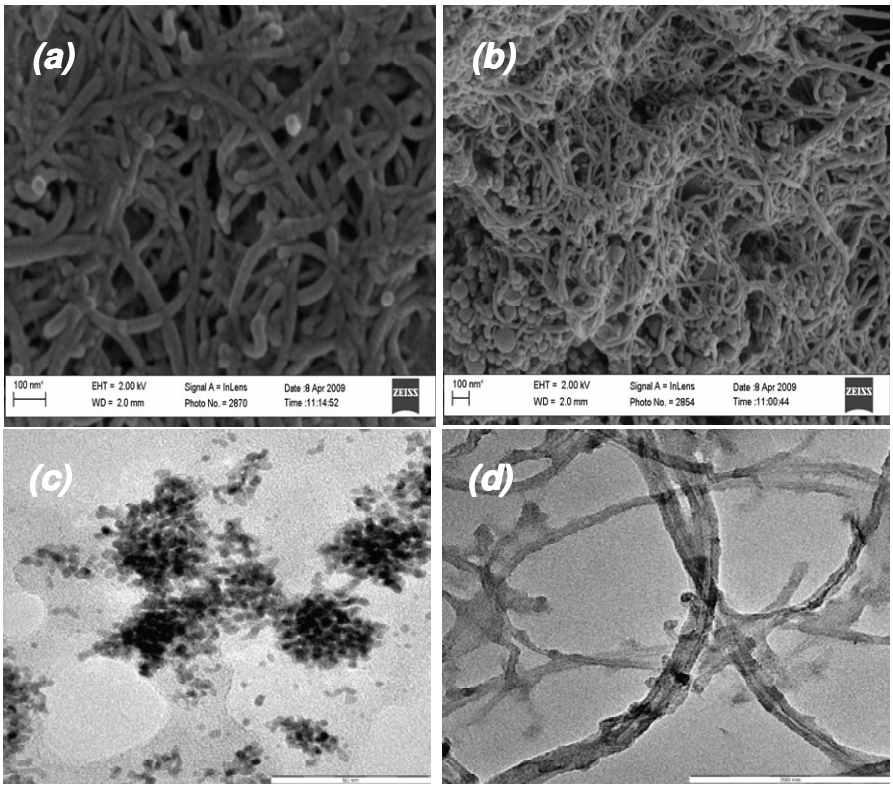

Figure 6.4: *Typical SEM images of MWCNT (a) and MWCNT/PtFeOCPc (b). Typical TEM images of PtFeOCPc (c) and MWCNT /PtFeOCPc (d)*

6.2. Electrochemical Properties

6.2.1. *Solution electrochemistry*

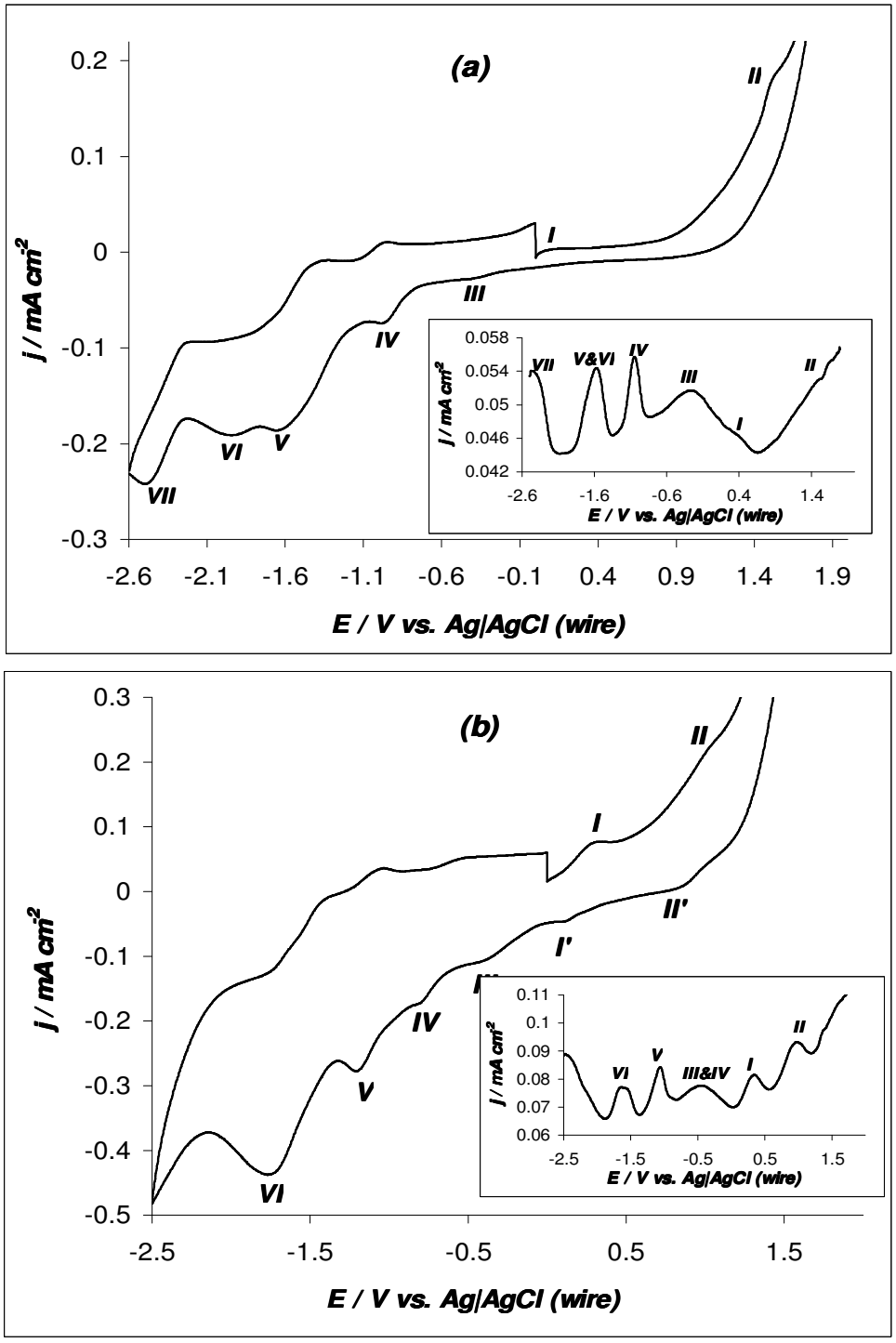

Figure 6.5: *Typical cyclic voltammograms for FeOCPc (a) and PtFeOCPc (b) recorded in DMF containing 0.1 M TBAP. Insets, corresponding square wave voltammograms*

Figure 6.5 shows the typical cyclic voltammograms and inset the corresponding square wave voltammograms obtained in DMF containing about 1 mM FeOCPc (a) and PtFeOCPc (b) in 0.1 M TBAP. The values of the redox potentials are summarised in Table 6.1. From the Table we can deduce that for the PtFeOCPc complex (Figure 6.5(b)), the oxidation and reduction processes denoted as I, I' and II, II' can be attributed to the metal centre (Fe^{3+}/Fe^{2+}) and the platinum metal coordinated to the phthalocyanine ring respectively. The other reduction processes are ascribed to the phthalocyanine ring. Peaks III and IV appear as single broad peak in the square wave voltammogram. Each of the two reduction process is considered as one-electron processes each, as the sum of their heights was comparable to the single broad peak. This suggests that the two processes occur close to each other and thus overlap as one peak.

For the FeOCPc complex (Figure 6.5(a)), the first oxidation and reduction process is ascribed to the metal centre while the second oxidation and the other reduction processes are ascribed to the phthalocyanine ring. It can be observed that the reduction processes at the FeOCPc complex occurred at more negative potentials compared to the PtFeOCPc complex; this suggests that the attachment of the platinum on the phthalocyanine ring reduces the electron density on the total conjugated MPc system hence easier reduction and more difficult oxidation, thus leading to the lower reduction potentials recorded for PtFeOCPc complex.

Table 6.1: *Redox potentials of FeOCPc and PtFeOCPc compounds recorded in DMF containing 0.1 M TBAP*

Compound	**Potential, $E_{1/2}$ (V vs. Ag|AgCl wire)**					
	VI	**V**	**IV**	**III**	**I**	**II**
FeOCPc	-2.42	-1.55	-1.03	-0.24	0.35	1.50
PtFeOCPc	-1.85	-1.27	-0.78	-0.44	0.39	1.04

6.2.2. *Electron transfer behaviour*: *cyclic voltammetry*

The surface electrochemistry of these MPc complexes when immobilised on MWCNT-modified EPPGEs was explored, first by examining their cyclic voltammetric evolutions in a solution of an outer-sphere redox probe, $[Fe(CN)_6]^{3-}/[Fe(CN)_6]^{4-}$. Figure 6.6 presents the comparative cyclic voltammograms of the various electrodes studied in 0.1 M $[Fe(CN)_6]^{3-/4-}$ 1.0 M KCl solution. When the same experiment was carried out in 1.0 M KCl alone, no significant redox process was observed compared to when the redox probe was present. This should perhaps not be surprising considering that it is usually very difficult to observe the redox couple (M^{3+}/M^{2+}) of surface-confined transition MPc complexes in aqueous solution.

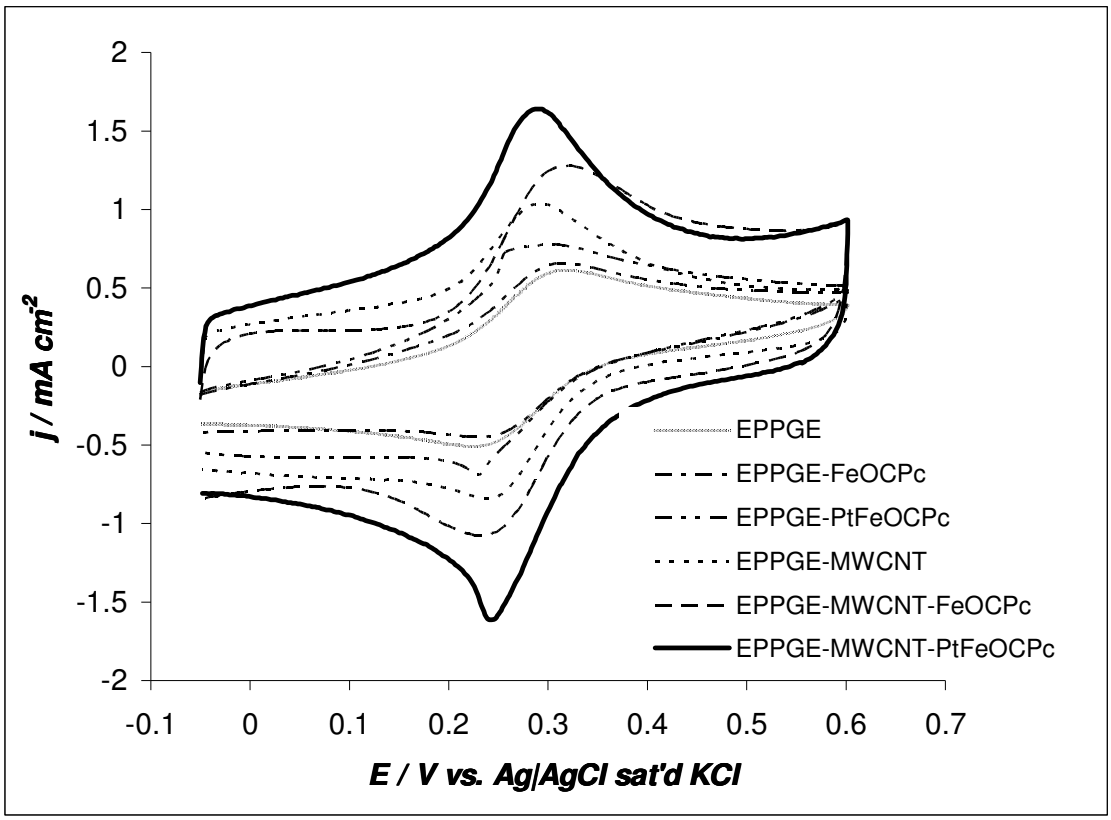

Figure 6.6: *Comparative cyclic voltammograms of the various electrodes in 0.1 M* $[Fe(CN)_6]^{3-/4-}$ *1.0 M KCl solution.*

The heterogeneous electron transfer behaviour was determined by analysis of the potential peak-to-peak separation (ΔE_p): the smaller the value the faster the electron transfer. The ΔE_p increases as EPPGE-MWCNT-PtFeOCPc (41 mV) < EPPGE-PtFeOCPc (44 mV) < EPPGE-MWCNT (56 mV) < EPPGE-MWCNT-FeOCPc (71 mV) < EPPGE- FeOCPc (78 mV) < EPPGE (90 mV), indicating that EPPGE-MWCNT-PtFeOCPc enhances faster electron transfer compared to other electrodes in the conditions employed. It is seen from the CV that the MWCNT-based electrodes exhibited higher current (Faradaic) response in the 0.2 – 0.35 V region as well as higher capacitive (non-Faradaic) response in

the -0.05 – +0.1 V region. This observation may be related to a change in diffusion regime (i.e., semi-infinite linear diffusion and / or thin layer diffusion processes arising from the redox process of electroactive species/electrolytes ($[Fe(CN)_6]^{3-}/[Fe(CN)_6]^{4-}$) trapped within the porous structure or in pockets in between the high surface area nanotubes) as described by Compton group.[6]

6.2.3. *Electron transfer behaviour: Impedimetric characterisation*

Figure 6.7(a) presents the Nyquist plots for the various electrodes studied in $[Fe(CN)_6]^{3-/4-}$ solution. The impedance spectra of the electrodes were satisfactorily fitted with the modified Randles equivalent electrical circuits (Figure 6.7(d)). The bare EPPGE electrode was fitted with circuit (i) while the other electrodes were fitted with circuit (ii) The fitting parameters involve the electrolyte resistance (R_s), electron-transfer resistance (R_{ct}), constant phase element (CPE), double layer capacitance (C_{dl}) and Warburg-type impedance (Z_w) which is associated with the diffusion of the ions of the redox probe.

The electron transfer rate constants (k^o) may be obtained from the R_{ct} values using the derived equations (6.1-3).[7,8]

$$R_{ct} = \frac{RT}{nFi_o} \qquad (6.1)$$

$$i_o = nFAk^o c_O^\infty c_R^\infty \qquad (6.2)$$

Combining equations (6.2) and (6.3), taking the activity coefficients (∞) equal to unity, and assuming the bulk concentrations of the oxidised and reduced species to be equal ($c_O^\infty = c_R^\infty = c$) such that the equilibrium potential ($E_{1/2}$) equals the formal redox potential ($E_{O/R}^\phi$), then the k^o becomes

$$k^o = k_{app} = \frac{RT}{n^2 F^2 A R_{ct} c} \qquad (6.3)$$

where n is the number of electron transferred (= 1) , *A* is the geometric area of the electrode, *c* is the concentration of the redox probe (in mol cm^{-3}, the concentration of $[Fe(CN)_6]^{3-}$ and $[Fe(CN)_6]^{4-}$ are equal), *R* is the ideal gas constant, *T* is the absolute temperature and *F* is the Faraday constant. The calculated values are shown in Table 6.2. The k^o values decreases as: EPPGE-MWCNT-PtFeOCPc (776 x 10^{-3} cm s^{-1}) > EPPGE-MWCNT (681 x 10^{-3} cm s^{-1}) > EPPGE-PtFeOCPc (176 x 10^{-3} cm s^{-1}) > EPPGE-MWCNT-FeOCPc (159 x 10^{-3} cm s^{-1}) > EPPGE-FeOCPc (151 x 10^{-3} cm s^{-1}) > EPPGE (20 x 10^{-3} cm s^{-1}) implying that electron transfer processes between the redox probe and the underlying EPPGE surface is faster at the EPPGE-MWCNT-PtFeOCPc compared to the other electrodes, corroborating the CV data. From the Bode plots, Figures 6.7(b) and (c), the slopes of the log *Z* vs. log *f* plot at the mid frequency region are less than the ideal −1.0 for pure capacitive behaviour, which is indicative of pseudocapacitive behaviour. Also, the EPPGE-MWCNT-PtFeOCPc shows the least impedance value compared to other electrodes. The data from the other Bode plot (i.e.,

–phase angle vs. log *f*) confirms the absence of ideal capacitive behaviour as the observed phase angles are less than the 90° expected of an ideal capacitive behaviour. It is only the bare EPPGE that shows a maximum at ~44°, close to the ideal Warburg value of 45°. This relaxation process is shifted to different phase angles upon modification, indicating that the $[Fe(CN)_6]^{3-/4-}$ redox process now takes place at the surface of the modifying films than directly on the bare EPPGE surface.

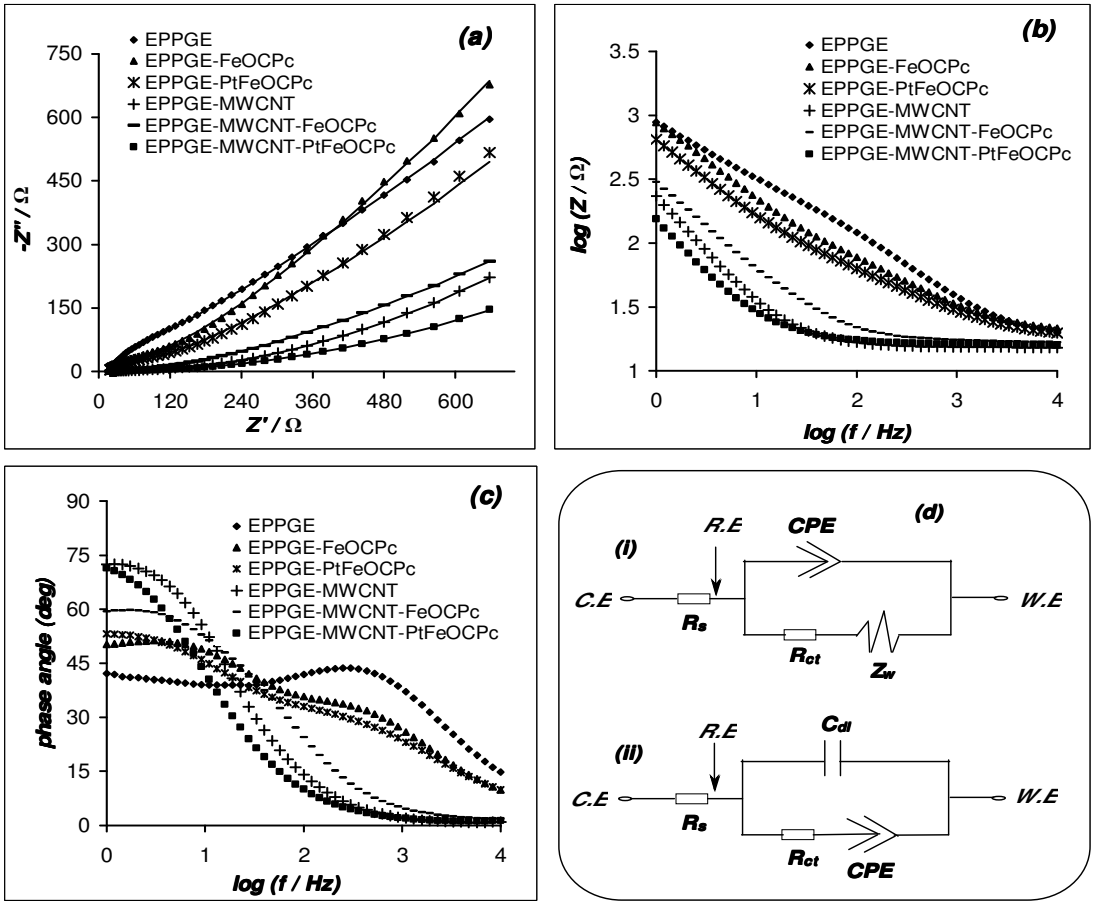

Figure 6.7: *Comparative Nyquist plots (a) and Bode plots: (b) and (c) of the various electrodes in 0.1 M* $[Fe(CN)_6]^{3-/4-}$ *1.0 M KCl solution. Equivalent electrical circuit used for fitting the measured data (d).*

Table 6.2: *Impedance parameters obtained using the electrical equivalent circuit in Figure 6.7 and* ΔE_p *values for the various electrodes studied in 0.1 M* $[Fe(CN)_6]^{3-/4-}$ *1.0 M KCl solution.*

ELECTRODES	**R_s / Ω**	**R_{ct} / Ω**	**CPE_1 /μF**	**n**	**C_{dl}/μF**	**$10^3 k^o$/cm s^{-1}**	**ΔE_p/mV**
EPPGE*	16.9±0.1	195.4±6.0	56.8±2.4	0.73±0.01	--	19.45±0.01	90
EPPGE-FeOCPc	21.5±0.3	25.2±1.6	386.9±7.5	0.59±0.01	6.5±0.3	150.63 ±0.01	78
EPPGE-PtFeOCPc	19.8±0.3	21.6±1.3	535.5±12.1	0.60±0.01	7.8±0.4	175.69 ±0.01	44
EPPGE-MWCNT	15.3±0.1	5.6±0.4	636.2 ±19.7	0.80±0.01	279.2±18.9	681.00 ±0.04	56
EPPGE-MWCNT-FeOCPc	17.2±0.1	23.4±0.9	903.3±7.5	0.63±0.03	45.0±5.2	158.48 ±0.01	71
EPPGE-MWCNT-PtFeOCPc	16.1±0.1	4.9±0.6	10.7±0.2	0.82±0.01	333.0±18.0	775.91±0.09	41

*Z_w of EPPGE is (433±3.81) x 10^{-6} Ω

6.3 Electrocatalytic Properties

6.3.1. *Electrocatalytic reduction of oxygen*

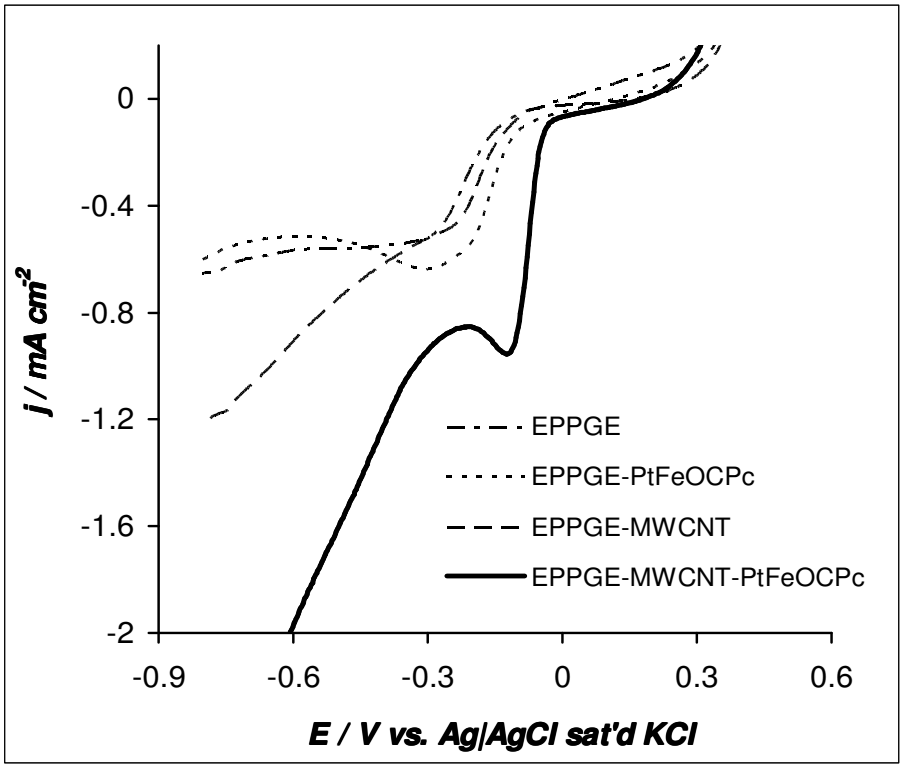

Figure 6.8: *Comparative linear sweep voltammetric curves of the electrodes in oxygen saturated 0.1 M NaOH solution. Scan rate: 10 mV* s^{-1}

Figure 6.8 compares the linear sweep voltammetric evolutions of bare EPPGE, EPPGE-PtFeOCPc, EPPGE-MWCNT and EPPGE-MWCNT-PtFeOCPc in oxygen saturated 0.1 M NaOH solution. A change in Gibb's free energy of reaction (ΔG) is related to the electrochemical potential (E) by the relationship;

$$\Delta G = -nFE \qquad (6.4)$$

where n is the number of electron transferred.

As a result, the onset potential for ORR is directly related to the activation energy of the reaction. It is evident from Figure 6.8 that the EPPGE-MWCNT-PtFeOCPc showed the least onset potential (~ 0.0 volt vs. Ag|AgCl saturated KCl) and peak potential (–0.1 V vs. Ag|AgCl saturated KCl) compared to other electrodes that showed onset potential at ~ –0.10 V vs. Ag|AgCl saturated KCl and peak potential at ~ –0.25 V vs. Ag|AgCl saturated KCl. In addition, the current density of the MWCNT-PtFeOCPc electrode (~1.20 mA cm^{-2}) is about twice (0.4 – 0.6 mA cm^{-2}) of the other electrodes. The higher performance of the MWCNT-PtFeOCPc electrode (in terms of onset potential, reduction peak potential and current density) clearly indicates faster charge transfer kinetics toward ORR compared to other electrodes. This result is remarkable when compared to recent work on gold nanoparticles[9] with onset potential of -0.08 V vs. Ag|AgCl and comparable to SnO_2-Au hybrid nanoparticles[10] with onset potential of 0.06 V vs. Ag|AgCl.

The kinetics of the ORR at the MWCNT-PtFeOCPc electrode was explored using the rotating disk electrode (Figure 6.9(a)). The Figure clearly shows that the current density increased as the rotation rate is increased, with a limiting current density of 5.52 mA cm^{-2} at 2,500 rpm. Figure 6.9(b) is the plot of j^{-1} versus $\omega^{-1/2}$ employing the Koutecky-Levich equation:

$$\frac{1}{j} = \frac{1}{J_{\text{Lev}}} + \frac{1}{J_{\text{kin}}} \qquad (2.12)$$

$$J_{kin} = nFkc_O \qquad (2.13)$$

$$J_{Lev} = 0.21nFD^{2/3}\gamma^{-1/6}c_{O_2}\omega^{1/2} \quad (2.14)$$

where j is the measured current density, j_{Lev} and j_{kin} are the limiting current density and the kinetic current density respectively, γ is the kinematic viscosity (0.01 cm^2s^{-1}),[7] ω is the angular frequency of rotation, D is the diffusion coefficient of oxygen in an aqueous solution (1.98 x 10^{-5} cm^2s^{-1}),[11,12] c_{O2} is the concentration of oxygen in solution (1.38 x 10^{-6} $molcm^{-3}$),[11,13] k is the kinetic rate constant for the catalyzed oxygen reduction reaction. The linearity of the plot is indicative that the reaction is first order, and controlled by kinetics at the electrode surface as well as mass transport of oxygen species. The number of electrons (n) transferred per oxygen molecule was calculated as 3.98±0.24, suggesting that ORR at MWCNT-PtFeOCPc electrode proceeds via a single 4-electron transfer.

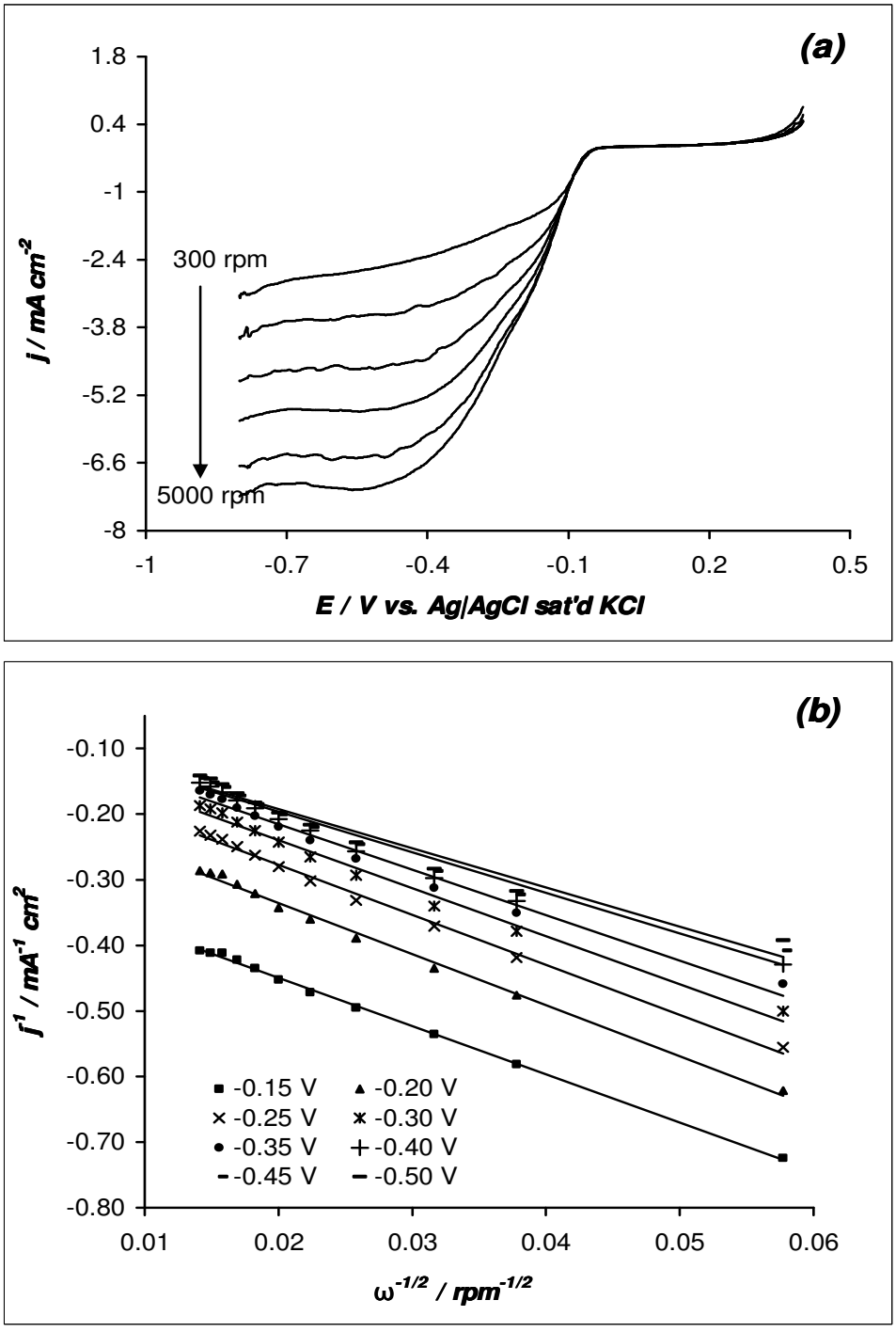

Figure 6.9: *(a) RDE polarization curves at different rotation rates for EPPGE-MWCNT-PtFeOCPc electrode in oxygen saturated 0.1 M NaOH solution scan rate 10 mVs^{-1}; (b) Koutecky-Levich plot obtained from RDE data*

J_{kin}, obtained from the intercept of the Koutecky-Levich plots, was calculated to be –13.8 mA cm^{-2} at both potentials of –0.45 and –0.50 V. The kinetic rate constant (k) was calculated as 2.78 x 10^{-2} cm s^{-1}. This value is slightly better than the reported 1.4 x 10^{-2} – 2.0 x 10^{-2} cm s^{-1} range for a glassy carbon modified with anthraquinone,[14] but in the same magnitude (1.96 x 10^{-2} – 5.87 x 10^{-2} cm s^{-1} range) obtained in alkaline media reported for gold nanoclusters catalyst[9] and tungsten carbide nanocrystals.[15]

Correcting the polarization curve for diffusion effects for first order reaction, one obtains:[16]

$$j_K = \left(\frac{j}{j_L - j} \right) \tag{4.4}$$

The j_k is related to the Tafel equation as Eq. (4.3):[16]

$$E_{app} = E_{eq} - b \log j_k \tag{4.3}$$

$$b = \frac{2.3RT}{\alpha n F} \tag{4.5}$$

where E_{app} is the applied potential, E_{eq} is the equilibrium potential, j_k is the kinetic current density, j_L is the limiting current density (plateau in RDE voltammogram), j is the measured current density at a given potential, R, T and F have their usual meaning, αn is the kinetic parameter for the electrode process. The plot of E_{app} versus log jk (exemplified in Figure 6.10 for 4000 rpm) yielded a slope of –180±0.04 mV dec^{-1} in the potential region between –0.24 and –0.38 V. The high value of the Tafel slope obtained is characteristic of porous electrode

with high internal surface area leading to high electrocatalytic activities. This value implies that ORR at the MWCNT-PtFeOCPc electrode might be limited by oxygen adsorption, a similar phenomenon also reported for Pt-containing electrodes.[17]

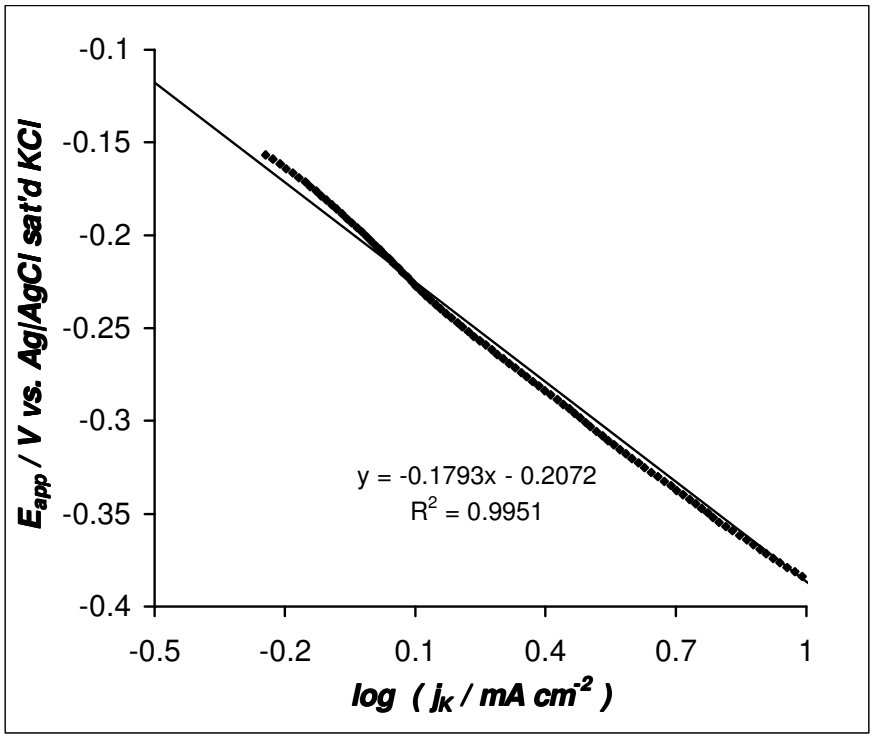

Figure 6.10: *Tafel plot of E_{app} vs. log j_K for oxygen reduction on EPPGE-MWCNT-PtFeOCPc electrode in oxygen saturated 0.1 M NaOH solution.*

6.3.2. *Electrocatalytic oxidation of formic acid*

6.3.2.1. *Comparative cyclic voltammetric response*

The electrocatalytic properties of EPPGE-MWCNT-PtFeOCPc for formic acid oxidation were studied in 0.5 M HCOOH + 0.5 M H_2SO_4 aqueous solution by cyclic voltammetry. Figure 6.11 presents the cyclic

voltammogramms of the various electrodes. The classical formic acid electro-oxidation peaks were observed only with the EPPGE-PtFeOCPc and EPPGE-MWCNT-PtFeOCPc electrodes, implying that electro-catalytic activity for the oxidation of formic acid takes place in the presence of the platinum containing catalysts. Two distinct oxidation peaks can be observed at ~0.20 and ~0.70 V for the forward scan and a backward oxidation peak at ~0.20 V. The peak at ~0.20 V is attributed to the direct oxidation of formic acid to CO_2 via the formation of an active intermediate specie ($-COO^-$)[18] or the "direct pathway", usually used to evaluate the electro-catalytic activity of the catalyst. The peak at ~0.70 V is attributed to the oxidation of adsorbed CO on the surface of the catalyst and formic acid by sites that have been poisoned by the adsorption of CO (poisoning of surface active sites) and the subsequent release of these sites by CO stripping and is usually referred to as the "CO pathway".[19,20,21] The reverse peak at ~ 0.20 V is related to the direct oxidation of formic acid to CO_2 after the adsorbed CO has been removed at increased electrode potential with the subsequent recovery of the surface active sites. Notice that unlike the EPPGE-PtFeOCPc, the EPPGE-MWCNT-PtFeOCPc showed a small reverse peak at around 0.8 V. A similar peak was observed recently by Maxakato *et al.*[22] and attributed it to further oxidation of the CO or FA.

It can be seen in Figure 6.11 that the onset for the electro-oxidation of formic acid in the EPPGE-PtFeOCPc and EPPGE-MWCNT-PtFeOCPc electrodes is almost immediate. The current densities of the forward

oxidation peaks are ~2.96 and ~2.55 mA cm^{-2} for the EPPGE-PtFeOCPc electrode; ~3.71 and ~2.51 mA cm^{-2} for the EPPGE-MWCNT-PtFeOCPc electrode. According to Zhou *et al.,*[16] the ratio of the current densities under the first and second forward oxidation is used to determine the pathway for the electro-oxidation of formic acid. A low ratio indicates that formic acid oxidation proceed via the "CO pathway" and a high ratio implies that formic acid oxidation proceed via the direct pathway. The ratios of the current densities calculated for EPPGE-PtFeOCPc and EPPGE-MWCNT-PtFeOCPc is ~1.2 and ~1.5 respectively. These mean that both electrodes favour the direct pathway. According to Chen *et al.,*[18] the ratio of the current densities under the first forward oxidation peak and the reverse oxidation peak essentially reflects the fraction of catalyst surface that is not poisoned by CO adsorption. A low ratio implies a low tolerance to CO poisoning, while a high ratio implies a high tolerance to CO poisoning. The ratios of the current densities calculated for EPPGE-PtFeOCPc and EPPGE-MWCNT-PtFeOCPc is approximately 1, meaning that both electrodes have high tolerance to CO poisoning. For the reverse oxidation, an oxidation peak at almost the same potential is observed, with a current density of ~4 mA cm^{-2} for the EPPGE-PtFeOCPc electrode; and ~5 mA cm^{-2} for the EPPGE-MWCNT-PtFeOCPc electrode. The direct oxidation process observed here is related to the promotional effect of the phthalocyanine as also postulated by Zhou *et al*.[16] for FeTSPc immobilised onto a Pt disc electrode.

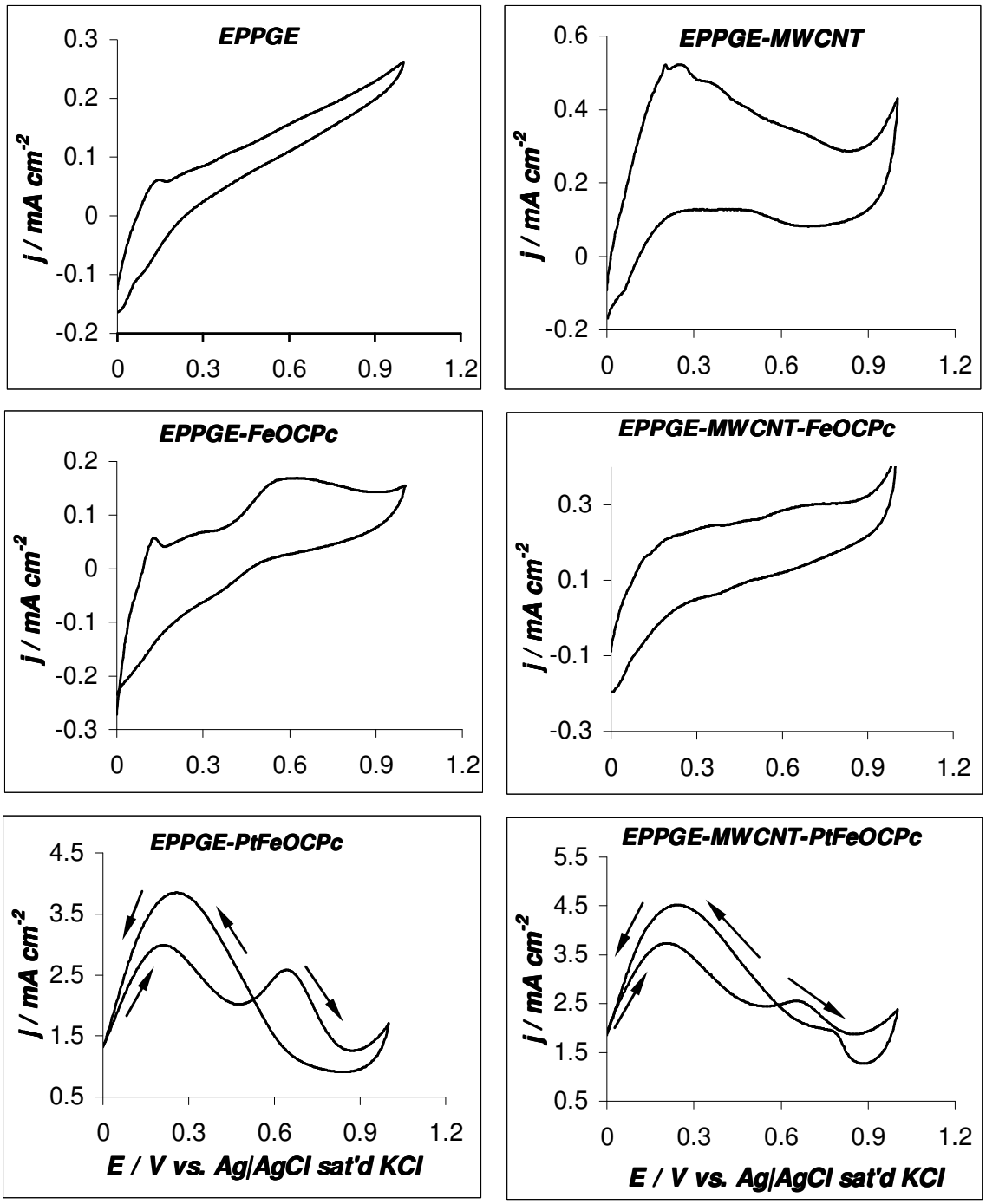

Figure 6.11: *Cyclic voltammograms of the various electrodes in 0.5 M H_2SO_4 containing 0.5 M HCOOH solutions*

The reason for this enhanced reaction is not yet fully understood, however, other workers[23,24] have attributed such observation to the enhanced dehydration reaction in the CO pathway that generates the CO_{ad} intermediates. Also, the electronic effect generated by the availability of electrons in the FeOCPc macrocycle could favour the electro-oxidation of formic acid by changing the electron distribution on the platinum surface, hence affecting the reaction pathway. It should be noted here that Pt nanoparticles alone electrodeposited onto MWCNT (MWCNT-Pt) showed poorer current response towards formic acid compared to the MWCNT-PtFeOCPc. This result is in agreement with the result reported by Maxakato *et al*.[22]

6.3.2.2. *Chronoamperometry experiment*

Chronoamperometry experiments were performed to provide further insights into the achievable current densities by the electrodes. Figure 6.12 presents the current – time curve of the electrodes studied, showing that the current density first drops to ~0.21 mA cm^{-2} and then to a steady value at ~0.13 mA cm^{-2} after about 2 min. for the EPPGE-PtFeOCPc electrode, while for the EPPGE-MWCNT-PtFeOCPc electrode, the current dropped initially to ~ 0.47 mA cm^{-2} then to a steady value at ~0.27 mA cm^{-2} after about 5 min. The stable current for the EPPGE-MWCNT-PtFeOCPc electrode is much higher than EPPGE-PtFeOCPc. The stability of the EPPGE-MWCNT-PtFeOCPc at high current

signifies better activity towards formic acid oxidation. This confirms our results from cyclic voltammetry.

An insight into the electrocatalytic rate constants (k_{cat}) at the two electrodes was obtained by employing the conventional equation below:[7]

$$\frac{j_{cat}}{j_{buff}} = \pi^{1/2}\left(k_{cat}c_o t\right)^{1/2} \qquad (6.5)$$

where j_{cat} and j_{buff} are the current densities in the presence and absence of formic acid, c is the bulk concentration and t is the time. A value of 41.09 cm^3 mol^{-1} s^{-1} was obtained for the EPPGE-MWCNT-PtFeOCPc and 10.95 cm^3 mol^{-1} s^{-1} for the EPPGE-PtFeOCPc, further confirming the higher electrocatalytic performance of the EPPGE-MWCNT-PtFeOCPc. There is no available literature to adequately compare the k_{cat} values determined in this work. However, the values are smaller than the 2.45 x 10^{-1} L mol^{-1} s^{-1} (i.e., 245 cm^3 mol^{-1} s^{-1}) reported by Blake and Hinshelwood[25] for gaseous formic acid. Considering the higher performance of the EPPGE-MWCNT-PtFeOCPc, all subsequent studies (unless otherwise stated) was devoted to this electrode.

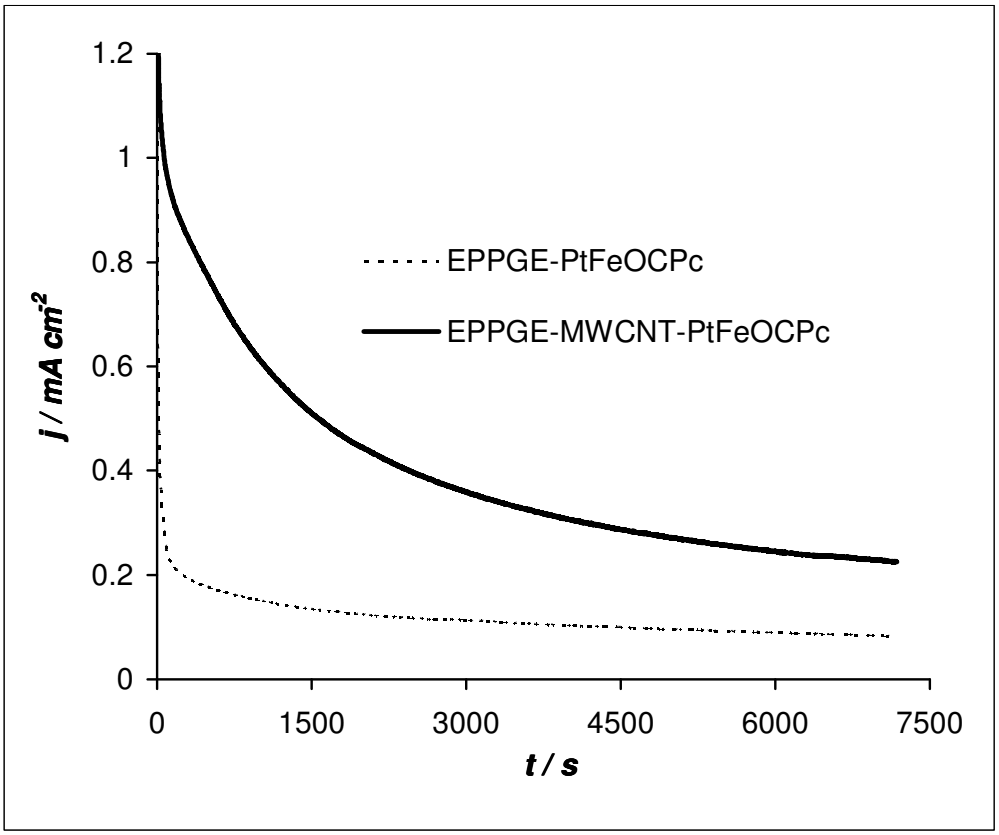

Figure 6.12: *Chronoamperometric curves of EPPGE-PtFeOCPc and EPPGE-MWCNT-PtFeOCPc in 0.5 M H_2SO_4 containing 0.5 M HCOOH solutions*

6.3.2.3. *Concentration studies: Tafel analysis*

The effect of formic acid concentration on the electrocatalysis was studied at concentrations ranging from 0.10 to 1.20 M formic acid in 0.5 M H_2SO_4 solution at EPPGE-MWCNT-PtFeOCPc. Figure 6.13(a) shows that the current density increases as concentration increases and starts to decrease at 0.90 M, meaning that mass transfer resistances and build up of interfacial CO_2 formed during the electro-oxidation process or the combination of both might be responsible for this deviation at high concentration.[26] Simply stated, at > 0.75 M the

catalyst becomes easily saturated, meaning that optimum catalysis occur at 0.75 M formic acid.

The electrocatalytic properties was investigated by analyzing the Tafel behaviour, using the conventional relationships for oxidation processes, equations (6.6) and (6.7):[7]

$$\eta = a + b \log j \qquad (6.6)$$

$$b = \frac{2.303\ RT}{(1-\alpha)nF} \qquad (6.7)$$

where η is the overpotential (difference between the applied potential and the open circuit potential), j is the current density, b is the Tafel slope, a is the Tafel constant relating to the exchange current density, α is the transfer coefficient, n is the number of electrons involved in the rate determining step, while other symbols retain their usual meaning. From the plots of η vs. log j (Figure 6.13(b)), the Tafel slopes were essentially the same (275 – 290 mV dec^{-1} range) at all concentrations, indicating that the same reaction mechanism is probably operating at all the concentrations of the formic acid studied. Assuming a 1-electron transfer process in the rate-limiting step of the overall electrocatalysis, the value of $(1-\alpha) \approx 0.2$, which implies that the transfer coefficient is close to unity.

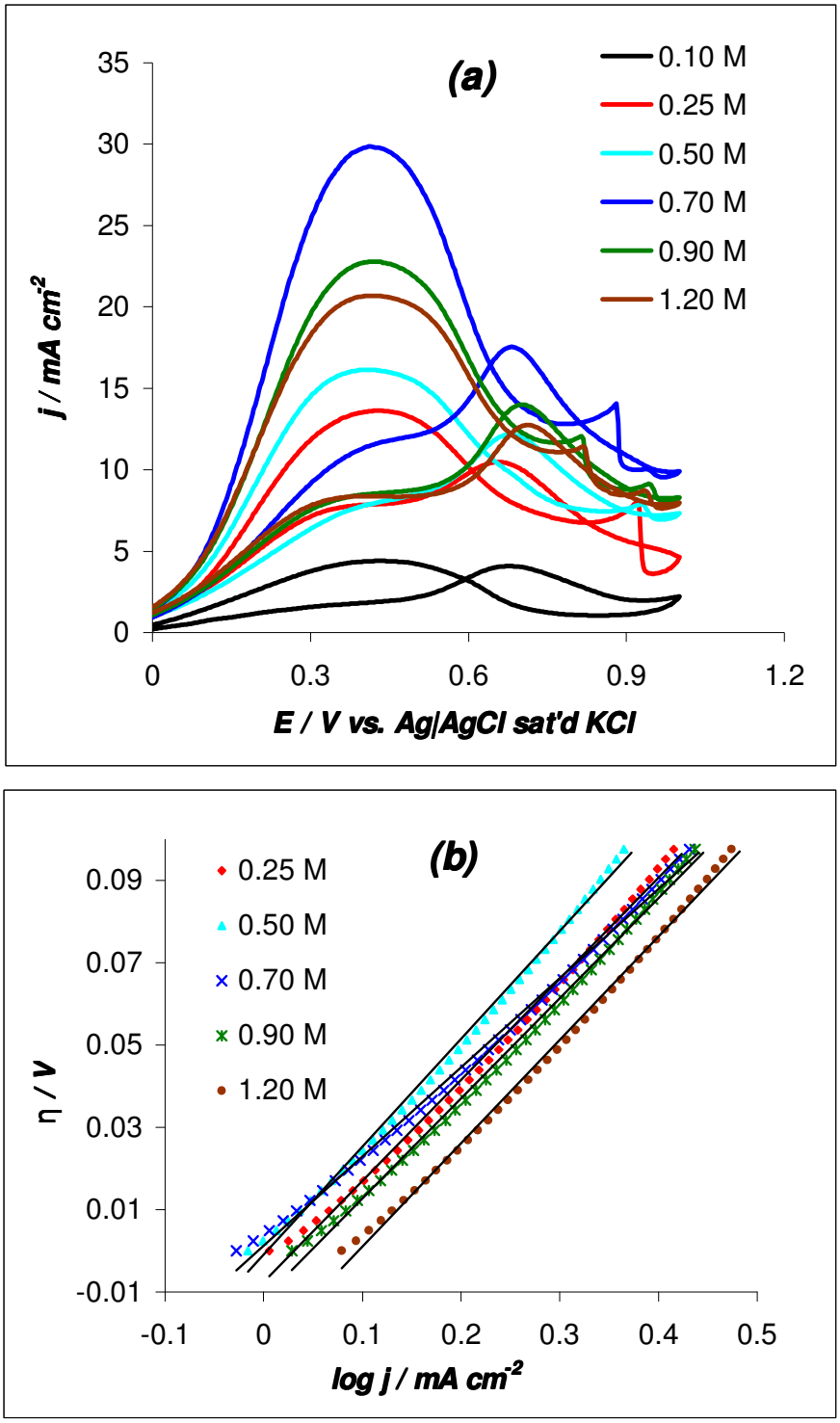

Figure 6.13: *Cyclic voltammetric evolutions following changes in concentration of formic acid (a), Tafel plots of η against log j at different concentration of formic acid (b)*

The proximity of the coefficient to unity is an indication that the probability of product formation is very high. The high value of the Tafel slope obtained is characteristic of porous electrode with high internal surface area leading to high electrocatalytic activities.[26]

6.3.2.4. *Electrochemical impedance spectroscopy experiments*

EIS was employed to further interrogate the electrocatalytic activity of the EPPGE-MWCNT-PtFeOCPc towards formic acid oxidation. Figures 6.14(a) presents the Nyquist plots while Figures 6.14(b) and 6.14(c) were the Bode plots obtained at different potentials measured in 0.5 M HCOOH + 0.5 M H_2SO_4 solutions. The Frumkin-Melik-Gaikazyan (FMG)[27] equivalent electrical (Figure 6.14(d)) was used to fit the EIS data. In the circuit the symbols C_{ad} represents the adsorption capacitance arising from the oxidation of carbonaceous species on the electrode surface, while other symbols retain their usual meaning. It can be seen from the figure that all measured spectra are in the same quadrant, the conventional positive Faradaic impedance, at all peak potentials measured, which is indicative of the absence of adsorbed intermediates. This is interesting considering that other workers such as Chen *et al.,*[21,29] Seland *et al.*[18] and Maxakato *et al.*[22] have observed negative Faradaic impedance and attributed such phenomenon to adsorbed intermediates resulting from the formation of chemisorbed

hydroxyl species that compete for surface adsorption sites against the CO. The implication of the data in Table 6.3 resulting from the modelling of this electrode should be emphasised. First, since the FMG electrical equivalent circuit used in fitting our measured data is popularly used for studying adsorbed organic molecules,[30] the presence of adsorbed species cannot be completely ruled out in this work. Second, the values of the R_s and Z_w are approximately the same. Ideally, R_s and Z_w values should not be affected by modification of the electrode surface.[31] Third, considering that electron transfer rate constant is inversely proportional to the C_{ad},[32,33] it suggests that reaction kinetics tends to be faster at higher potentials (≥ 0.90 V). Thus, the low adsorption capacitance at more positive potential suggests some oxidative removal of carbonaceous species present on the electrode surface. The corresponding Bode plots clearly show the phase angles of the electrocatalytic processes as 65° and ≥ 70°, confirming the presence of CPE and the pseudo-capacitive nature of the electrode since the angle is less than the 90° for an ideal capacitive behaviour. The slopes from the plot of log Z vs. log f were ~ -0.68 and -0.05 at mid and high frequency regions respectively, indicative of pseudo-capacitive and resistive behaviour at these frequency regions.

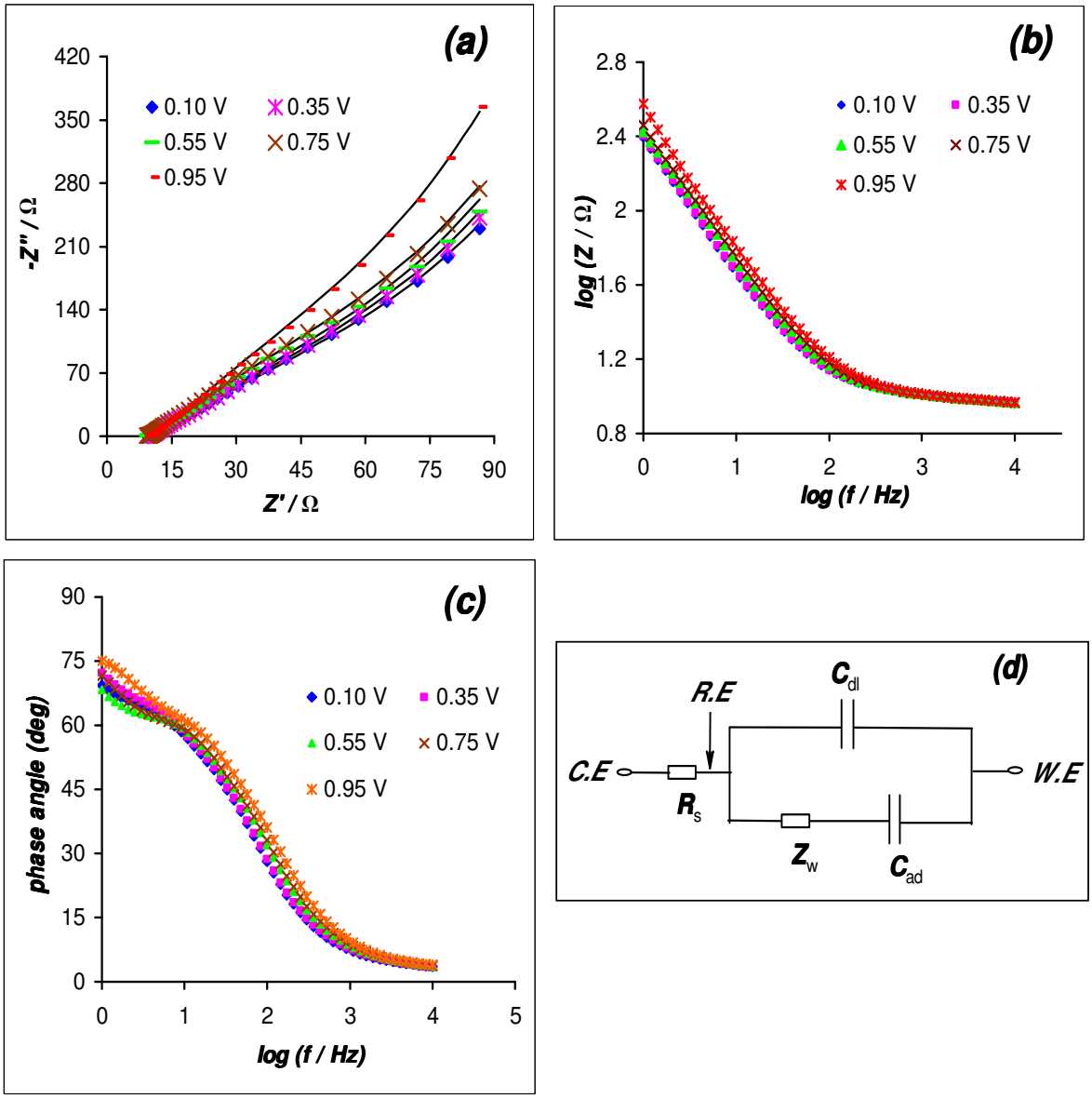

Figure 6.14: *Typical Nyquist(a), Bode (b and c) plots and equivalent circuit (d) used to fit the spectra obtained at different potentials (0.10, 0.35, 0.55, 0.75 and 0.95 V) for EPPGE-MWCNT-PtFeOCPc in 0.5 M H_2SO_4 containing 0.5 M HCOOH.*

Table 6.3: *Impedance data obtained for EPPGE-MWCNT-PtFeOCPc electrode studied in 0.5 M H_2SO_4 containing 0.5 M HCOOH at different potentials using the electrical equivalent circuit in Figure 6.14.*

Bias Potential / V vs. Ag/AgCl sat'd KCl	**R_s / Ω**	**C_{dl}/μF**	**C_{ad}/mF**	**10^3 Z_w / Ω**
0.10	9.82 ±0.10	133.70 ±7.42	0.88 ±0.04	2.72 ±0.14
0.35	9.75 ±0.10	121.40 ±6.93	0.79 ±0.03	2.89 ±0.14
0.55	9.80 ±0.10	117.70 ±5.49	0.92 ±0.08	2.15 ±0.09
0.75	9.73 ±0.08	102.00 ±4.63	0.78 ±0.03	2.26 ±0.09
0.95	9.63 ±0.07	80.10 ±3.57	0.51 ±0.01	2.37 ±0.09

6.3.2.5. *Tolerance to carbon monoxide poisoning*

Adsorption of CO-like species on the surface of the electrocatalyst is used to evaluate the extent to which an electrocatalyst can tolerates poisoning in a fuel cell system such as direct formic acid fuel cell (DFAFC).[34,35] Thus, we conducted a preliminary experiment to determine the tolerance of the proposed electrocatalyst for formic acid oxidation towards CO. Figure 6.15 shows the comparative CVs of EPPGE-PtFeOCPc (Figure 6.15(a)) and EPPGE-MWCNT-PtFeOCPc (Figure 6.15(b)) in 0.5 M H_2SO_4 solution (**I**), 0.5 M H_2SO_4 saturated with CO (**II**), and 0.5 M FA containing 0.5 M H_2SO_4 saturated with CO (**III**). The MWCNT-PtFeOCPc also shows the unique reverse peak at ~ 0.8 V as in Figure 6.11. The peak potential for CO oxidation at the EPPGE-PtFeOCPc is slightly (~ 40 mV) more positive than at the EPPGE-MWCNT-PtFeOCPc, meaning that the removal of CO from the EPPGE-PtFeOCPc electrode will be slightly difficult.[30] Secondly, from the electrocatalytic waves of (**III**) in both figures, the ratio of the current density of the forward anodic peak to the reverse anodic peak of 2.18 and 1.12 were obtained for EPPGE-PtFeOCPc and EPPGE-MWCNT-PtFeOCPc, respectively, meaning that EPPGE-MWCNT-PtFeOCPc tolerates CO poisoning than its EPPGE-PtFeOCPc counterpart.

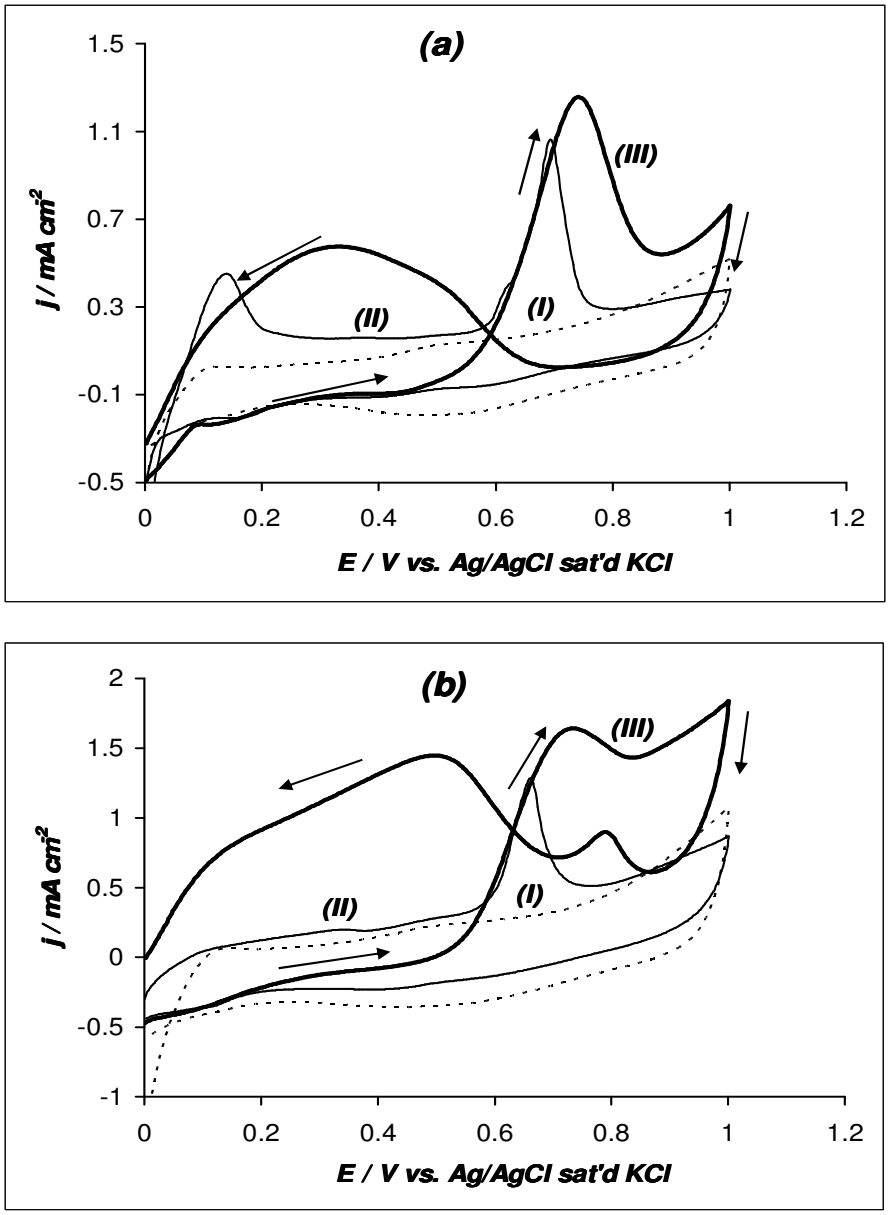

Figure 6.15: *Comparative cyclic voltammograms of EPPGE-PtFeOCPc (a) and EPPGE-MWCNT-PtFeOCPc (b) electrodes studied in 0.5 M H_2SO_4 (I), CO saturated in 0.5 M H_2SO_4 (II) and CO saturated in 0.5 M H_2SO_4 and 0.5 M HCOOH (III)*

References

1. O.V. Dolotova, O.L. Kaliya, *Russ. J. Coord. Chem*. **33** (2007) 111
2. J. Yang, D. Sung, J. Li, X. Yang, J. Yu, Q. Hao, W. Liu, J. Liu, Z. Zou, J. Gu, *Electrochimica Acta,* **54** (2009), 6300
3. J. Prabhuram, T.S. Zhao, C.W. Wang, J.W. Guo, *J. Power Sources*, **134** (2004), 1
4. J.G. Guan, W. Wang, R.Z. Gong, R.Z. Yuan, L.H Gan, K.C. Tam, *Langmuir,* **18** (2002), 4198
5. Z-Z. Zhu, Z. Wang, H-L. Lin*, Appl. Surf. Sci*., **254** (2008) 2934
6. I. Streeter, G.G. Wildgoose, L. Shao, R.G. Compton, *Sens. Actuat. B,* **133** (2008), 462
7. A.J. Bard, L.R. Faulkner, *Electrochemical Methods: Fundamentals and Applications*, 2nd ed., John Wiley & Sons, Hoboken NJ, 2001
8. H.H. Girault, *Analytical and Physical Electrochemistry*, EPFL Press, Lausanne, Switzerland, 2004, Chapter 7
9. W. Chen, S. Chen, *Angew. Chemie, Int. Ed*., **48** (2009) 4386
10. W. Chen, D. Ny, S. Chen, *J. Power Sources* **195** (2010) 412
11. J. Zagal, P. Bindra, E. Yeager, *J. Electrochem. Soc*. **127** (1980) 1506
12. K. Gubbins, R. Walker, *J. Electrochem. Soc.,* **112** (1965) 469
13. W.G. Wilke, *solubilities of inorganic and metal organic compounds*, Vol 2, 4th ed., American Chemical Society, Washington,D.C. 1965 p.1219
14. K. Vaik, U. Maeorg, F.C. Maschion, G. Maia, D.J. Schiffrin, K.

Tammeveski, *Electrochim. Acta* **50** (2005) 5126

15. H. Meng, P.K. Shen, *Electrochem. Commun*. **8** (2006) 588
16. I. Koc, M. Camur, M. Bulut, A.R. Ozkaya, *Catalysis Lett*. **131** (2009) 370
17. K. Tammeveski, T. Tenno, J. Claret, C. Ferrater, *Electrochim. Acta* **42** (1997) 893
18. F. Seland, R. Tunold, D.A. Harrington, *Electrochim. Acta*, **53** (2008), 6851
19. X. Zhou, C. Liu, J. Liao, T. Lu, W. Xing*, J. Power Sources*, **179** (2008), 481
20. B. Liu, H.Y. Li, L. Die, X.H. Zhang, Z. Fan, J.H. Chen, *J. Power Sources*, **186** (2009), 62
21. W. Chen, J. Kim, S. Sun, S. Chen*, Langmuir*, **23** (2007), 11303
22. N.W. Maxakato, K.I. Ozoemena, C.J. Arendse, *Electroanalysis*, **22** (2010), 519
23. T. Iwasita, X.-H. Xia, E. Herrero, H.-D. Liess, *Langmuir,* **12** (1996) 4260
24. J. Cavalier, S.G. Sun, *J. Electroanal. Chem.,* **199** (1986) 471
25. P.G. Blake, C. Hinshelwood, *Proc. Royal Soc. of London Series A*, *Math. Phys. Sci.,* **255** (1960), 444
26. M. Zhao, C. Rice, R. I. Masel, P. Waszczuk, A. Wieckowski*, J. Electrochem. Soc.,* **151** (2004), A131
27. P.K. Shen, C. Xu, *Electrochem. Commun*., **8** (2006), 184

28. G. Nurk, H. Kasuk, K. Lust, A. Janes, E. Lust, *J. Electroanal. Chem*., **533** (2003), 1

29. W. Chen, J. Kim, L-P. Xu, S. Sun, S. Chen, *J. Phy. Chem. C,* **111** (2007), 13452.

30. F. Ye, S. Chen, X. Dong, W. Lin, *J. Nat. Gas. Chem*., **16** (2007), 162

31. J. Pillay, K.I. Ozoemena, *Electrochem. Commun*., **9** (2007), 1816

32. J. Pillay, K.I. Ozoemena, R.T. Tshikhudo, R.M. Moutloali, *Langmuir*, **26** (2010), 9061

33. S.E. Creager, T.T. Wooster, *Anal. Chem.* **70** (1998), 4257

34. F. Hu, C. Chen, Z. Wang, G. Wei, P.K. Shen, *Electrochim. Acta*, **52** (2006), 1087

35. A. N. Gavrilov, E. R. Savinova, P. A. Simonov, V. I. Zaikovskii, S. V. Cherepanova, G. A. Tsirlina, V. N. Parmon, *Phys. Chem. Chem. Phys.,* **9** (2007), 5476